Final Draft Report

On

LONGITUDINAL CRACKING AND SPALLING IN LONG SPAN FLORIDA POST-TENSIONED BULB-T GIRDERS

State Study No. 0667
WPI 0510667
State Job No. 99700-3511-119
Contract No. B-8606

Submitted to

State of Florida
Department of Transportation

By

Kamafiq, Ph.D., P.E.

July 20, 1994

Report No.	2. Government Accession No.	3. Recipient's Catalog No.

Title and Subtitle	5. Report Date
,ongitudinal Cracking and Spalling in Long Span 'ost Tensioned Bulb-Tee Girders	6. Performing Organization Code

Author(s)	8. Performing Organization Report No.
:amal Tawfiq, Ph.D., P.E.	

Performing Organization Name and Address	10..Work Unit No.
'AMU/FSU College of Engineering)epartment of Civil Engineering :525 Pottsdamer Street 'allahassee, Fl 32316	11. Contract or Grant No.

2. Sponsored Agency Name and Address	13. Type of Report and Period Covered
:tate of Florida Department of Transportation .esearch Center :05 Suzannee Street, M.S. 30 'allahassee, Fl 32301	14. Sponsoring Agency Code

5. Supplementary Notes

'repared in cooperation with the Federal Highway Administration

5. Abstract

In this study, full-scale field tests and a number of finite element models were used to nvestigate the longitudinal cracking and spalling in long span Florida bulb-t girders. The full-cale test consisted of two (2) 75 foot long bulb-t girders which were constructed to form a 150 oot long continuous girder. The instrumentation plan was developed after an analytical study of he bulb-t girder. Fifty-seven (57) internal strain gages were placed in high stress regions prior o concrete casting. Prior to testing, forty-four (44) additional strain gages were mounted to the urface of the girder. The gages were monitored during the post-tensioning of the strands in each uct, as the live loads were applied and during the grouting of the ducts.

The FEA modeling consisted of two-dimensional and three-dimensional models. The two-imensional models were used to examine the effects of various types in the bulb-t girders. Ducts anufactured with either high density polyethylene or galvanized steel were examined. Also, ducts ith a round or oval shapes were examined. The four ducts analyzed in the two-dimensional models ere oval polyethylene, oval steel, round polyethylene and round steel. The forces caused by trand wedging and grouting pressure in bulb-t girders were applied to the two-dimensional models. he results indicate that round steel ducts are most effective in reducing strains in the concrete eb. Models with oval polyethylene ducts had the highest strains in concrete web. The three-imensional models were used to compare the stresses and deflections in full-scale girders. The hree-dimensional models were also used to examine any stress concentration that occurs at the end f the transition zone.

The strains predicted by the FEA were compared with the filed (field) results to verify the validity f the analytical solution. There was a close correlation between the strains predicted by the odels and the actual field results. Therefore, the finite element models developed for this roject offer an effective means to evaluate stresses in long span post-tensioned girders. The esults indicate: wedging and grouting forces will cause significant stresses in bulb-t girders, ound shapes are more effective in reducing concrete web strains, steel ducts are more effective n reducing concrete web strains and measured friction coefficients fall within the recommended ange in the AASHTO code.

. Key Words	18. Distribution Statement
ost Tension, Grout, Strand edging, Ducts	No restriction. This document is available to the public through the National Technical Information Service, Springfield Va. 22161

Security Classif. (of this report)	20. Security Classif. (of this page)	21. No. of Pages
nclassified	Unclassified	

DISCLAIMER

The opinions, findings and conclusions expressed in this publication are those of the authors and not necessarily those of the Florida Department of Transportation and the Federal Highway Administration.

Prepared in cooperation with the Florida Department of Transportation and the Federal Highway Administration.

ACKNOWLEDGMENTS

The author would like to express his gratitude and sincere regards are extended to Dr. Mohsen Shahawy from the Florida Department of Transportation for his invaluable suggestions and creative criticism to this undertaking. Thanks to Dr. Moussa Issa for his constructive review. Also, thanks to John Poulson a graduate student at the department of Civil Engineering for his outstanding efforts in sample preparation, laboratory testing and analysis of results. My appreciation is extended to the Civil Engineering Department at FAMU/FSU College of Engineering for providing us with the needed facilities. Lastly, I acknowledge the support provided to us by the Florida Department of Transportation. Without their support this task would not have been feasible.

TABLE OF CONTENTS

List of Tables

List of Figures

Notation

F	=	total force caused by pressure acting on the duct wall (LB)
F_n	=	force acting on each node (LB)
$F_{u\text{-}in}$	=	the in-plane deviation force effect per unit length of tendon (K/FT)
$F_{u\text{-}out}$	=	the out-of-plane deviation force effect per unit length of tendon (K/FT)
F_c	=	stress corresponding to strain, Ecf
f_c	=	peak stress obtained from a cylinder test
K	=	wobble friction coefficient (FT^{-1})
k	=	factor to increase the postpeak decay in stress, taken as 1.0 for (ErVE'e) less than 1.0 and as a number greater then 1.0 for (EVE',) greater then 1
n	=	number of nodes on the inner duct surface
P	=	pressure acting inside the duct (PSI)
P_u	=	the factored tendon force (KIP)
R	=	the radius of curvature of the tendon at the considered location (FT)
SA	=	surface area of the duct wall (IN^2)
α	=	sum of the absolute values of angular change of prestressing steel path from jacking end, or from the nearest jacking end if tensioning is done evenly at both ends, to the point under investigation (RAID)
O_{pf}	=	loss in prestressing steel stress due to friction (KSI)
Apl	=	stress in the prestressing steel at jacking (KSI)
E_C	=	tangent stiffness when E_{cf} equals zero
ϵ_d	=	strain at a given point
ϵ'_C	=	strain at maximum stress, f_r
μ	=	coefficient of friction (1/RAD)

Abstract

In this study, full-scale field tests and a number of finite element models were used to investigate the longitudinal cracking and spalling in long span Florida Bulb-T girders. The full-scale test consisted of two (2) 75 foot long Bulb-T girders which were constructed to form a 150 foot long continuous girder. The instrumentation plan was developed after an analytical study of the Bulb-T girder. Fifty-seven (57) internal strain gauges were placed in high stress regions prior to concrete casting. Prior to testing, forty-four (44) additional strain gauges were mounted to the surface of the girder. The gauges were monitored during the post-tensioning and grouting of the strands in each duct. The gauges were also monitored when the slab dead load compensation was applied to the girders. In addition, a friction analysis was performed using data from the field test.

The FEA modeling consisted of two-dimensional and three-dimensional models. The two-dimensional models were used to examine the effects of various duct types in the Bulb-T girders. Ducts manufactured with either high density polyethylene or galvanized steel were examined. Also, daunts with a round or oval shapes were examined. The four ducts analyze in the two-dimensional models were oval polyethylene, oval steel, round polyethylene and round steel. The forces caused by strand wedging and grouting pressure in Bulb-T girders were applied to the two-dimensional models. The results indicate that round steel ducts are most effective in reducing strains in the concrete web. Models with oval polyethylene ducts had the highest strains in concrete web. The three-dimensional models were used to compare the stresses and deflections in full-scale girders. The three-dimensional models were also used to examine any stress concentration that occurs at the end of the transition zone.

The strains predicted by the FEA were compared with the field results to verify the validity of the analytical solution. There was a close correlation between the strains predicted by the models and the actual field results. Therefore, the finite element models developed for this project offer an effective means to evaluate stresses in long span post-tensioned girders. The results indicate: wedging and grouting forces will cause significant stresses in Bulb-T girders, round shapes are more effective in reducing concrete web strains, steel ducts are more effective in reducing concrete web strains and measured friction coefficients fall within the recommended range in the AASHTO code.

Chapter 1
Introduction

Precast prestressed concrete girders were developed in the early 1950s. By the end of the 1950s, AASHTO standardized types II, III and IV girders. These girders became very popular throughout the USA and Canada. Numerous advancements have been made in prestressing technology since the 1950s, and, more efficient girder shapes are possible. Recently, girders have been designed with a wide top flange, narrow web and a large lower flange. These girders are commonly referred to as Bulb-T girders.

The Florida Department of Transportation developed the Florida Bulb-T in the early 1980s. The Eau Gallie Bridge was the first bridge that was built with the Florida Bulb-T. The Eau Gallie Bridge had 145 foot spans and was completed in 1990. Since the successful use of the Florida BulbT in the Eau Gallie Bridge, the Bulb-T girder has been a popular design choice in Florida. The girder is pretensioned in the casting yard so that it can support its self weight during transportation and erection. The girders typically have three ducts to allow for post-tensioning. Each duct generally has between nine and twelve 0.6" diameter post-tensioning strands. The post-tensioning is used to make the girder continuous over the supports, and to provide additional prestressing to support the weight of the slab and live loads.

Some small changes in the design and construction of Florida Bulb-T girders have been allowed by the FDOT. Recently, oval shaped post-tensioning ducts have been used instead of round ducts. The larger cross-sectional are of an oval duct allows more PT strands to be placed in a single duct without increasing the web thickness. In the Edison Bridge, the oval ducts were manufactured with high density polyethylene. Also in the Edison Bridge, the ducts had a curvature in both the longitudinal and transverse directions at the ends of the girder. During the post-tensioning of the girders, several cracks were observed in the web that followed the path of the post-tensioning ducts. A thorough examination of the stresses caused by the post-tensioning operations is necessary to understand why these cracks occurred, and to prevent future problems with Florida Bulb-T girders.

The post-tensioning process of a single duct can be simplified into the following sequence. The desired number of strands are fed through the ducts of the girders that will be made continuous. The strands are anchored at one end and tensioned at the other end using a hydraulic jack. The strands at the live end are then anchored, and the remaining amount of the prestressing force is applied to the other end. AASHTO and MOT require that the ducts be grouted soon after posttensioning.

The grout is pumped through the duct to seal and bond the strands. The grout is applied at the end of the continuous girder with the lowest elevation. This makes it less likely that air voids will be present in the ducts after grouting. A grouting pressure of 75 psi at the live end is often sufficient to seal the ducts. Several conditions may arise that require grouting pressures greater that 75 psi. The primary cause would be a blockage in the duct. Also bridges with a greater inclination will require greater pressures at the live end.
The stresses of interest in this study are oriented transverse to the length of the girder. The two dimensional cross-section of a Bulb-T girder shown in Figure l. l can be used to visualize the transverse stresses caused by post-tensioning operations. The strands that will be inside each duct have an upward component due to the parabolic trajectory of the duct and strand. Figure 1.2 shows the strands in the oval polyethylene duct with the upward force applied to each strand. This upward force will cause both upward and outward forces where the strands are touching the ducts. This mechanism will be referred to as strand wedging. Grouting pressure acts on the inner surface of the duct and will cause stresses in the concrete surrounding the duct. Figure 1.3 shows a grouting pressure applied to an oval polyethylene duct.

The effects of the grouting pressure, strand wedging, and type of duct will be thoroughly examined in this report. In addition several friction tests will be performed. A number of different ducts have been used in 72" Bulb-T girders. They include a round steel duct, oval steel duct, round polyethylene duct and oval polyethylene duct. These ducts will be examined in this paper. The ducts used in the analysis are shown in Figure 1.4. The effects of the duct shape will be distinguished from the effects of the duct material.

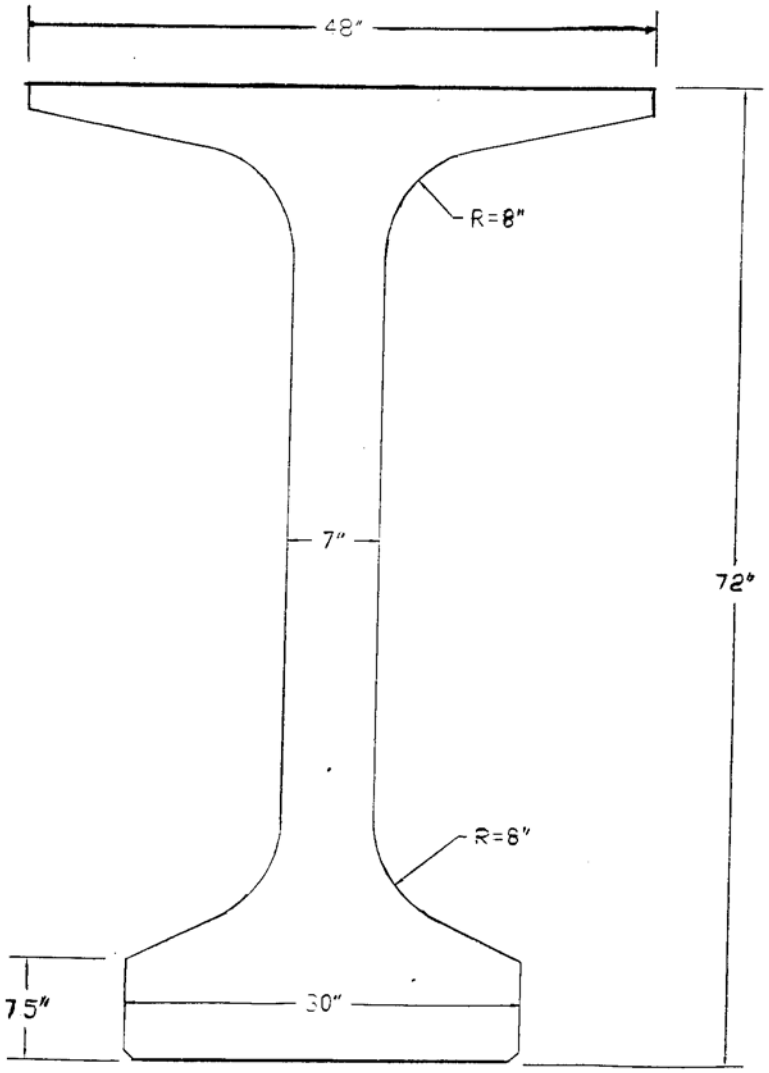

Figure 1.1 Cross Section of Florida Bulb-T Girder

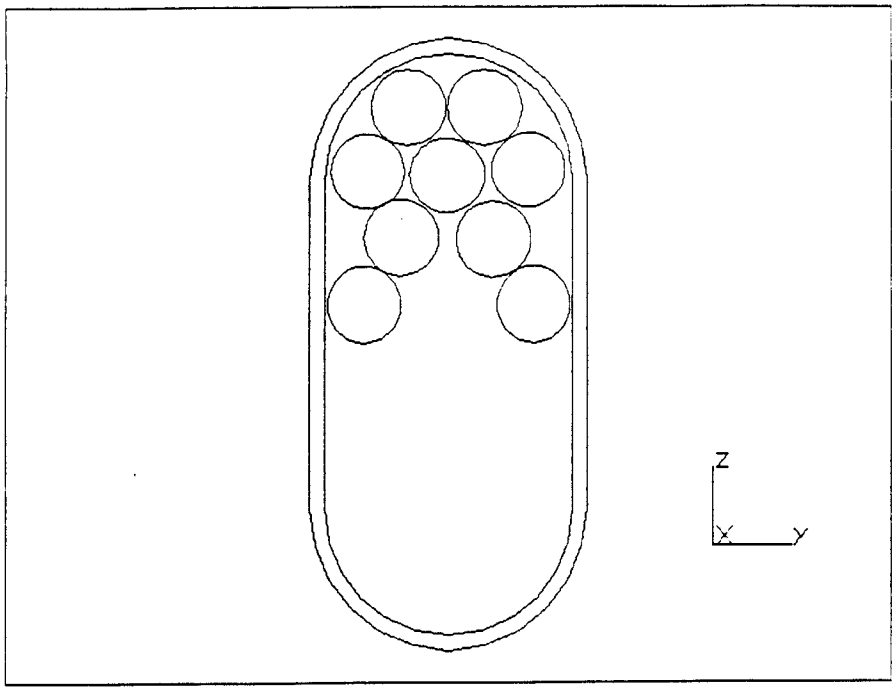

Figure 1.2 Post-Tensioning Strands in an Oval Polyethylene Duct

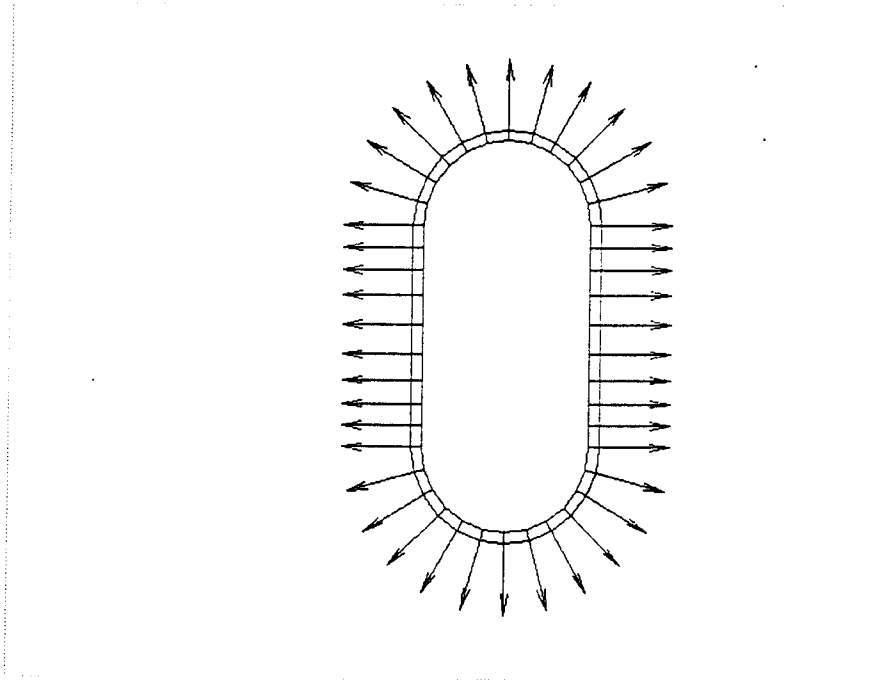

Figure 1.3 Grout Pressure Acting on an Oval Polyethylene Duct

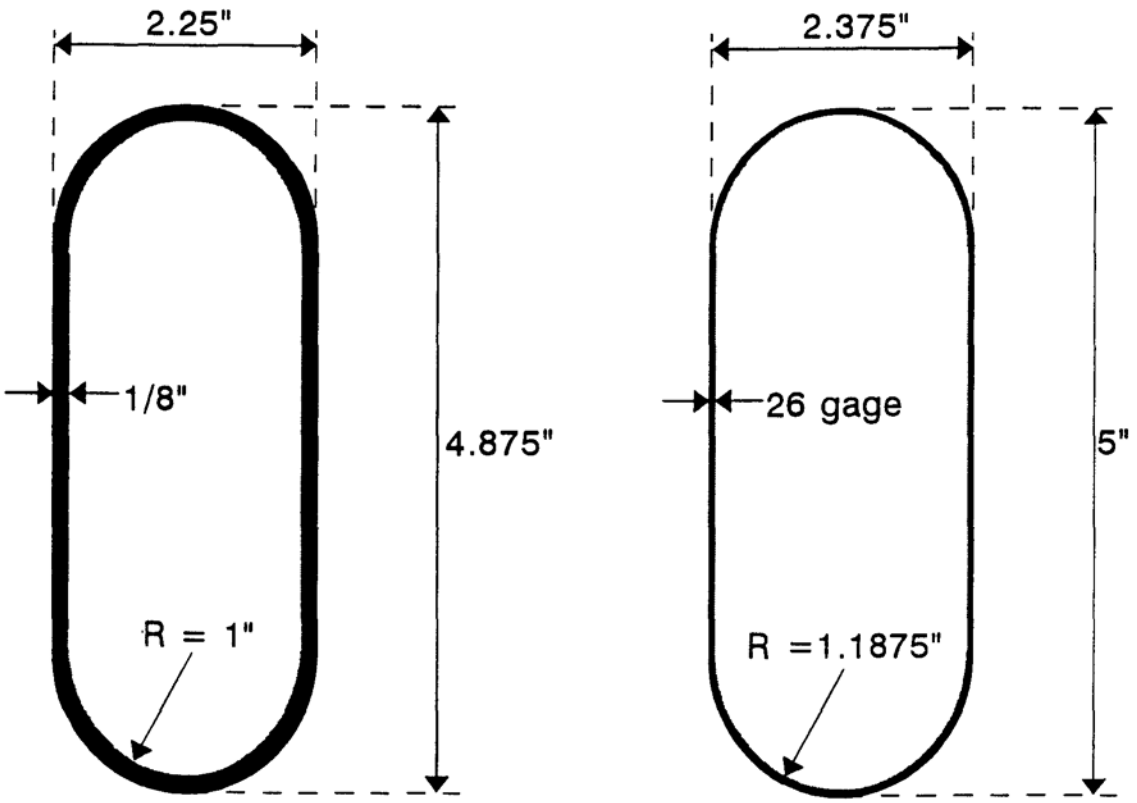

(a) Oval Polyethylene Duct

(b) Oval Steel Duct

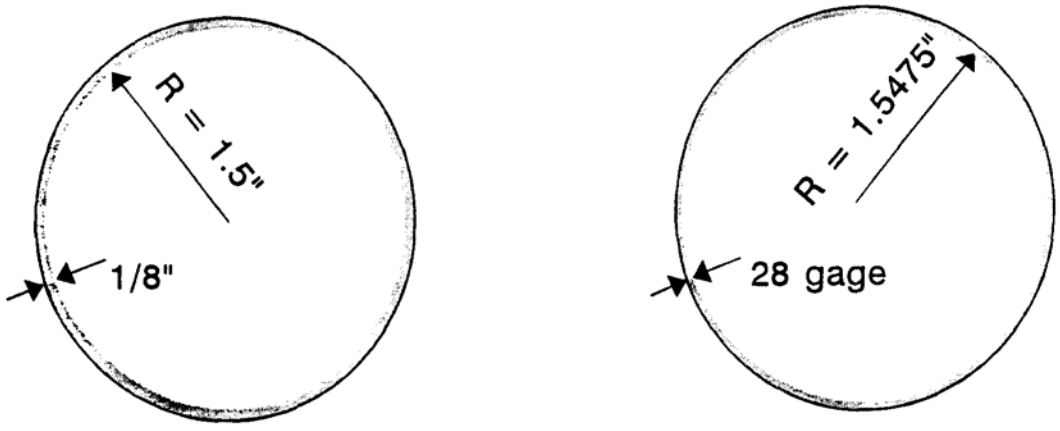

(c) Round Polyethyelene Duct

(d) Round Steel Duct

Figure 1.4 Ducts Used in Florida Bulb-Tee Girders

Chapter 2

Literature Review

2.1 1994 LRFD AASHTO Code

The current code discusses the effects of strand wedging, grouting of ducts and friction loss in post-tensioned girders. Section 5.10.4.3, entitled "Effects of Curved Tendons," discusses both in-plane force effects and out-of-plane force effects. Figure 2.1 shows the figure that is given in the code that illustrates the effects of out-of-plane forces. The in-plane force is given by equation 5.10.4.3.1-1 in the LRFD code and is shown below as equation 2-1.

$$F_{u\text{-}In} = \frac{P_u}{R} \qquad 2\text{-}1$$

$F_{u\text{-}in}$ = the in-plane deviation force effect per unit length of tendon (K/FT)

P_u = the factored tendon force (KIP)

R = the radius of curvature of the tendon at the considered location (FT)

In-plane forces will be most severe in regions of large curvature (small radius.) When several strands are in a single duct, the in-plane force acting on each strand will create out-of-plane forces. The out-of-plane forces are caused by the wedging of the strands against the duct wall. The code gives equation 5.10.4.3.2-1 to estimate the out-of-plane force effect. This equation is shown below as equation 2-2.

$$F_{u\text{-}out} = \frac{P_u}{\pi R} \qquad 2\text{-}2$$

$F_{u\text{-}out}$ = the out-of-plane deviation force effect per unit length of tendon (K/FT)

P_u = the factored tendon force (KIP)

R = the radius of curvature of the tendon in a vertical plane at the considered location

While the equation given to compute the in-plane force effects, equation 2-1, is valid for any curved tendon, the equation given to compute out-of plane force effects is an approximation. It is apparent when examining Figure 2.1 that the number of strands, shape of the duct and the strand orientation will affect the actual out-of-plane forces. The calculation of the out-of-plane forces will be thoroughly examined in chapter 3.

Section 5.4.6 of the LRFD code is entitled "Ducts." This section of the code discusses the minimum radius of curvature and cross-sectional areas of polyethylene and galvanized ducts. The only limitation on the use of polyethylene ducts is that they should not be used in areas where the radius of curvature is less that 30.0 feet. In section 5.4.6.1, the code states that "The effects of grouting pressure on the ducts and the surrounding concrete shall be investigated."

Section 5.9.5.2.2 of the LRFD code discusses the friction between the duct wall and the prestressing tendons. Equation 5.9.5.2.2b-1 is given to compute the friction loss. This equation is shown below as equation 2-4.

$$\Delta f_{pF} = f_{pj}(I - e^{(Kx+\mu\alpha)} \qquad 2\text{-}4$$

Δf_{Pf} = loss in prestressing steel stress due to friction (KSI)

Δf_{pj} = stress m the prestressing steel at jacking (KSI)

K = wobble friction coefficient (FT"')

μ = coefficient of friction (1 /RAD)

α = sum of the absolute values of angular change of prestressing steel path from jacking end, or from the nearest jacking end if tensioning is done evenly at both ends, to the point under investigation (RAD)

The code states that experimental values of K and g should be used. However, the code gives a table of values if experimental results are not available. This table is shown as Table 2.1 in this report.

2.2 1993 FDOT Investigation of the Edison Bridge

An experimental investigation was conducted by Dr. Moussa Issa of the Florida Department

of Transportation/Structural Research Center (FDOT/SRC) to investigate cracking in the Edison bridge. Unit two south was the last unit to be constructed in the south bound of the Edison bridge. Girders four and five of span two south were chosen for the experimental program. In addition, the Structural Research Center decided to investigate a girder that cracked during the first stage of posttensioning unit three south. Girder four, of span six south was the cracked girder. The objectives of this experimental program were to study the effect of grouting pressure and evaluate the bursting stress in the Bulb-Tee web during post-tensioning. In addition, any crack development during the construction process was monitored along with the crack width and propagation with time after the first stage of post-tensioning.

Embedded vibrating wire and electric resistance strain gauges were used to monitor strain and temperature changes. These strain gauges were used to monitor the state of stress in the web during the first and second stages of post-tensioning and grouting of the ducts. Besides these gauges, surface strain gauges were used across the crack to measure the cracks during the remaining stages of construction. A data acquisition system was used to continuously monitor and store the data collected c om the vibwing wire gauges at a preset time. In addition, a high speed system was used to collect the data obtained from the embedded electric resistance strain gauges.

The effects of grouting pressure in the ducts were determined for two models, one Bulb-Tee girder with an oval duct and the other with a round duct. The round duct maximum tension stresses were approximately half those for the oval duct (180 psi and 373 psi, respectively). A pumping pressure of 125 psig is common to inject grout in the field. The analytical model predicted a limit of 150 psig. However, field observations show a grouting pressure ranging between 50 to 130 psig. Analytically predicted transverse tension stresses compared favorably with the experimental stresses (150 to 140 psi, respectively). These typical comparisons were made one inch .away from the tip of the duct.

Cracks appeared during the first and second stages of post-tensioning. Most of these cracks were hairline cracks that developed near the transition zone and the web. Crack widths were between 0.003 and 0.001 in. and less. A five foot long crack developed during the first stage of posttensioning twenty feet from the end of the beam before grouting girder five (Unit 2S-Span 2S). This crack developed along the trajectory of tendon two. There were no cracks at the top of duct three.

During the grouting of girder four (Unit 3S-Span 6S), the cracks increased by 0.0018 in. in the transverse direction of the web. Also, water leakage was observed from a crack that developed during the second stage of post-tensioning tendon three. The American Concrete Institute (ACI) recommends permissible crack widths in reinforced concrete structures of 0.016 in. for interior exposure and 0.013 in. for exterior exposure. However, the Bulb-Tee girders developed longitudinal hairline cracks along the post-tensioning ducts. Five girders suffered severe longitudinal cracks and web spalling during the construction of the bridge.

The experimental results from two weeks of data collection after the second stage of post tensioning revealed that the cracks did not propagate or increase in width.

Based on the experimental investigation, and from field observations, the following conclusions were drawn by Dr. Issa:

l. The analytical model indicated that the bursting stresses in the oval duct are approximately twice those in the round duct under the same loading conditions. More research or test data is required before changing into the three round metal duct system.

2. It was observed in the field that 75 psig is sufficient to accomplish grouting. Also, an average maximum pressure of 125 psig was observed in the field for units 2S and 3S.

3. The orientation of tendons one and two and the wedging action of the strands in the ducts created a lateral splitting force in the transition zone and the web.

4. It is possible that some of the cracks developed internally in the precast yard during the pulling of the steel "rabbit" through the duct. Field personnel reported that the steel "rabbit" could not be pulled easily through some ducts. This was possible due to a closing of the polyethylene duct. These internal splitting cracks will propagate from the tips of the oval duct to the surface, during the post-tensioning of the tendons.

5. The placement and orientation of tendons one and two, side by side at the end, and their 3-D (space) trajectories in the end zone created a horizontal (transverse) splitting force. The transition zone and the web were not designed for such a force. It is very difficult for construction workers to install and locate the ducts in the end zone.

6. The possible variation of crack intensity and location depends on the splitting force and the tendon sharp curvature in the end blocks.

7. The experimental results showed an average transverse strain of 32 ps (stress = 140 psi) at an average grouting pressure of 100 psig.
8. The analytical model stress of 150 psi matches very well with the experimental stress of 140 psi for the same location at 100 psig simulated grout pressure.
9. An average transverse strain in the web after the second stage of post-tensioning was 125 μs (stress = 550 psi) along the three tendons.
10. The high cracking strains (>150 μs) were a result of the deformed duct shape after casting and/or the location of the duct or a combination of both. This conclusion was made because high strains and cracks were seen randomly at different sections and along the tendons. Sometimes these cracks develop in the web of the girder and propagate along the tendon toward the transition zone or toward the middle of the girder.
11. Field inspectors mentioned that fair amounts of ducts were reduced to a minimum dimension of $1\pm^{1}/4$ in. (steel "Rabbit" thickness = lf'/4 in.). For this shape, the "rabbit" could cause internal web splitting cracks between the girder ducts at the casting yard.
12. The problems of bug holes were related to the improper and/or nonuniform compaction of the concrete. This was a conclusion by the State Materials Office.
13. Based on the analytical model, round duct tension stress were about half the tension stresses of the oval duct.
14. The maximum temperature (100°F) occurred between 10 and 11 AM, and the minimum temperature(80°F) occurred between 6 and 7 AM.
15. During the grouting of girder four (unit 3S, span 6S), the crack at section one increased by 0.0018 in. in the transverse direction (Splitting crack).
16. Concrete Admixtures can be used to ease the placement of concrete in sections congested with reinforcing steel.
17. An average transverse strain of 60 gs (stress=264 psi) was recorded along tendons one and two during the first stage of post-tensioning.
18. For uncracked sections, an average of 125 gs (stress=550 psi) was recorded due to the first and second stages of post-tensioning, deck weigh and composite action along the tendons at different sections.

19. An average thermal strain of ±30 gs was observed cycling accordingly with the concrete and external temperature. After placing concrete for the deck, the strain variation was about t17 gs and then stabilized.
20. During the second stage of post-tensioning, at 15 feet from the end of girder 4 (unit 3 S, span 6S) the transverse (splitting) crack in the web between tendons two and three was 0.0066 in. While the other surface cracks along tendons one and two were stable and did not propagate. A maximum crack width of 0.0002 in. was observed.
21. The splitting force from bearing of the curved tendons, and the transverse force from the wedging action of the strands were the most probable cause for the girder cracking. 22. Tendon elongation is affected by the variation of the force due to the friction losses along the tendon length. Friction losses should be considered in translating tendon elongation measurements into tendon forces. The elongation measurement provides a measure of the average force along the length of the tendon, whereas the gauge pressure gives the force in the tendon at the anchorage. That is why the 90% stressed girder end was developing cracks in that girder only near the transition zone.

Based on the experimental investigation, and from field observations, the following recommendations were suggested by Dr. Issa:

1. Limit the grout pressure to 150 psig (Analytical model supported by experimental results).
2. Stop the use of polyethylene ducts. Use metal round/oval ducts instead(preferably round metal duct).
3. Provide transverse confinement steel to control bursting cracks near the transition zone and web. This will help in confining the bottom two tendons.
4. Increase the transition zone of the end girders by three feet.
5. It is recommended to obtain concrete core samples from the cracked girders and two of the instrumented girders to check for any interior splitting cracks.
6. Concrete admixtures can be used to ease the placement of concrete in sections congested with reinforcing steel.
7. It is recommended to pull (stress) the tendons for 50% of the iackina load from hnth ends

Use this method for the first and second stages of post-tensioning. This method of symmetrical stressing of the tendons will reduce the high concentrated stresses at the jacking end girders.

8. Consider using internal vibrators when external vibrators are not fully effective. Formation of bug holes and internal voids between ducts is due to insufficient compaction energy. Recommendation by State Materials Office.
9. Model the bulb-tee by using a non-linear finite element analysis model.
10. Further research to study the effect of grouting, post-tensioning, duct size and shape for the Florida Bulb-Tee

Type of Tendons and Sheathing	Wobble Coefficient, K (1/FT)	Curvature Coefficient, μ (1/RAD)
Tendons in rigid and semi-rigid galvanized ducts - 7-wire strands	0.0002	0.05-0.25
Pre-greased tendons - wires and 7-wire strands	0.0003-0.0020	0.05-0.15
Mastic-coated tendons - wires and 7-wire strands	0.0010-0.0020	0.05-0.15
Rigid steel pipe deviators	0.0002	0.25 Lubrication probably required

Table 2.1 Wobble and Curvature Coefficients from 1994 LRFD AASHTO

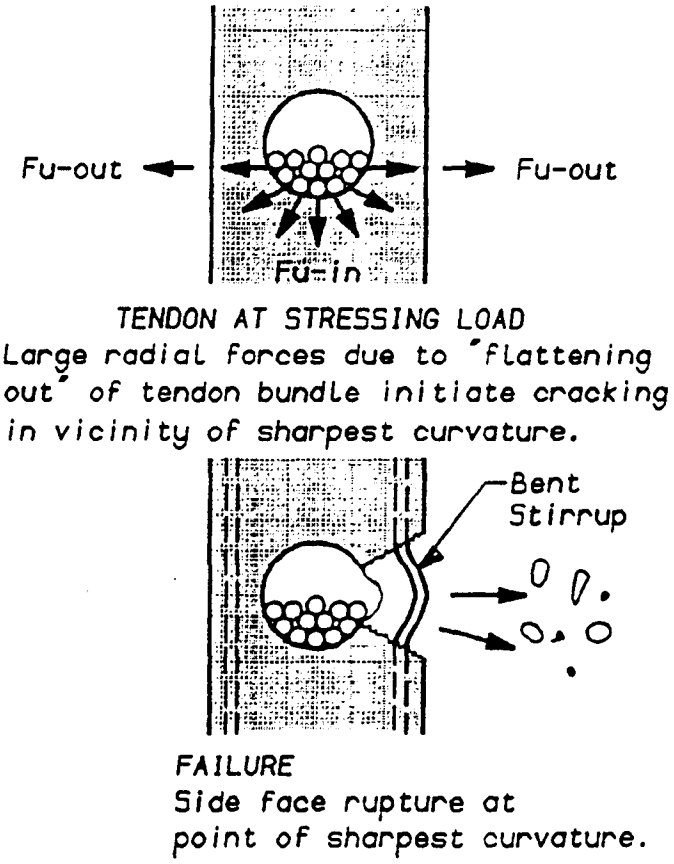

Figure C5.10.4.3.2-1 - Effects of Out-of-Plane Forces

Figure 2.1 Effects of Out-of-Plane Forces

Chapter 3
Computer Modeling

3.1 General

The testing program consisted of two full-scale Bulb-T girders and a number of finite element models. More than 100 finite element models were analyzed in order to examine the stresses in the concrete web caused by the post-tensioning operations. The results from the field tests will be used to examine the accuracy of the finite element models. One of the full-scale girders will be manufactured with oval steel ducts and the remaining girder will be manufactured with round steel ducts.

A finite element analysis package called Algor was used to model the Bulb-T. The computer model was built using specific details of the test girders. The properties of the materials and loading conditions must be defined before a finite element analysis can be started. Finite element models will assume all materials are honuogenerxus and isotropic. Models will be analyzed with a linear concrete stress-strain relationship and a non-linear stress-strain relationship. The primary forces acting on the duct during post-tensioning, in the two-dimensional models, are caused by strand wedging and grouting pressure. The magnitude and location of these forces must be quantified prior to building the model. A standard coordinate system will be used for all of the two and three-dimensional finite element models. Two-dimensional models will be built in the y-z plane. Z will be the vertical direction and y will be the horizontal direction. The x direction will be along the length of the girder.

3.2 Calculation of Wedging Forces

The upward force on each strand at any point can be calculated knowing the prestressing force and curvature at that point. The curvature at any point can be determined knowing the parabolic equation expressing the height of the strand as a function of the distance along the girder. If the parabolic equation is f(x) then the curvature at any point is given by equation 3-1.

$$K(x) = \frac{f''(x)}{\left(1 + (f'(x)^2\right)^{3/2}} \qquad (3\text{-}1)$$

The upward force caused by the prestressing force, P, and curvature, K(x) is given by the equation 3-2.

$$F(x) = P\text{-}K(x) \qquad (3\text{-}2)$$

The upward force was calculated for the strands in each duct throughout the length of the test girders.

Given the upward force on each strand, and the strands orientation in relation to each other and the duct surface, the outward forces acting on the inner duct surface can be determined. For this analysis it was assumed that the strands were cylindrical with a 0.6" diameter. It was also assumed that adjacent strands touched each other at one tangent point. Any line that passes from the center of one circle (strand) to the center of an ***adjoining*** circle (strand) will' by definition pass through the tangent point of those two circles (strands.)

The wedging effect of the strands can best be modeled as a truss. Figure 3.1 shows a truss model for one of the test sections. For a given strand *orientation,* the center of each strand is connected to the center of adjacent strands through the tangent points. Similarly the strands touching the duct inner wall are connected to the tangent point with truss members that may only transmit axial forces. The *tangent* points connecting the strands and the duct inner wall are restrained for moving in any direction. These restraints are noted in the Figure by the symbol Tyz, (translation restrained in Y and Z directions.) The upward force is then applied to the center of each cylinder, and the truss can be solved. The results that are most important for this study are the reaction on the duct surface. These truss problems are easily solved using Algor finite element analysis software.

The orientation of the strands will affect the geometry of the truss and the reactions that act on the duct wall. There are an infinite number of strand orientations that may be present in the girders, and the strand orientation may change along the length of the girder. Several different orientations were examined for each duct. Each trial *orientation* was graphically determined so that

there was a minimal amount of free space in the top half of the ducts. The most severe orientation for each duct was used for the remainder of the study. Due to the different wall thicknesses and shapes, the orientations are different for each of the four ducts.

3.3 Calculation of Pressure Forces

The pressure acts on the inner surface of the duct in a direction normal to that surface. The total force caused by the pressure acting on the inner surface is given by the following equation:

$$F = P\text{-}SA \qquad (3\text{-}3)$$

F = total force (lbs)

P = pressure (psi)

SA = surface area (in^2)

For the two-dimensional model, the surface area is the circumference of the duct times the unit -thickness of one inch. Assuming the distance between each node is constant throughout the length of the duct's inner surface, the force acting on each node can be determined by the following equation:

$$F_n = \frac{F}{n} \qquad (3\text{-}4)$$

F„ = force acting on each node (lbs)

F = total force caused by pressure (pressure x surface area) (lbs)

n = number of nodes on the inner duct surface

3.4 Development of Non-linear concrete model

The non-linear stress strain curve for concrete was developed using relationships found from a number of different references. The method follows the technique used by Collins and Mitchell in their 1991 text. The general equation used to calculate the stress at any point, knowing the strain at that point and a number of other constants, was developed by Thorenfeldt, Tomaszewicz and Jensen

based on the work of Popovics. This equation is shown below as equation 3-5.

$$f_c = \frac{\frac{f'_c \cdot n \cdot \epsilon_{cf}}{\epsilon'_c}}{n - 1 + (\frac{\epsilon_{cf}}{\epsilon'_c})^{nk}} \qquad (3\text{-}5)$$

where:

$$n = \frac{E_c}{(E_c - E'_c)} \qquad (3\text{-}6)$$

$$E'_c = \frac{f'_c}{\epsilon'_c} \qquad (3\text{-}7)$$

f_c = stress corresponding to strain, ϵ_{cf}

f'_c = peak stress obtained from a cylinder test

ϵ_{cf} = strain at a given point

ϵ'_c = strain at maximum stress, f'_c

E_c = tangent stiffness when ϵ_{cf} equals zero

k = factor to increase the postpeak decay in stress, taken as 1.0 for $(\epsilon_{cf}/\epsilon'_c)$ less than 1.0 and as a number greater then 1.0 for $(\epsilon_{cf}/\epsilon'_c)$ greater then 1.0

The design strength of the test specimens was 6,000 psi, which is typical for Bulb-T girders. The initial concrete tangent stiffness was found from equation 3-8.

$$E_c = \omega_c^{1.5} \cdot 33 \cdot \sqrt{f'_c} \qquad (3\text{-}8)$$

Collins and Mitchell recommend equation 3-9 to determine n.

$$n = 0.8 + \frac{f'_c}{2{,}500} \qquad (3\text{-}9)$$

A compressive strength of 6,000 psi results in a value of 3.2 for n.

$$n = \frac{E_c}{(E_c - E'_c)} \qquad (3\text{-}6)$$

$$E'_c = \frac{f'_c}{\epsilon'_c} \qquad (3\text{-}7)$$

Knowing the compressive strength and n, Equations 3-6 and 3-7 can be combined to give the expression for the maximum strain, ϵ'_c, shown in equation 3-10.

$$\epsilon'_c = \frac{f'_c}{(E_c - \frac{E_c}{n})} \qquad (3\text{-}10)$$

The decay factor, k, increases with increased compressive strength. Collins and Mitchell suggest the following equation to determine k based on the compressive strength.

$$k = 0.67 + \frac{f'_c}{9{,}000} \qquad (3\text{-}11)$$

Using a compressive strength of 6,000 psi, k is found to be 1.34.

All of the values obtained in this section are then substituted into equation 3-5 and a numbe of points are obtained that are used to plot the stress strain curve for concrete. Figure 3.2 shows the

plotted stress strain curve.

The shear modulus (G), bulk modulus (K) and volumetric strain (ev) are needed at a number of different stress values to fully define the nonlinear behavior. These values can be obtained knowing Young's Modulus and Poisson's Ratio using the following relationships.

$$G = \frac{E}{2(1 + \upsilon)} \qquad (3\text{-}12)$$

$$K = \frac{E}{3(1 - 2\upsilon)} \qquad (3\text{-}13)$$

$$\upsilon_t = \upsilon_x + \upsilon_y + \upsilon_z \qquad (3\text{-}14)$$

Young's Modulus can be determined at any strain by taking the citrivative of equation 3-5 with respect to strain. The derivative can be determined by using a log transform on the expression. The resulting relationship is shown below in equation 3-15.

$$E = \frac{d_\sigma}{d_\epsilon} = e^{\ln\left(\frac{f'_c \cdot n \cdot \epsilon_{cf}}{\epsilon'_c}\right) - \ln\left(n - 1 + \left(\frac{\epsilon_{cf}}{\epsilon'^{nk}_c}\right)\right)} \cdot \left(\frac{1}{\epsilon_{cf}} - \left(\frac{1}{n - 1 + \left(\frac{\epsilon_{cf}}{\epsilon'_c}\right)^{nK}}\right) \cdot \left(\frac{nk(\epsilon^{nk - 1})}{\epsilon'^{nk}_c}\right)\right)$$

3-15

Poisson's ratio for concrete increases as stress increases. The relationship shown in Figure 3.3 was used for the analysis. This Figure shows Poisson's ratio to be constant until the stress/strength ratio exceeds 80%.

The relationships presented in this section were used to create a table with all of the various properties at numerous locations on the nonlinear concrete stress strain curve. These results are

shown in Table 3.1. Figure 3.4 shows a plot of stress vs shear modulus and Figure 3.5 shows a plot of stress vs bulk modulus for 6,000 psi concrete. Young's modulus was taken as 4,100,000 psi in the linear finite element models.

3.5 Two-Dimensional Finite Element Pressure Models

A two dimensional finite element model was used to examine the stresses caused by grout pressure in the post-tensioning process. The effects of pressure were examined independently from all other loads. Models were examined for each of the four duct types: oval polyethylene, oval steel, round polyethylene and round steel which will be further referred to as OP, OS, RP and RS respectively. Four different grouting pressures were studied: 75 psi, 100 psi, 125 psi and 150 psi. Table 3.2 shows the abbreviations used to distinguish between different models. In this table the model name appears in the left column. The additional five columns show which characteristics define the model.

Algor finite element analysis software was used to build the models and perform the analysis. Algcor's automatic mesh generation was. used to establish a mesh of approximately 1,200 elements in the girder. In addition, approximately 30 elements were generated in the cross-section of the duct. The nonlinear concrete model developed in section 3.1.3 was used in the non-linear analysis. Figure 3.6 shows the mesh for the models with oval ducts. Figure 3.7 shows the mesh for the models with round ducts.

The forces caused by the pressure were then applied on each node acting in a direction normal to the surface. Finally the model had to be restrained before the resulting stresses could be determined. There are a number of different ways that the model can be restrained. Rigid supports, elastic "spring" supports, truss elements or any combination can be used. For these two-dimensional pressure models the forces caused by the pressure were symmetrical in all directions, and the resultant force equals zero. Because the pressure does not cause a resultant force that is resisted by the boundary conditions, the location and type of boundary conditions has little effect on the stresses caused by the pressure. The bottom of the girder was restrained by rigid supports in the Z direction on the lower flange, two elements on the side of the lower flange were restrained with rigid supports in the Y direction.

3.6 Two-Dimensional Finite Element Models Including Strand Wedging

The same two dimensional mesh was used for models that included strand wedging. The truss models described in section 3.1.1 were solved to determine the forces that should be applied to the inner duct wall to simulate the strand wedging. These forces had horizontal and vertical components. The sum of the horizontal forces acting on one side of the duct equals the sum of the horizontal forces acting the opposite side of the duct. Therefore the sum of the horizontal forces in each duct equals to zero. Since the wedging forces are transmitted to the concrete on each side of the duct, there is no effect on the boundary conditions due to the horizontal forces. However, the vertical components of the forces have a significant effect on the boundary conditions.

The vertical forces have a resultant upward force equal to the vertical force applied to the strands. For example if duct 1 has 9 strands, and each strand has an applied upward force of 100 lbs., the sum of the vertical reactions acting on the duct will equal 900 lbs.. The boundary conditions that restrain the model must then resist this 900 lbs. upward force. Errors with the two dimensional models arise when resultant upward forces are restrained by boundary elements.

For example, consider a model that ham three ducts with nine strands in each duct. Also, each strand has an upward force of 100 lbs., and the model is restrained on the bottom flange. The effects of the boundary conditions can be seen by examining free body diagrams made by cutting the model beneath each of the three ducts. If the model is cut beneath the top duct then it can be seen that the concrete beneath the top duct must resist 900 lbs. of upward force. If the model is cut beneath the middle duct then it can be seen that the concrete beneath the middle duct must resist an upward force of 1,800 lbs. Likewise the concrete beneath the third duct must resist and upward force of 2,700 lbs.. Therefore, the stresses in the web will decrease with height. If the model was restrained on the top flange then the stresses would increase with height. Thus, the boundary conditions will have a significant impact on the resulting stresses in the web. In a three-dimensional model or in actual filed conditions, the upward forces would be resisted by the self weight and applied loads. Therefore the two-dimensional model will not be used to model the vertical components of the forces. The two-dimensional model will be used to examine stresses caused by the horizontal wedging forces and grouting pressure. The three dimensional model will examine the effects of the vertical components of the wedging forces, and other stresses caused by applied loads.

3.7 Three Dimensional Finite Element Models

A three dimensional finite element model was developed to evaluate the stresses that will act on an actual field girders. However, it is not possible to model all of the stresses acting on the girder in one three dimensional model. The three dimensional model developed for this project will examine the stresses in the Bulb-T caused by self weight, applied loads, pretensioning and post-tensioning forces. Using a personal computer, it was not possible to build a model that contained posttensioning ducts with a parabolic profile. Therefore, the effects of strand wedging and grouting pressure were not considered in the three dimensional model. However, the effects of wedging and grout pressure from the two-dimensional models can be added to the results from the threedimensional model to gain a complete view of the stresses in actual Bulb-T girders.

3.7.1 Three Dimensional Bulb-T Models

The parabolic shape of each duct was approximated as a series of segments in the model. The segments were connected to nodes at their joints. The software then treated the connected segments as truss elements. There was a concrete section, group of rodes in the pi;me perpendicular t:; the length, for every two feet of length throughout the length of the girder. At each of these sections the vertical node spacing was approximately four inches. Thus, it was possible to connect the truss elements every two feet along the length of the girder, the truss could be connected to any of a number of nodes spaced about four inches apart vertically. All of the nodes where the truss elements were connected were located along the centerline of the girder so that only the vertical eccentricity changed. Figures 3.8 shows a three dimensional solid model with the end block, transition zone and interior sections.

Approximating the parabolic tendon profile as straight segments can result in a good overall model if the model is developed carefully. Errors in modeling are most likely to be created at joints where the truss elements change direction. Consider the section of the girder from the end block to the center of a simply supported girder. The strands will be at the top of girder near the end block and will drop to the maximum eccentricity before the center of the girder. Throughout this parabolic shape the curvature will be upward. This curvature will cause stresses acting upwards towards the center along the curved portion of the tendons. The calculation of these stresses was described in

detail in section 3.1.1. The truss model must be carefully developed so that at all of the joints, there is an upward curvature. If there is a downward curvature then errors in the model will occur.

Model Name	Oval (0) or Round (R)	Table 3.2 Symbols Polyethelyne (P) or Steel (S)	Used in Finite Element Models Linear Concrete E (LC) or Non-linear Concrete E (NC)	Strand Wedging (S if present)	Pressure Magnitude 75 psi = P1 100 psi = P2 125 psi = P3 150 si =. P4
OPLCPI	0	P	LC		P1
OPLCP2	0	P	LC		P2
OPLCP3	0	P	LC		P3
OPLCP4	0	P	LC		P4
OPNCPI	0	P	NC	-	P1
OPNCP2	0	P	NC		P2
OPNCP3	0	P	NC		P3
OPNCP4	0	P	NC		P4
OPLCSP	0	P	LC	S	P1
OPLCSP	0	P	LC	S	P2
OPLCSP	0	P	LC	S	P3
OPLCSP	0	P	LC	S	P4
OSLCPI	0	S	LC		P1
OSLCP2	0	S	LC		P2
OSLCP3	0	S	LC		P3
OSLCP4	0	S	LC		P4
OSNCP1	0	S	NC		P1
OSNCP2	0	S	NC		P2
OSNCP3	0	S	NC		P3
OSNCP4	0	S	NC		P4
OSLCSP	0	S	LC	S	P1
OSLCSP	0	S	LC	S	P2
OSLCSP	0	S	LC	S	P3
OSLCSP	0	S	LC	S	P4
RPLCP1	R	P	LC		P1
RPLCP2	R	P	LC		P2
RPLCP3	R	P	LC		P3
RPLCP4	R	P	LC		P4
RPNCP1	R	P	NC		P1
RPNCP2	R	P	NC		P2
RPNCP3	R	P	NC		P3
RPNCP4	R	P	NC		P4
RPLCSP	R	P	LC	S	P1
RPLCSP	R	P	LC	S	P2
RPLCSP	R	P	LC	S	P3
RPLCSP	R	P	LC	S	P4
RSLCPI	R	S	LC		P1
RSLCP2	R	S	LC		P2
RSLCP3	R	S	LC		P3
RSLCP4	R	S	LC		P4
RSNCP1	R	S	NC		P1
RSNCP2	R	S	NC		P2
RSNCP3	R	S	NC		P3
RSNCP4	R	S	NC		P4
RSLCSP	R	S	LC	S	P1
RSLCSP	R	S	LC	S	P2
RSLCSP	R	S	LC	S	P3
RSLCSP	R	S	LC	S	P4

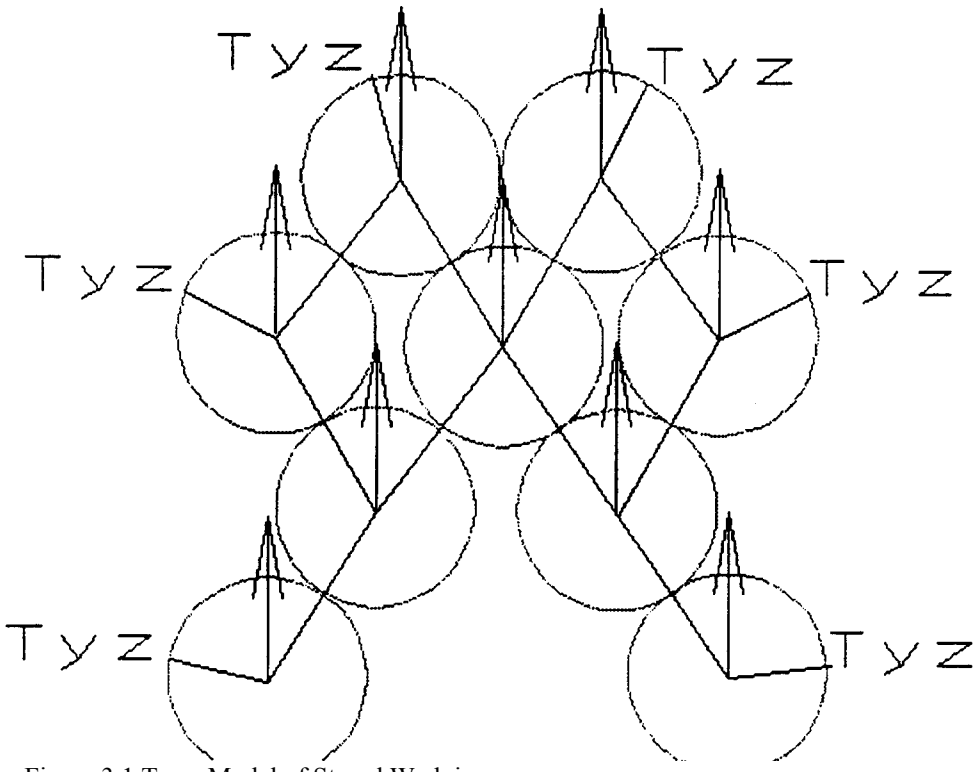

Figure 3.1 Truss Model of Strand Wedging

Table 3.1 Non-Linear Concrete Model

f C	(compressive strength)	= 6,000
n	(curve fitting factor)	= 3.2
e'C	(strain at max stress)	= 0.002129
EO	(tangent stiffness at 0 strain)	= 4,098,386

Stress (psi)	Strain (%)	Young's Modulus (psi)	Poisson's Ratio (%)	Volumetric Strain (%)	Shear Modulus (psi)	Bulk Modulus (psi)
0	0	4,098,386				
1,024	0.00025	4,090,145	0.190	0.0003	1,718,548	2,199,003
2,040	0.00050	4,023,167	0.190	0.0007	1,690,406	2,162,993
3,025	0.00075	3,828,637	0.190	0.0010	1,608,671	2,058,407
3,939	0.00100	3,448,713	0.190	0.0014	1,449,039	1,854,147
4,732	0.00125	2,860,761	0.197	0.0017	1,195,271	1,572,020
5,354	0.00150	2,095,954	0.233	0.0022	849,941	1,308,336
5,772	0.00175	1,237,830	0.300	0.0028	476,088	1,031,525
5,975	0.00200	395,935	0.300	0.0032	152,283	329,946
5,854	0.00225	(1,462,269)	0.300	0.0036	(562,411)	(1,218,558)
5,385	0.00250	(2,217,252)	0.300	0.0040	(852,789)	(1,847,710)
4,781	0.00275	(2, 543, 241)	0.300	0.0044	(978,170)	(2,119, 368)
4,141	0.00300	(2,535,294)	0.300	0.0048	(975,113)	(2,112,745)
3,530	0.00325	(2,328,495)	0.300	0.0052	(895,575)	(1,940,413)
2,984	0.00350	(2,035,445)	0.300	0.0056	(782,863)	(1,696,204)
2,514	0.00375	(1,727,837)	0.300	0.0060	(664,553)	(1,439,864)
2,118	0.00400	(1,442,689)	0.300	0.0064	(554,880)	(1,202,241)

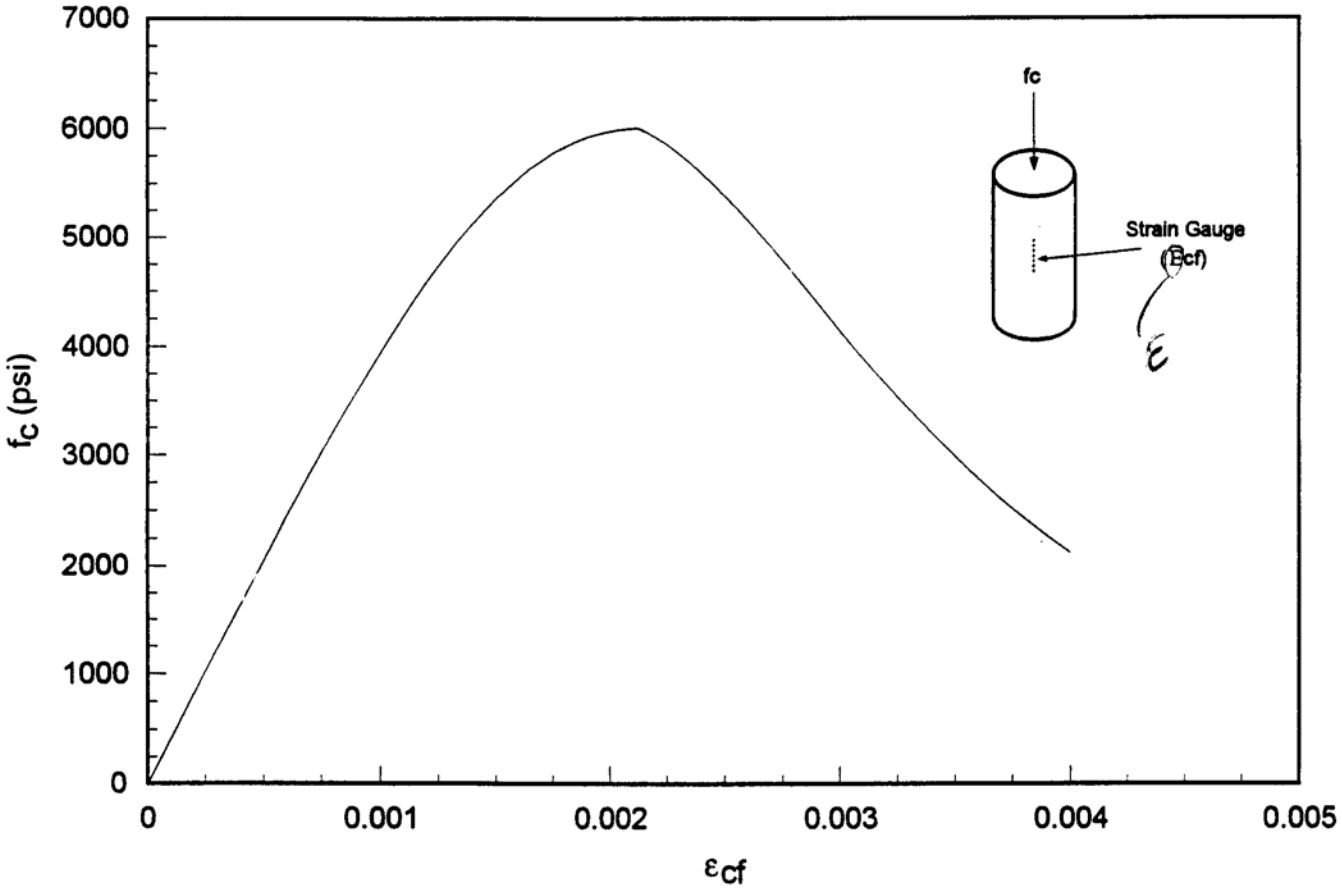

Figure 3.2 Non-Linear Concrete Stress Strain Relationship

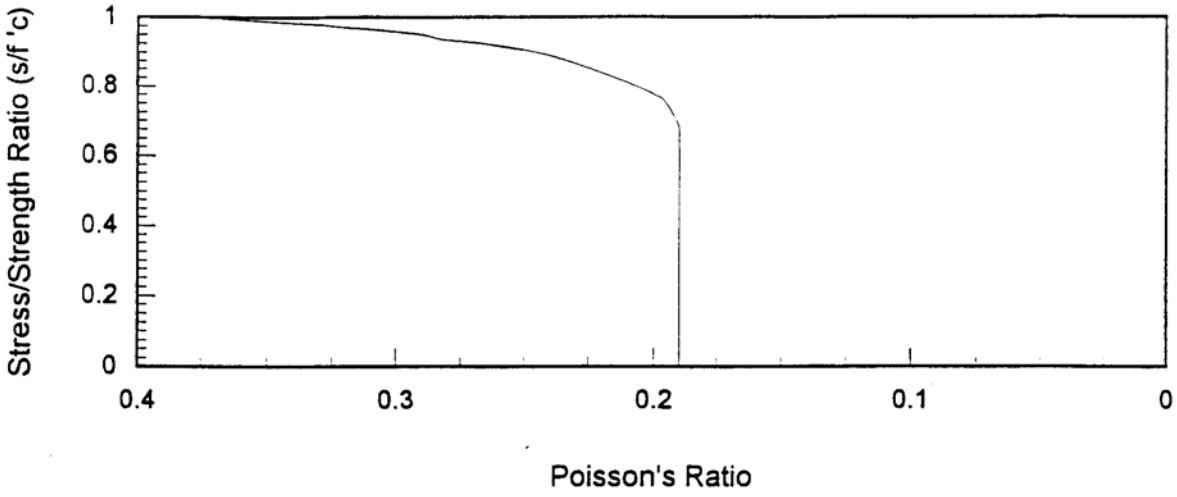

Figure 3.3 Relationship between Stress/Strength Ratio and Poisson's Ratio for 6,000 psi Concrete

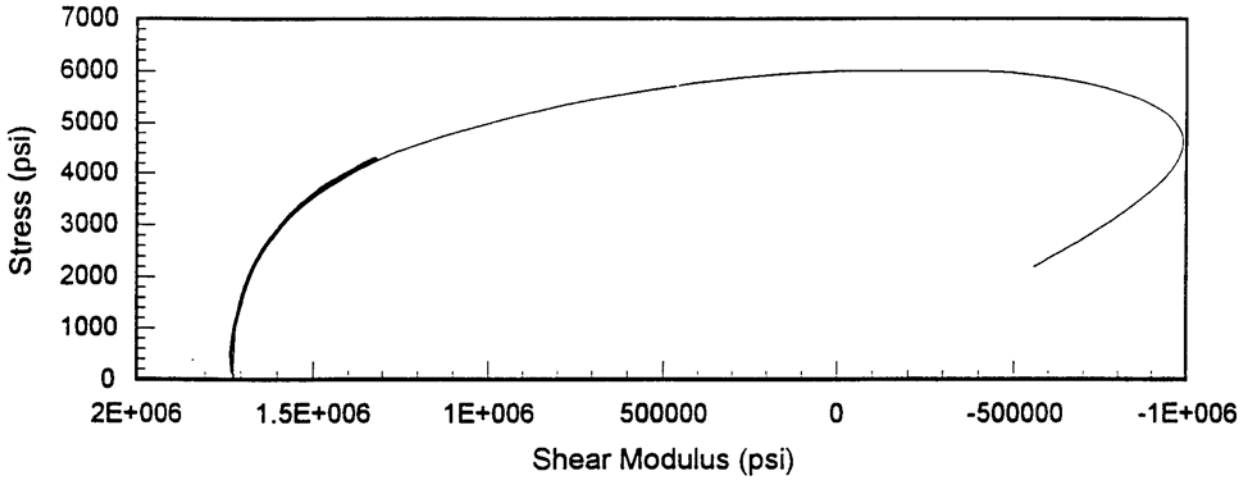

Figure 3.4 Stress vs Shear Modulus for 6,000 psi Concrete

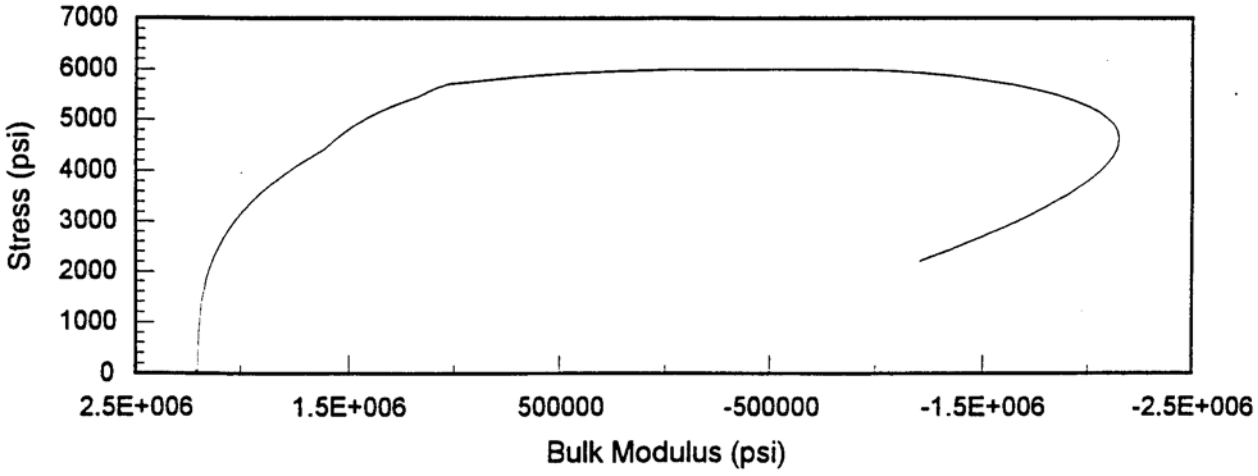

Figure 3.5 Stress vs Bulk Modulus for 6,000 psi Concrete

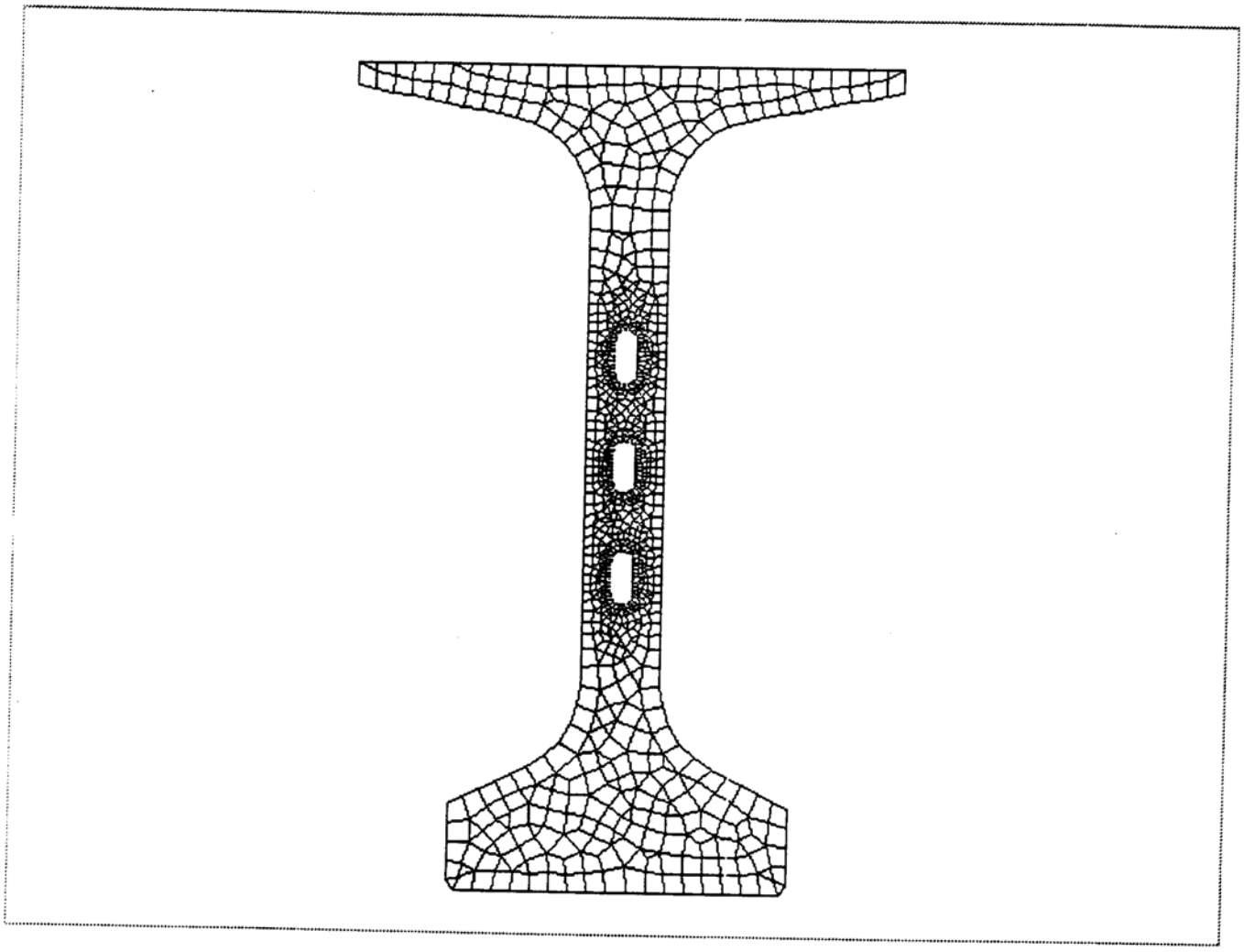

Figure 3.6 Two-Dimensional Mesh of Models with Oval Ducts

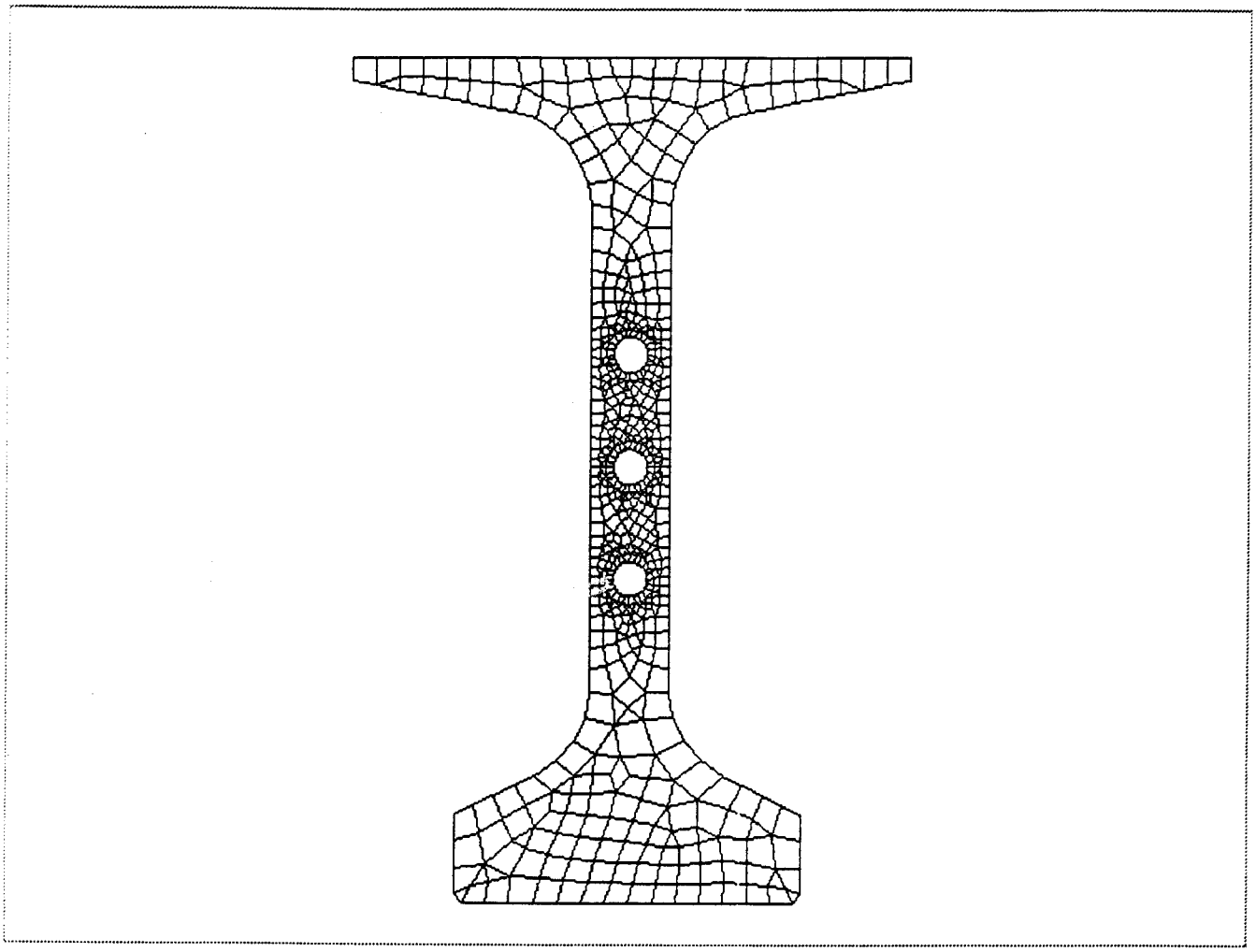

Figure 3.7 Two-Dimensional Mesh of Models with Round Ducts

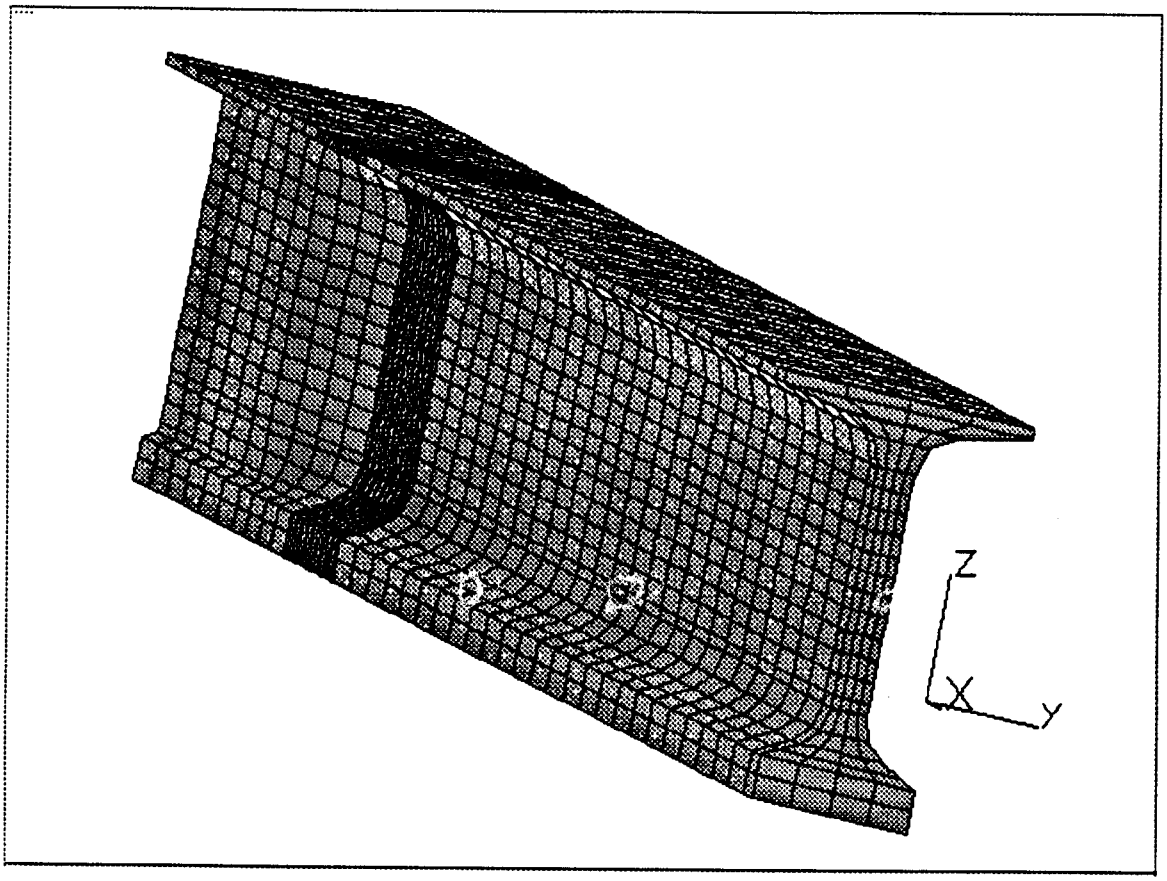

Figure 3.8 Three-Dimensional Bulb-T Finite Element Model

Chapter 4
Field Study

4.1 General

Full scale 72" Florida Bulb-T girders were manufactured, instrumented and tested. Each of the test girders were 75' long. The two 75' girders were post-tensioned together to form a twp span continuous beam. Each of the girders had three ducts, and nine 0.6" diameter strands were placed in each duct for post-tensioning. Typical end block sections for full scale girders will be used at the exterior ends of both girders. The interior section, end block section and transition zone of the Bulb-T girders are shown in Figures 4.1 to 4.3.

4.2 Design of Bulb-T Girders

The design of the test girders was performed following the 1994 LRFD AASHTO code. The prestressing reinforcement was designed to carry the self weight of the simply supported girder. A minimum amount of prestressing was desirable so that more post-tensioning could be performed before adding external loads. The post-tensioning ducts were located so that a maximum amount of post-tensioning force could be applied with a minimum amount external loads. This resulted in a duct profile with a lower eccentricity than would be typical in most Bulb-T girders. However, the duct curvature in the test girders was approximately equal to the curvature in field girders because the test girders were 75' long, compared with a typical length of approximately 150'. A trial and error design process was followed until a suitable duct profile was obtained. The location of the ducts is shown in Figure 4.4 and Table 4.1. Figure 4.4 also shows the Bulb-T test setup.

The final design uses twelve 0.5" prestressing strands to carry the shelf weight of the girder, and duct. The prestrssing reinforcement design is shown in Figure 4.5. The post-tensioning sequence will begin at the lowest duct and proceed to the top duct. After the strands in the lower two ducts are tensioned a uniformly distributed load of 1.2 kips per foot will be applied to the beam for slab dead load compensation. The strands in the top duct will then be tensioned.

The friction losses and elongations were calculated following the 1994 LRFD AASHTO

code, using a coefficient of friction, p, equal to 0.1. Table 4.2 shows the expected elongations during each stage of the post-tensioning process. Figures 4.6 to 4.8 show the expected tendon stress in each duct during each stage of post-tensioning.

Figures 4.9 and 4.10 show the end block and transition zone of one of the test girders prior to the placement of the forms and casting. Figure 4.11 shows the placement of the oval ducts in one of the test girders. Figure 4.12 shows the interior end of one of the test girders and figure 4.13 shows end block after casting.

4.3 Instrumentation of Test Girders

The test girders were instrumented with both internal and external gauges. A total of 57 internal gauges were placed in the two girders prior to the placement of the concrete. Forty-four external gauges were placed on the girder surface prior to testing. In addition, four deflection gauges were used to monitor camber and deflection.

The locations of the internal gauges were finalized after an extensive finite element analysis reveUed severer critical locations around the post-tensioning ducts. Four sections were chosen to be heavily instrumented, these sections are identified as sections A,B,C and D. One section at the end of the transition zone of each girder was instrumented (sections A and D.) In addition an additional section 4' closer to the center of the girder from the first section was instrumented (sections B and C.) The mid-span of each girder was instrumented with 5 external strain gauges. The mid-span locations are referred to as sections E and F. Figure 4.14 shows the locations of the instrumented sections on the girder with the oval ducts (sections A, B and E.) Figure 4.15 shows the locations of the instrumented sections on the girder with the round ducts (sections C, D and F.) The gauges were placed in areas of high stress caused by strand wedging and grouting pressure. The gauge labeling plan, denoting symbols used for gauge identification, is shown in Table 4.3. Figures 4.16 to 4.19 show the specific locations of the internal gauges at sections A, B, C and D, respectively. Figures 4.20 to 4.23 show the locations of the external gauges at the same sections. Figure 4.24 shows two of the internal gauges, secured with plastic cable ties, at section C prior to the concrete casting.

The gauges installed along the duct will be used to measure the strain on the duct surface. All of these gauges were installed on the lowest duct, duct 1. The locations of these gauges are

shown in Figures 4.25 and 4.26. Figure 4.27 shows one of the gauges applied to the round duct. Presumably the grout pressure will decrease as the distance from the grouting end increases. Ideally the strain gradient will be used to quantify the reduction in pressure. In addition to embedded and external surface gauges, deflection gauges will be installed at the center of each span.

4.4 Testing Procedure

The following testing procedure will be used to load the test girders. The girders have been cast as two simply supported 75' girders. One of the girders has oval ducts while the other girder has round ducts. The girders will be placed end to end to form a continuous two span 150' girder. The ducts over the interior support will be spliced together. A construction joint will then be poured between the interior ends of the girders. After the joint has cured, testing will be ready to begin.

Nine 0.6" diameter strands will be fed through each of the post-tensioning ducts. First the strands in lowest duct, duct l, will be tensioned. The strands were required to be bundled so that they could be pulled through the round ducts. After bundle was pulled through the girders, the bundled portion was removed having the nine separated strands. Figure 4.28 shows the bundled strands and figure 4.29 shows the bundle being inserted into the end block. A jacking force of 255 kips (132 ksi) will be applied at the oval end of the continuous girder. Then a jacking force of 366 kips (189 ksi) will be applied at the round end of the girder. Finally, a jacking force of 366 kips (189 ksi) will be applied at the oval end. Figure 4.30 shows the strands in duct 1 secured by wedges at the end block and the strands in duct 2 ready for post-tensioning. Figure 4.31 shows the jack configured to tension nine strands.

A loadcell will be installed at the round end during the first stage of post-tensioning so that a friction test may be performed. In addition, by recording the elongation and liftoff pressure, enough data for a detailed friction analysis should be acquired. The same procedure will be used to post-tension the center duct, duct 2. An applied load of 1.2 kips per foot will then be applied to the girder. Finally the top duct, duct 3, will be post-tensioned following the same procedure. Grout will then be injected into the ducts from the oval end. The opposite end will be sealed after the grout has filled the duct. The grout pressures will then be increased to the maximum possible value while the gauges are monitored.

Table 4.1Locationof Ducts in Test Girders

x	Duct 1	Duct 2	Duct	x	Duct 1	Duct 2	Duct
0				38	21.0	28.5	36.0
1				39	21.3	28.8	36.3
2	60.1			40	21.6	29.1	36.6
3	57.3			41	22.0	29.5	37.0
4	54.6			42	22.4	29.9	37.4
5	51.9			43	22.8	30.3	37.8
6	49.4			44	23.2	30.7	38.2
7	47.0	61.9		45	23.7	31.2	38.7
8	44.7	59.0		46	24.2	31.7	39.2
9	42.5	56.2		47	24.7	32.2	39.7
10	40.4	53.5		48	25.3	32.8	40.3
11	38.5	51.0	63.5	49	25.9	33.4	40.9
12	36.6	48.6	60.6	50	26.5	34.0	41.5
13	34.8	46.3	57.8	51	27.2	34.7	42.2
14	33.1	44.1	55.2	52	27.9	35.4	42.9
15	31.5	42.1	52.8	53	28.6	36.1	43.6
16	30.0	40.2	50.5	54	29.4	36.9	44.4
17	28.6	38.5	48.3	55	30.2	37.7	45.2
18	27.4	36.9	46.4	56	31.0	38.5	46.0
19	26.2	35.4	44.5	57	31.9	39.4	46.9
20	25.1	34.0	42.9	58	32.8	40.3	47.8
21	24.1	32.8	41.4	59	33.7	41.2	48.7
22	23.3	31.7	40.0	60	34.7	42.2	49.7
23	22.5	30.7	38.9	61	35.7	43.2	50.7
24	21.8	29.8	37.8	62	36.7	44.2	51.7
25	21.3	29.1	37.0	63	37.8	45.3	52.8
26	20.8	28.5	36.3	64	38.9	46.4	53.9
27	20.5	28.1	35.7	65	39.9	47.4	54.9
28	20.2	27.8	35.3	66	40.9	48.4	55.9
29	20.1	27.6	35.1	67	41.8	49.3	56.8
30	20.0	27.5	35.0	68	42.5	50.0	57.5
31	20.0	27.5	35.0	69	43.2	50.7	58.2
32	20.1	27.6	35.1	70	43.7	51.2	58.7
33	20.1	27.6	35.1	71	44.2	51.7	59.2
34	20.3	27.8	35.3	72	44.5	52.0	59.5
35	20.4	27.9	35.4	73	44.8	52.3	59.8
36	20.6	28.1	35.6	74	44.9	52.4	59.9
37	20.8	28.3	35.8	75	45.0	52.5	60.0

x = distance from end of girder (ft)
y = distance from bottom of girder to center of duct (in)

Table 4.2 Expected Strand Elongation

Duct	Operation	Predicted Elongation (in)
Duct 1	Apply 132 ksi at Oval End	6.5
	Apply 189 ksi at Round End	2.8
	Apply 189 ksi at Oval End	0.96
Duct 2	Apply 132 ksi at Oval End	6
	Apply 189 ksi at Round End	2.6
	Apply 189 ksi at Oval End	0.83
Duct 3	Apply 132 ksi at Oval End	5.7
	Apply 189 ksi at Round End	2.5
	Apply 189 ksi at Oval End	0.7

Table 4.1 Gauge Labeling Plan

First letter is A,B,C or D

A	=	oval near end block
B	=	oval near center
C	=	round near center
D	=	round near end block
E	=	oval at center
F	=	round at center

Second letter and number

D 1	=	near duct 1 (lowest duct)
D2	=	near duct 2 (center duct)
D3	=	near duct 3 (upp r duct)

Third two symbols

VN	=	vertical gauge north of duct
VS	=	vertical gauge south of duct
H1	=	first horizontal gauge above duct
H2	=	second horizontal gauge above duct
H3	=	third horizontal gauge above duct

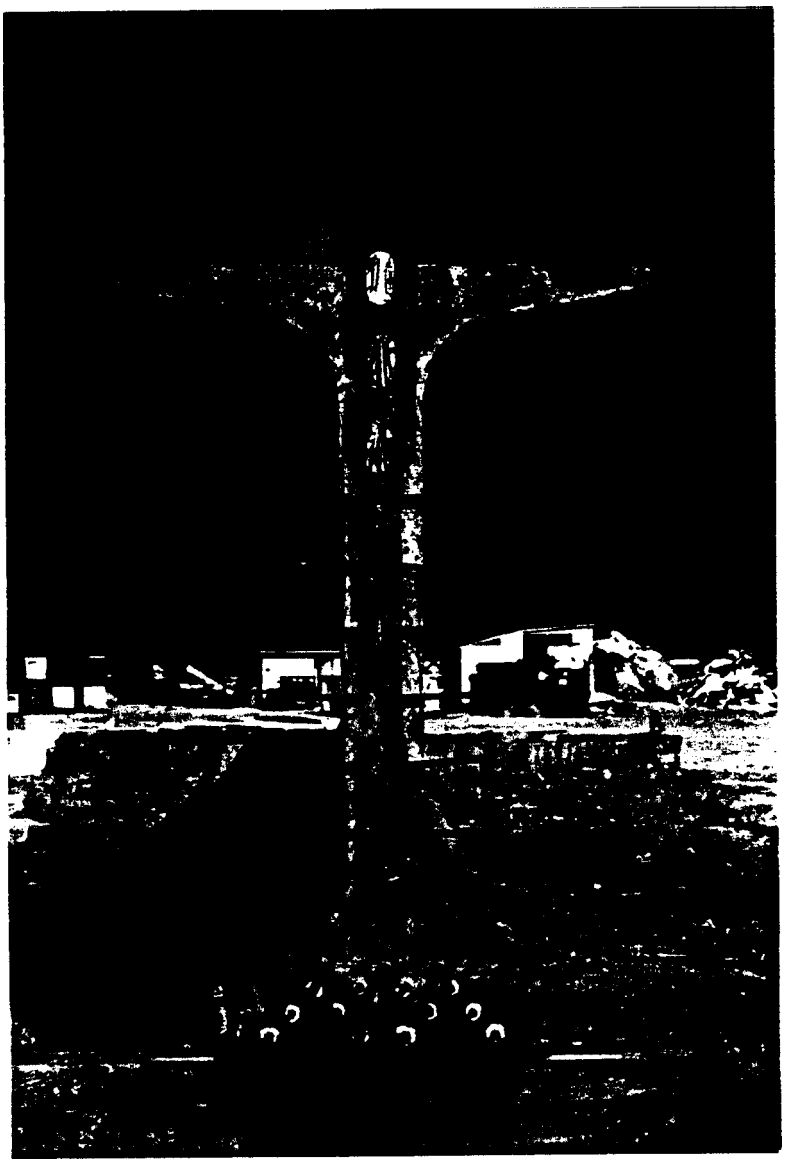

Figure 4.1 Typical Interior Section of a Bulb-T

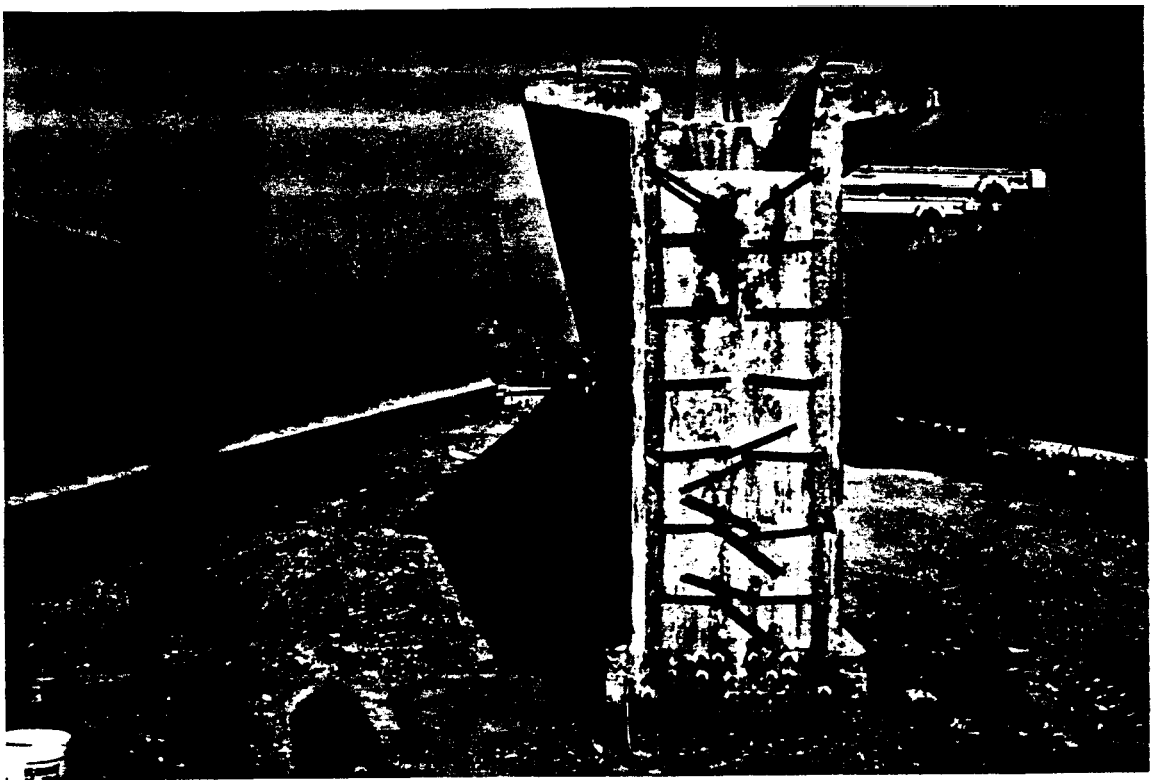

Figure 4.2 Typical End Block Section of a Bulb-T Girder

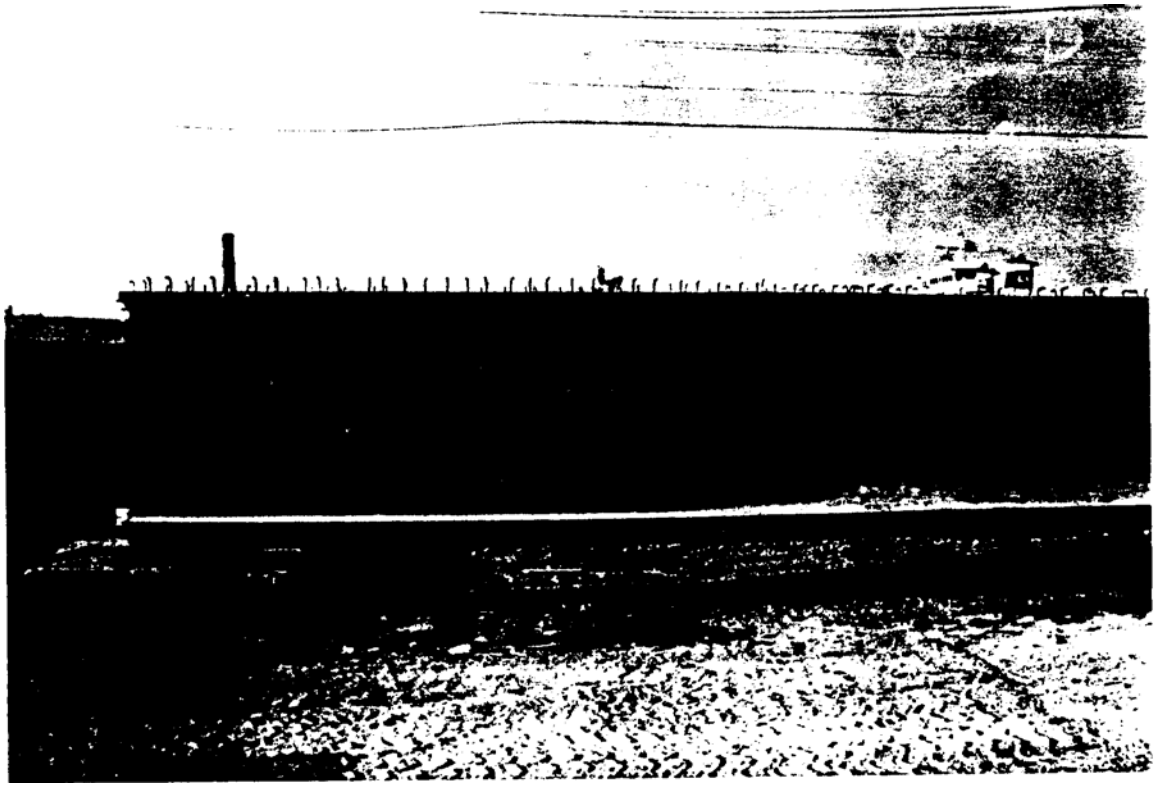

Figure 4.3 Tranzition Zone of a Bulb-T Girder

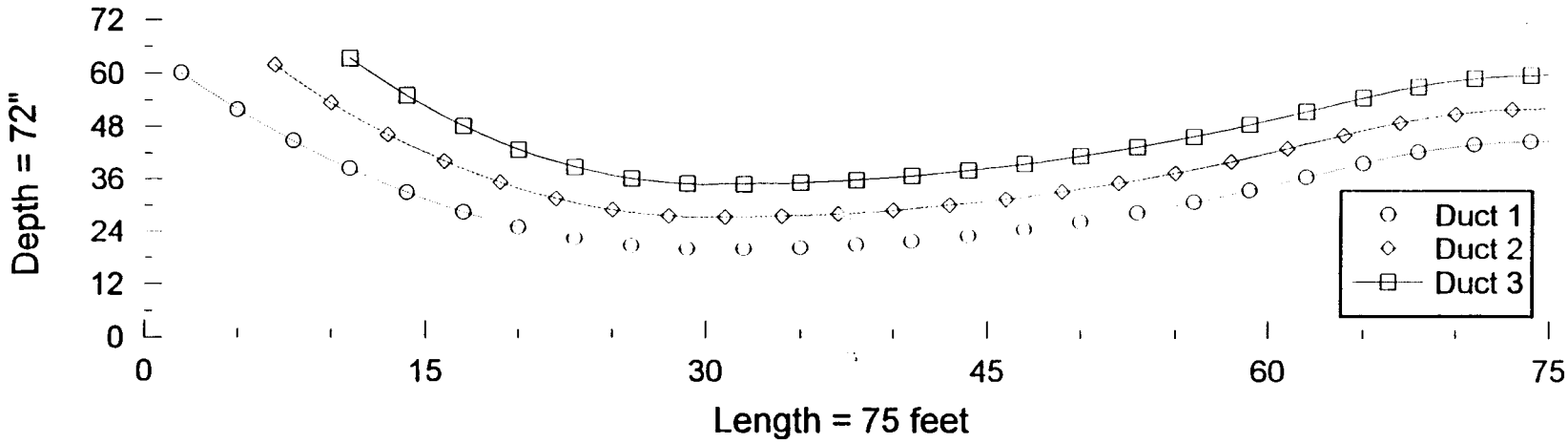

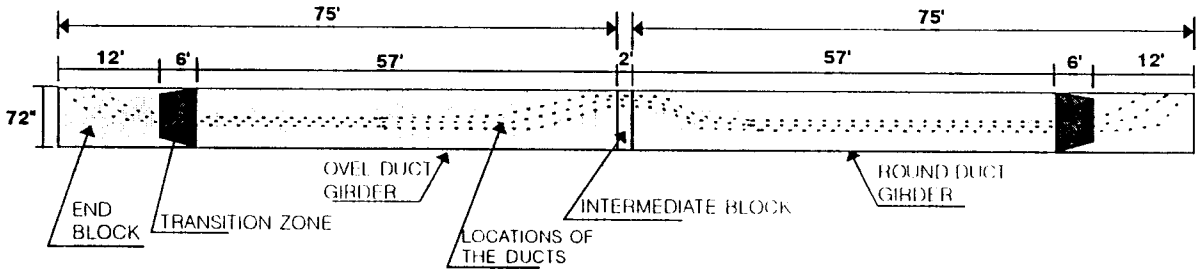

FULL SCALE TEST GIRDERS

Figure 4.4 Location of Ducts and test setup

Bottom Flange:

12 - 1/2", 270k LR strands, tensioned to 31kips each

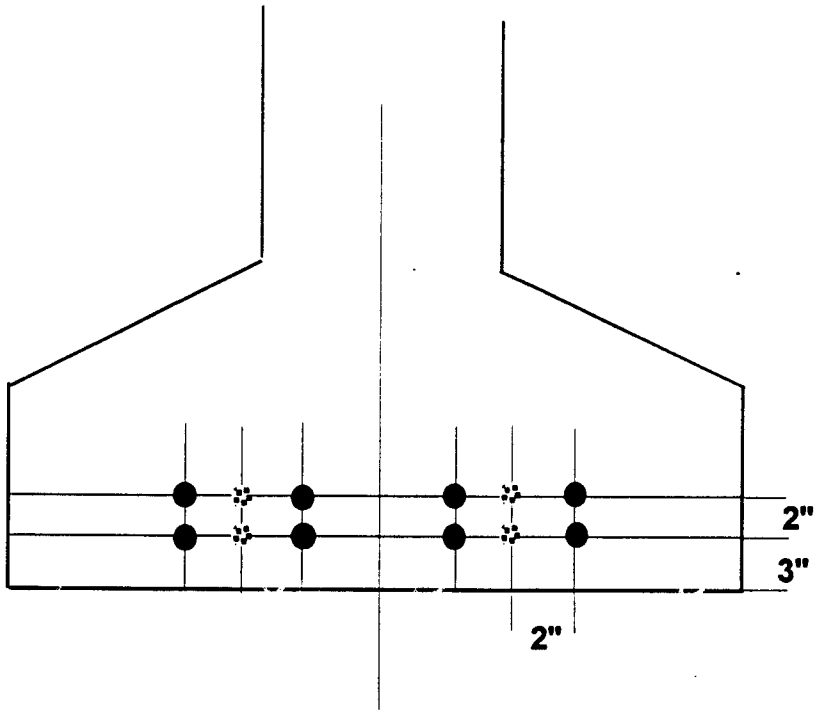

● = fully bonded strand

⁘ = debonded to 7.5' from end of girder

Top Flange:

4 - 1/2", 270k LR strands, tensioned to 5 kips each

allow 2" cover to top of girder

Figure 4.5 Design of Prestress in Field Girders

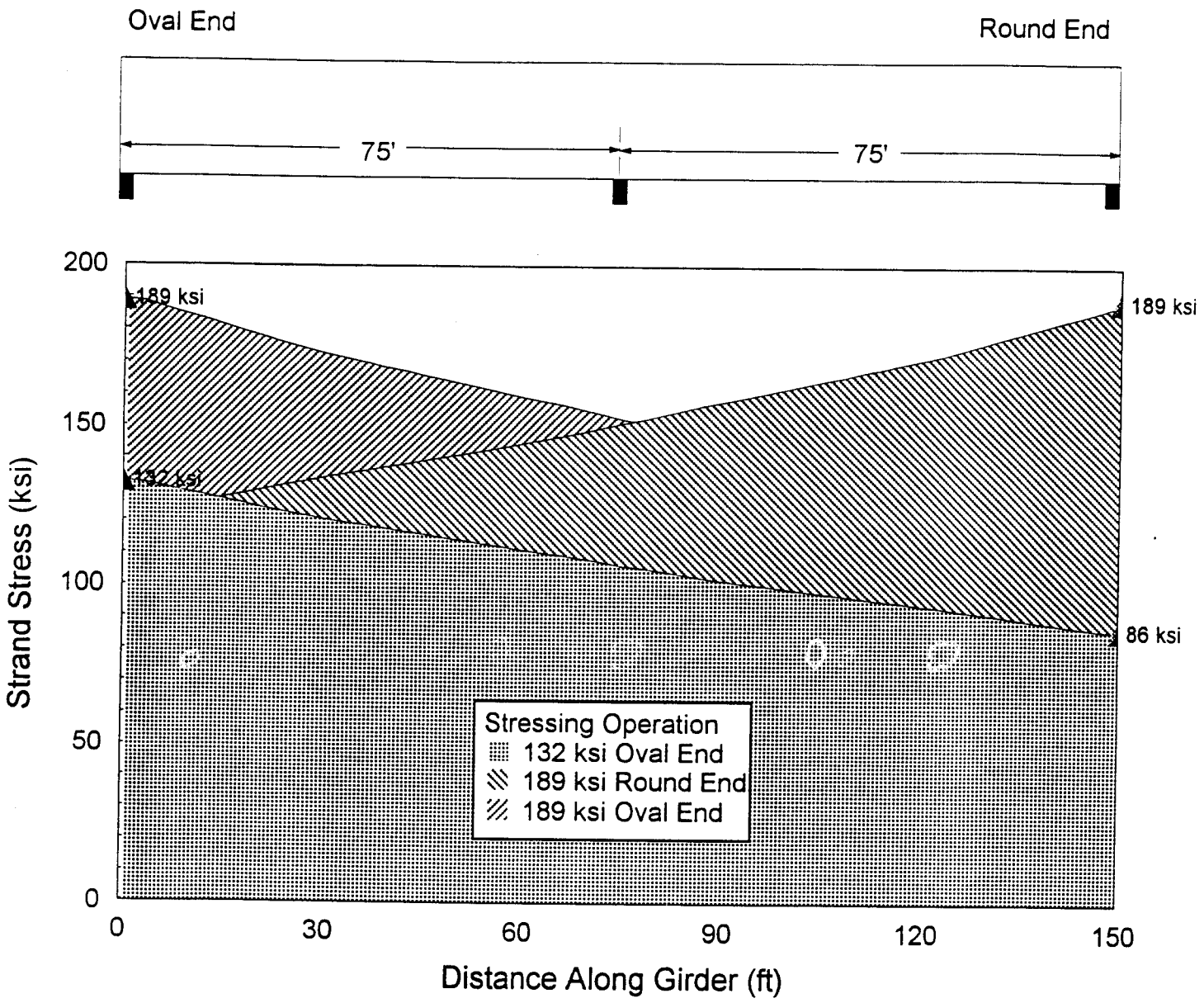

Figure 4.6 Expected Post-Tensioning Losses in Duct 1

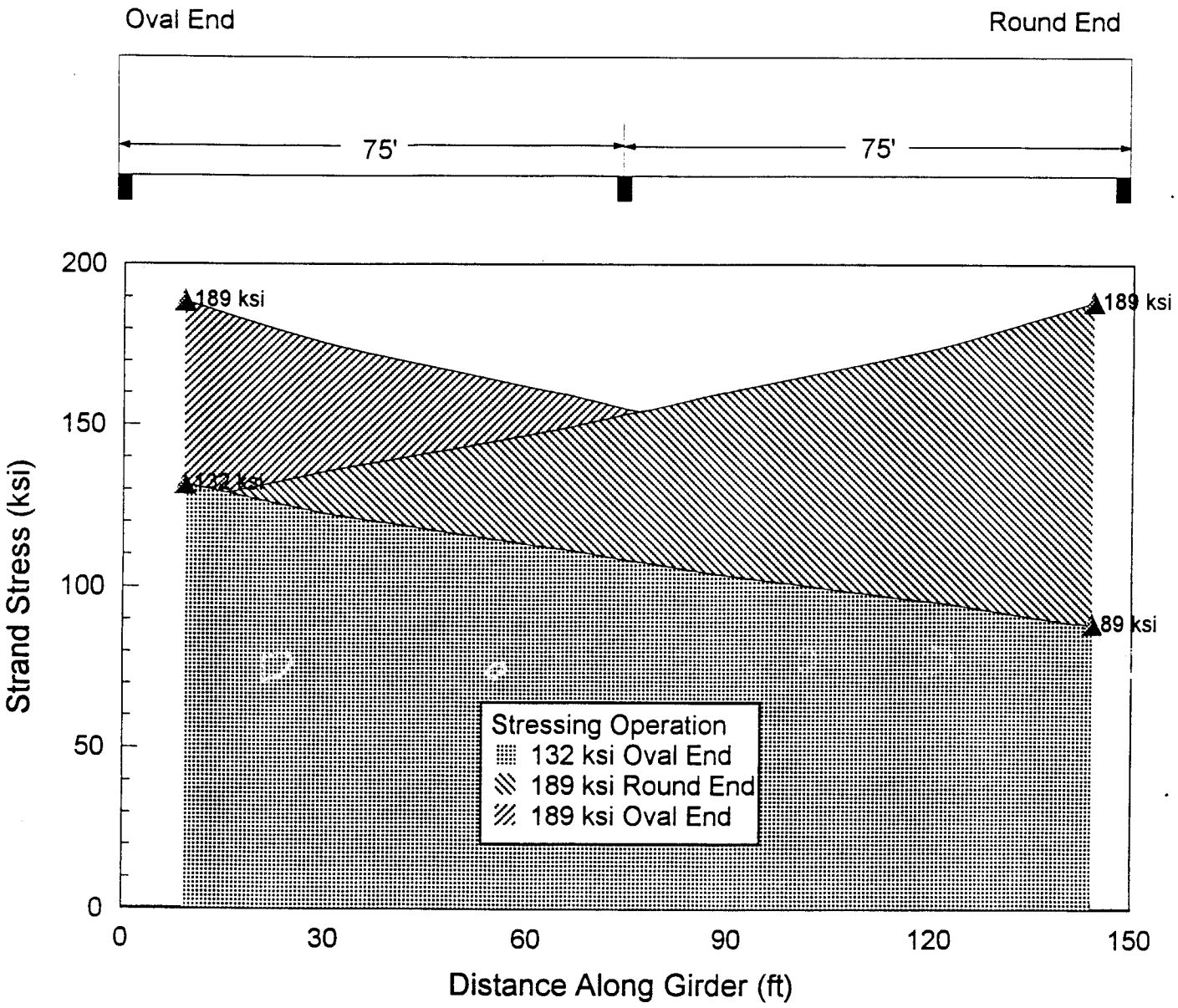

Figure 4.7 Expected Post-Tensioning Losses in Duct 2

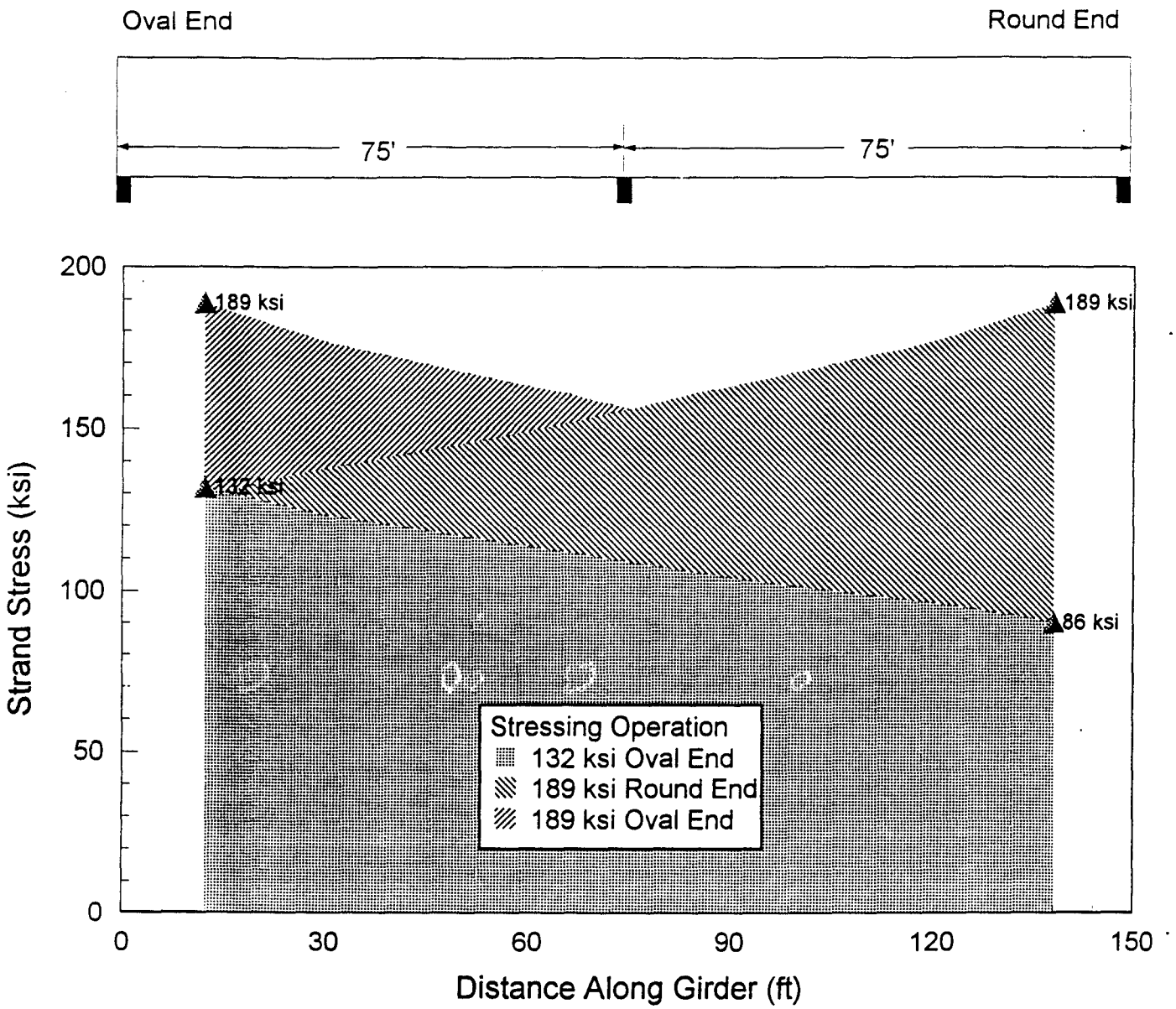

Figure 4.8 Expected Post-Tensioning Losses in Duct 3

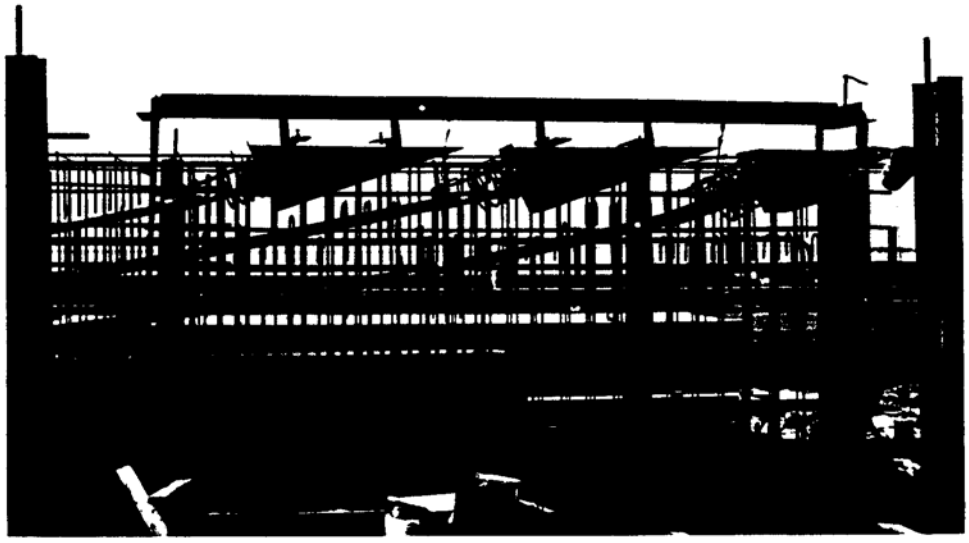

Figure 4.9 End Block Section of a Test Girder Before Casting

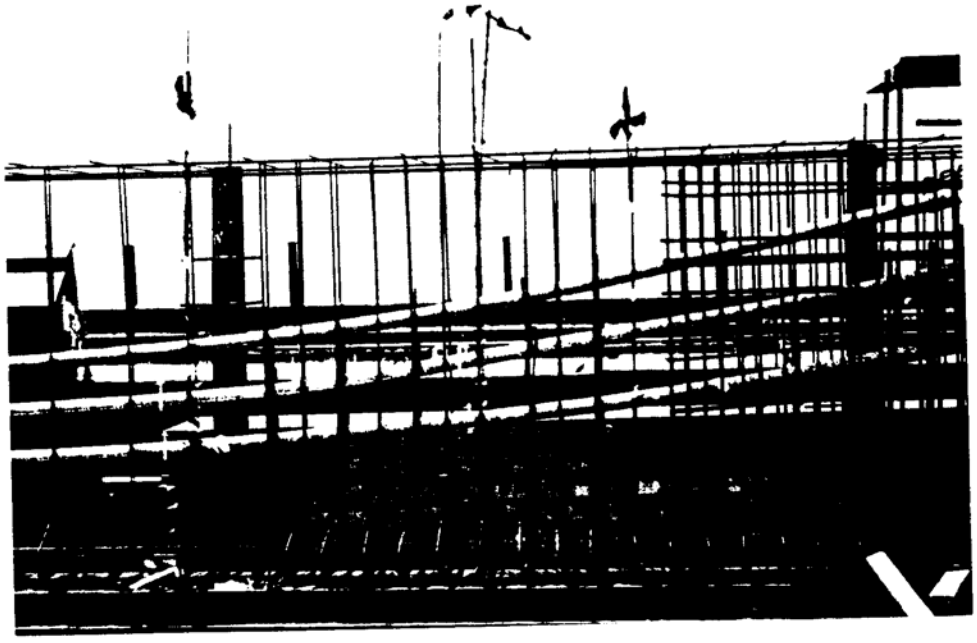

Figure 4.10 Transition Zone of a Test Girder Before Casting

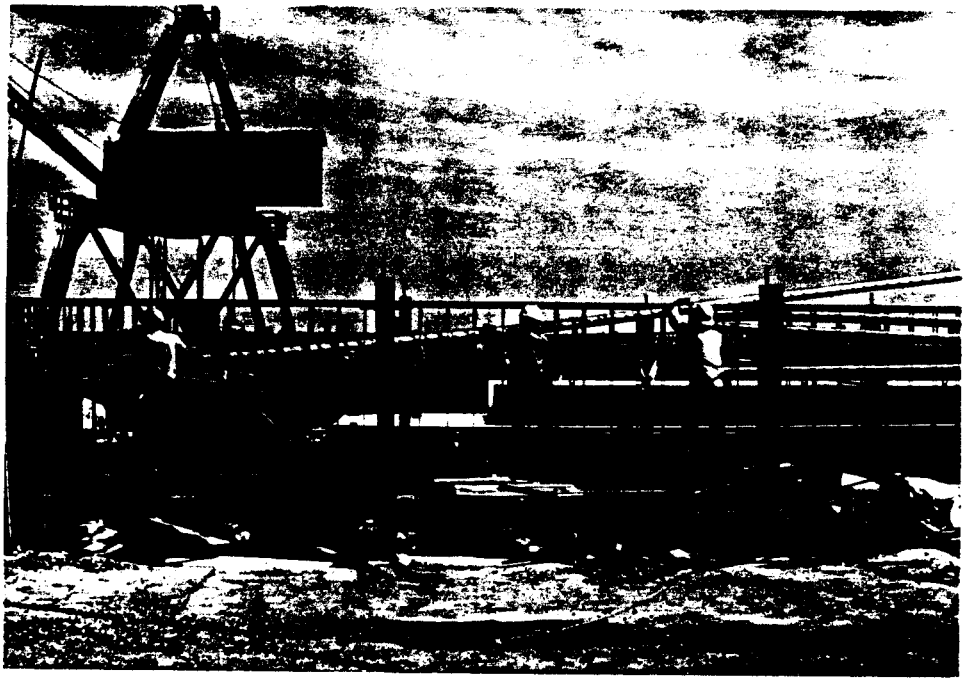

Figure 4.11 Placement of Oval Ducts in Bulb-T test Girder

Figure 4.12 Interior Section of a Bulb-T Girder Before Casting

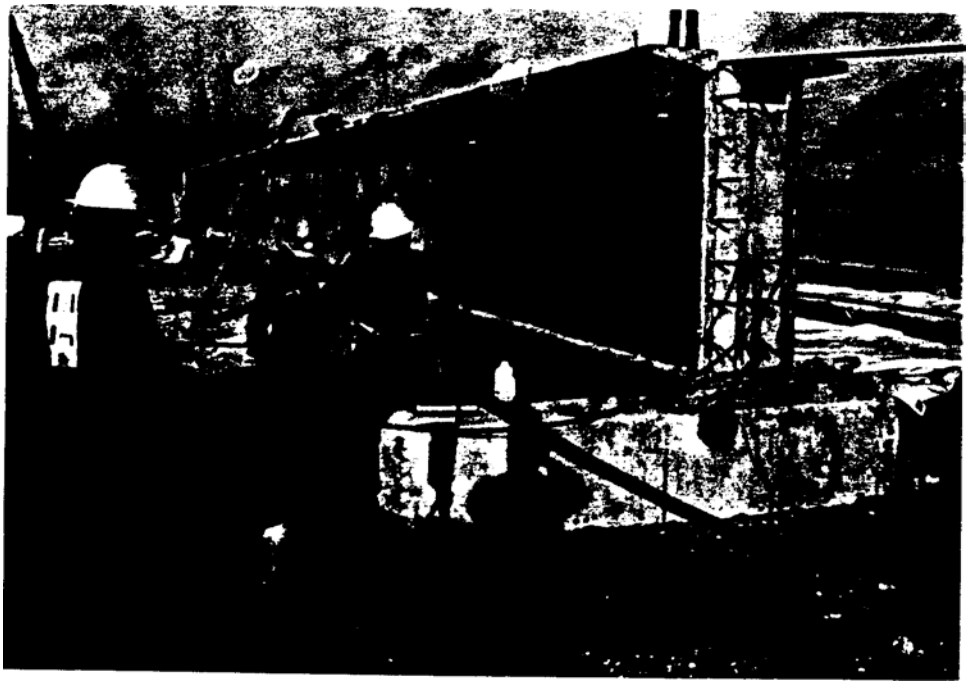

Figure 4.13 End Block Section of a Bulb-T Girder Before Post-

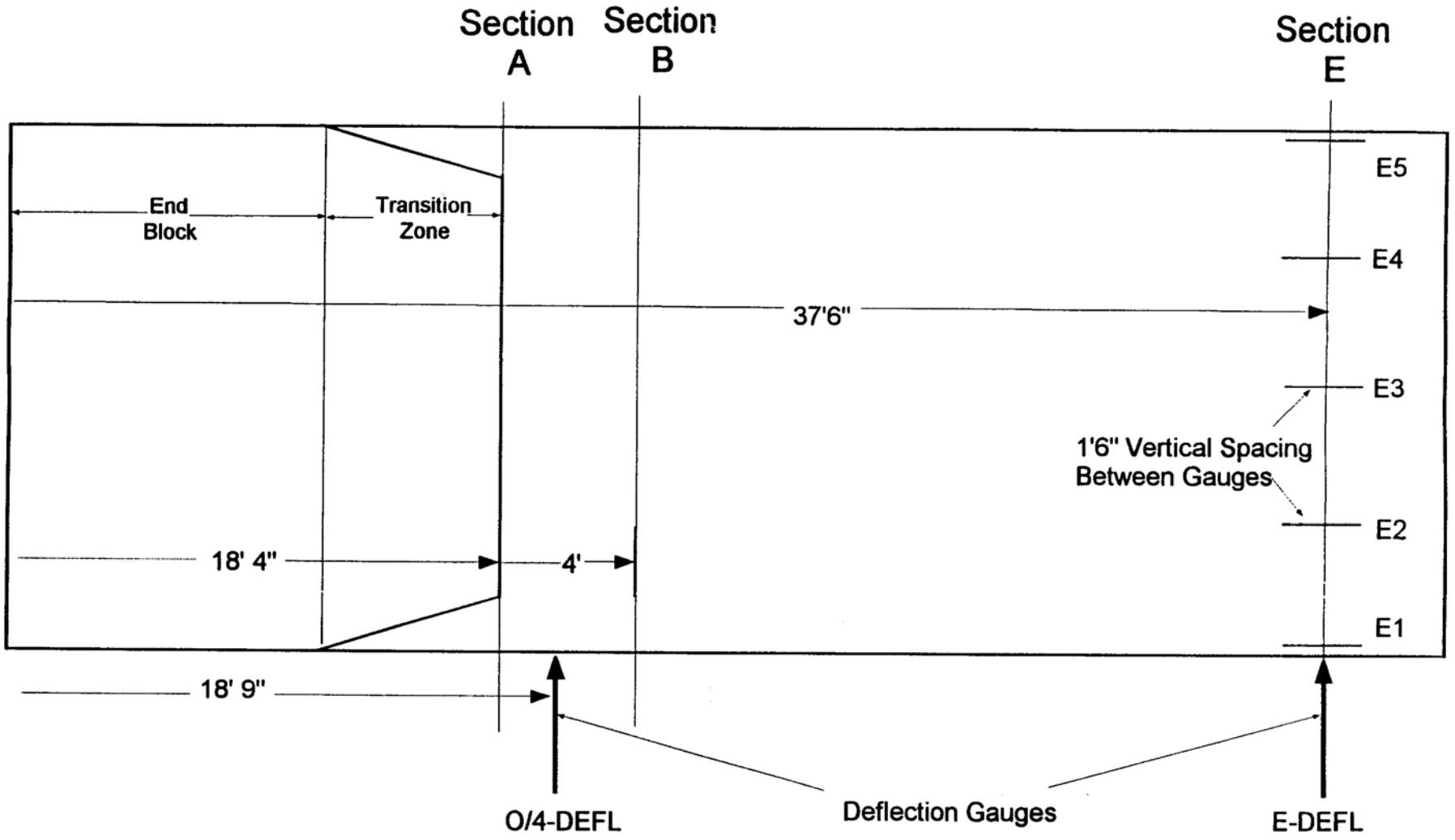

Figure 4.14 Location of Instrumented Sections on Girder with Oval Ducts

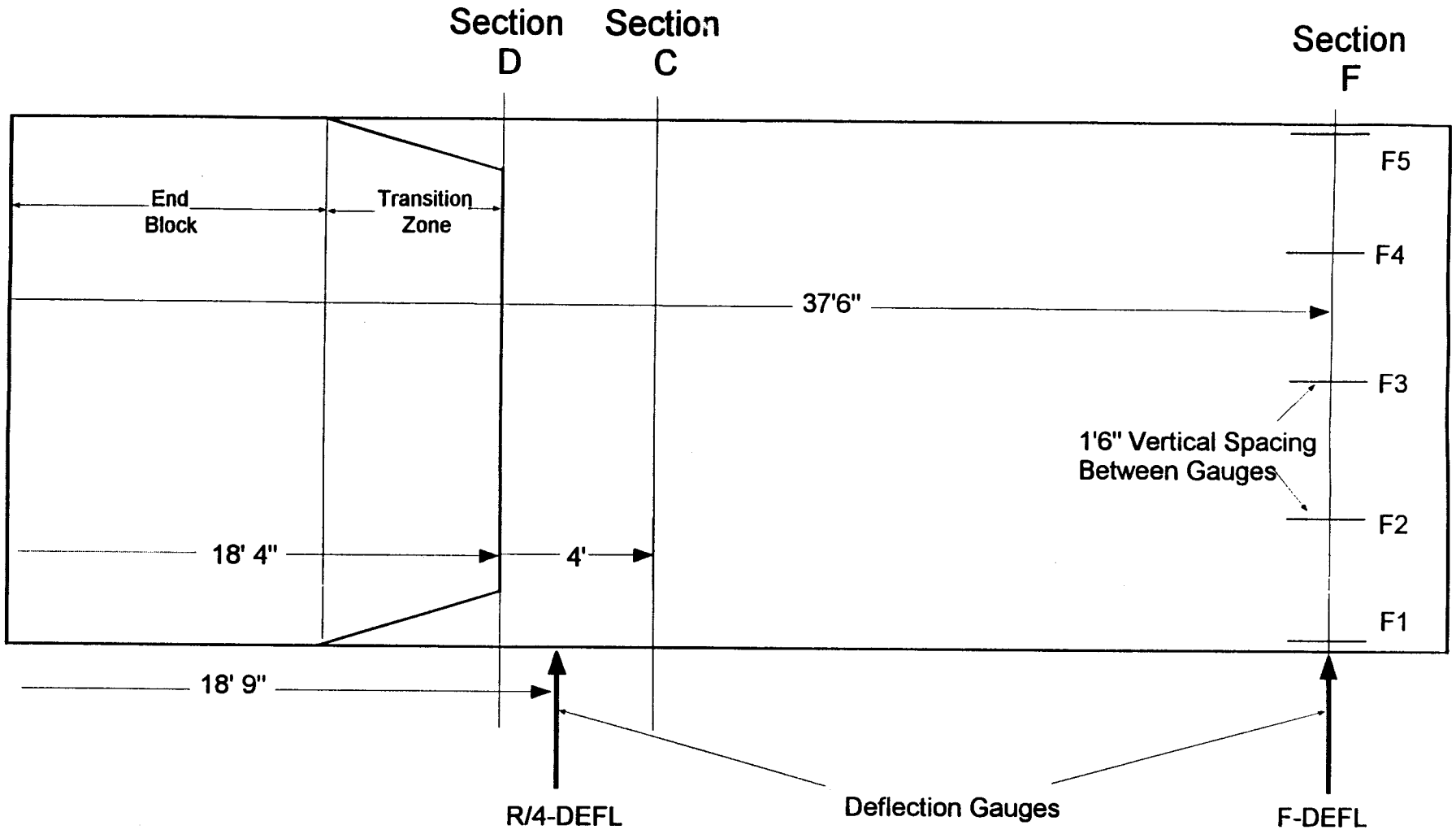

Figure 4.15 Location of Instrumented Sections on Girder with Round Ducts

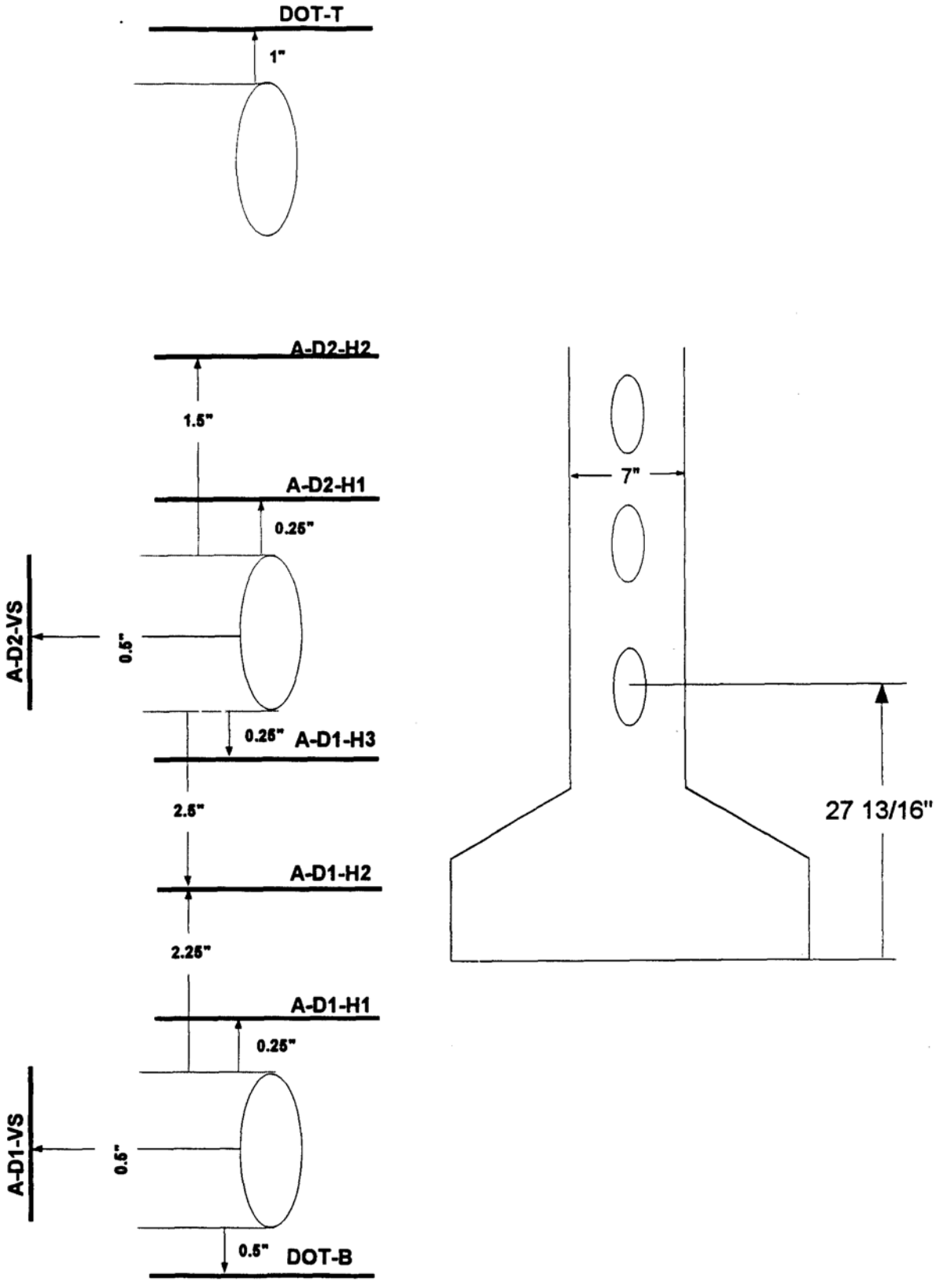

Figure 4.16 Internal Gages at Section A

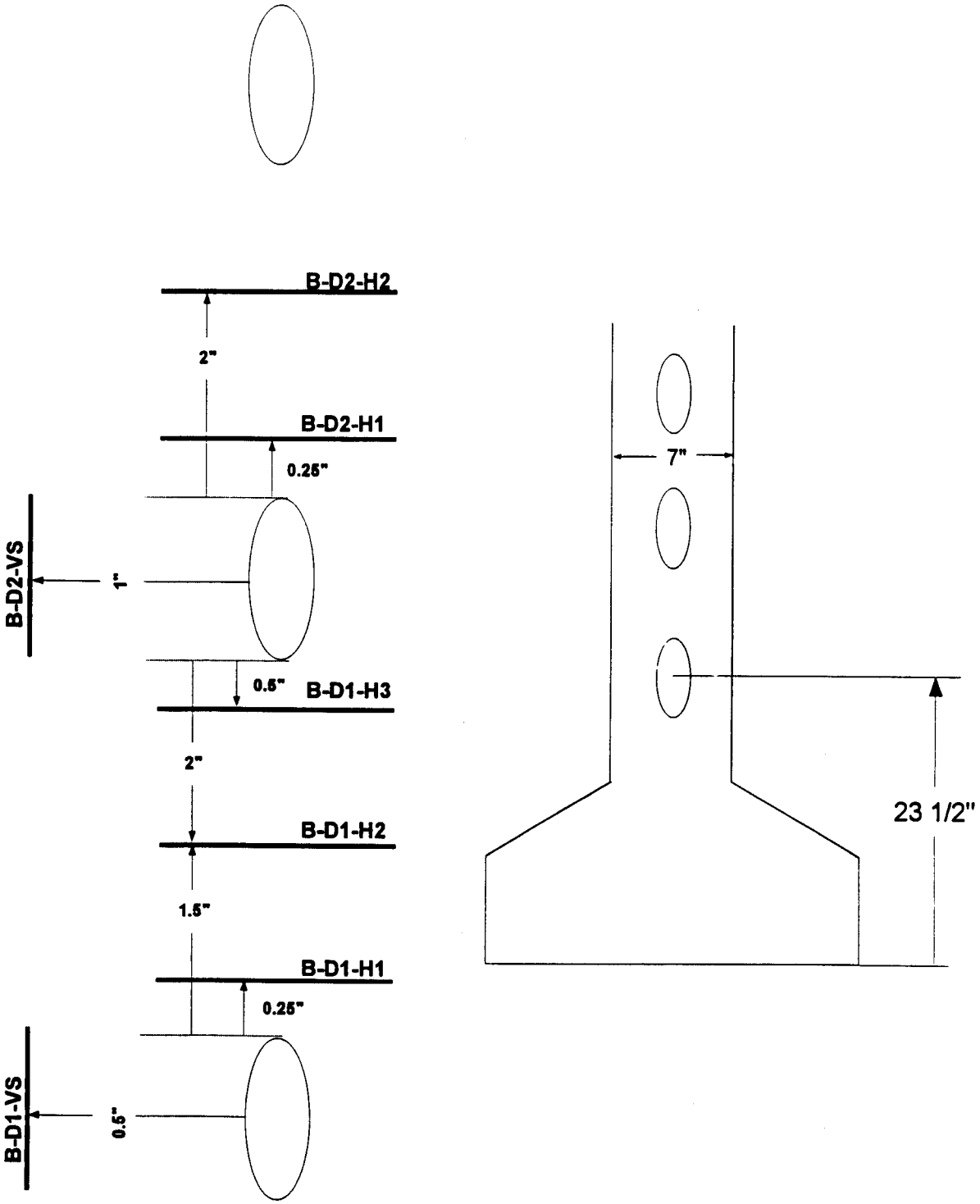

Figure 4.17 Internal Gages at Section B

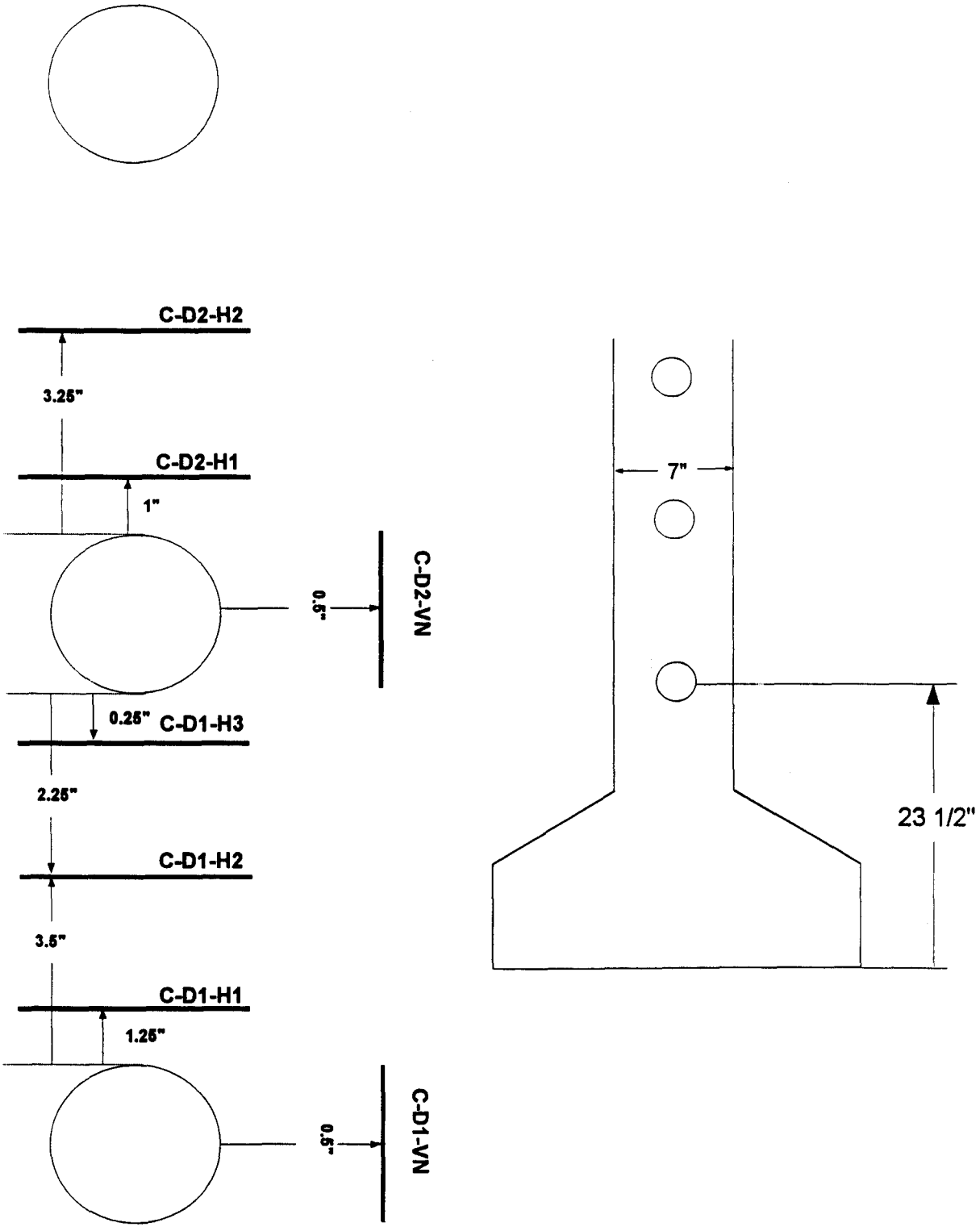

Figure 4.18 Internal Gages at Section C

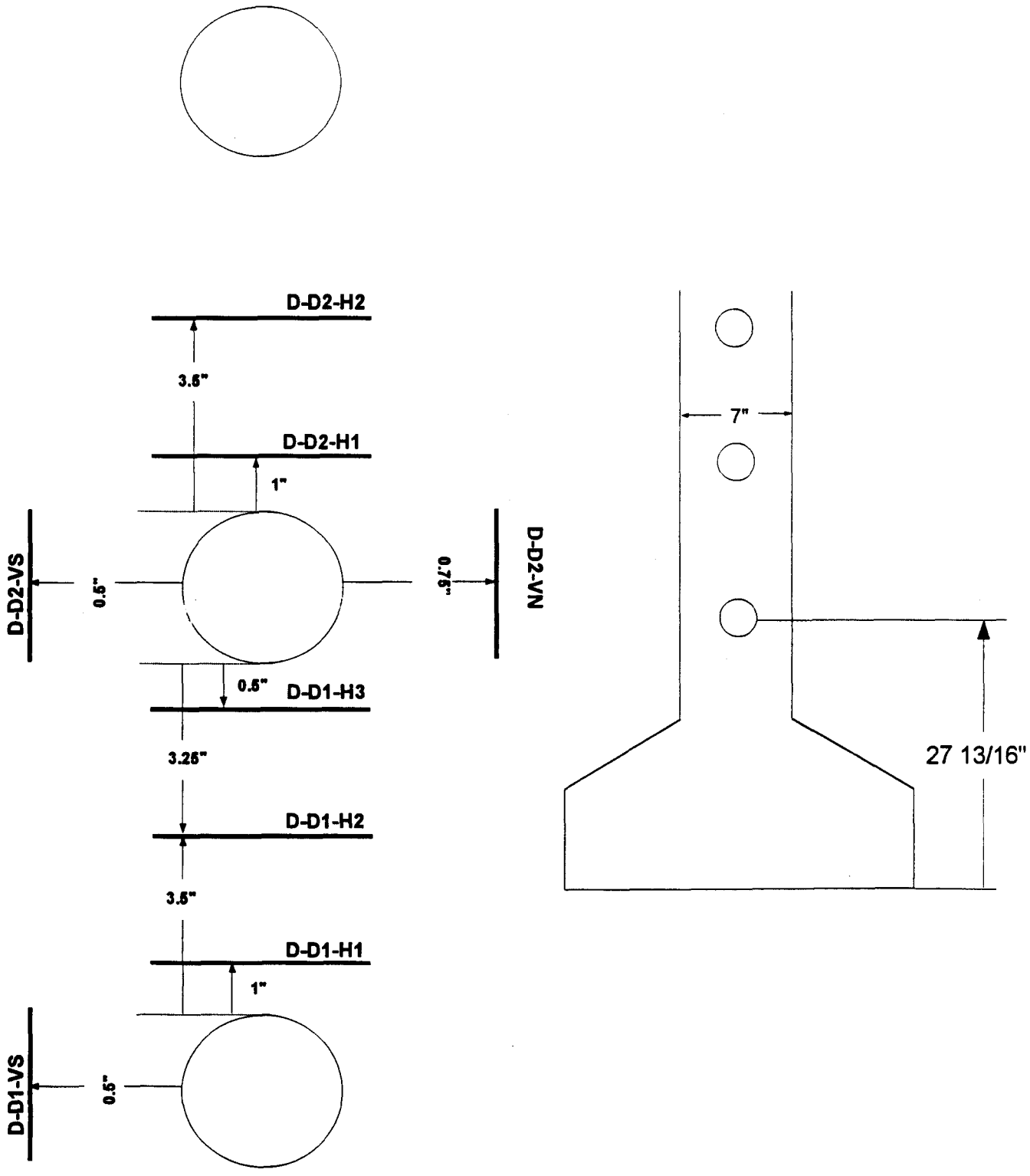

Figure 4.19 Internal Gages at Section D

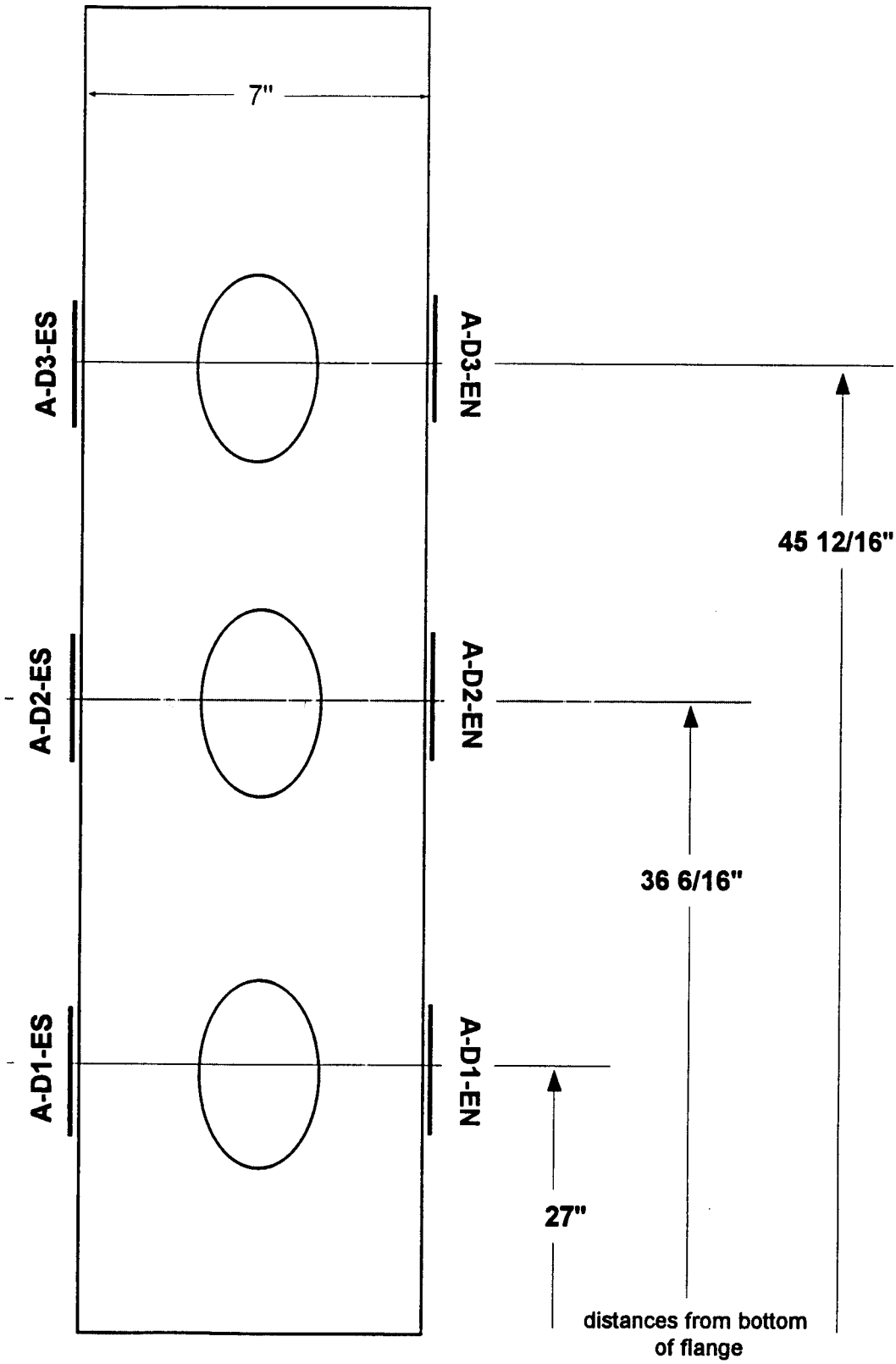

Figure 4.67 External Gages at Section A

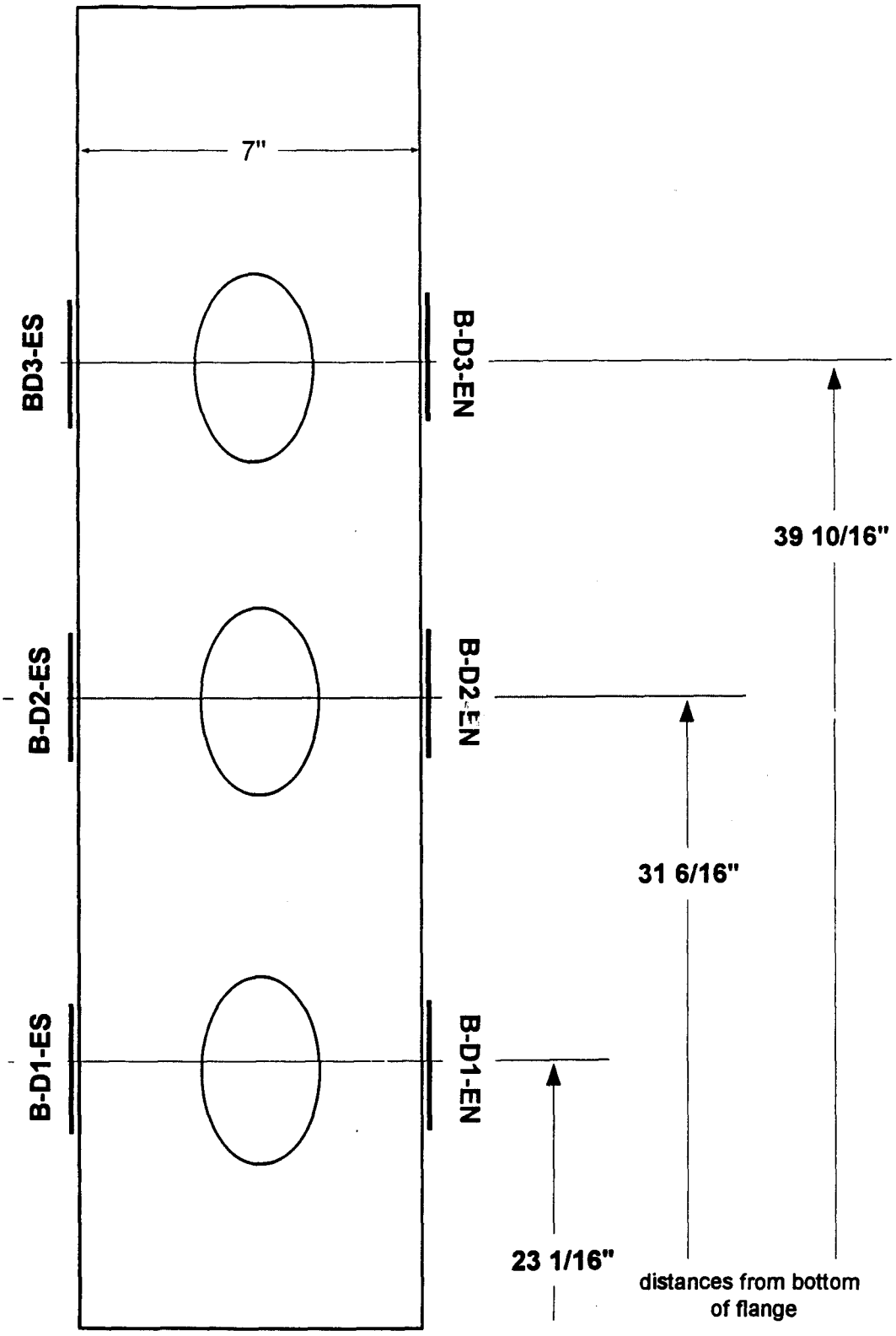

Figure 4.21 External Gages at Section B

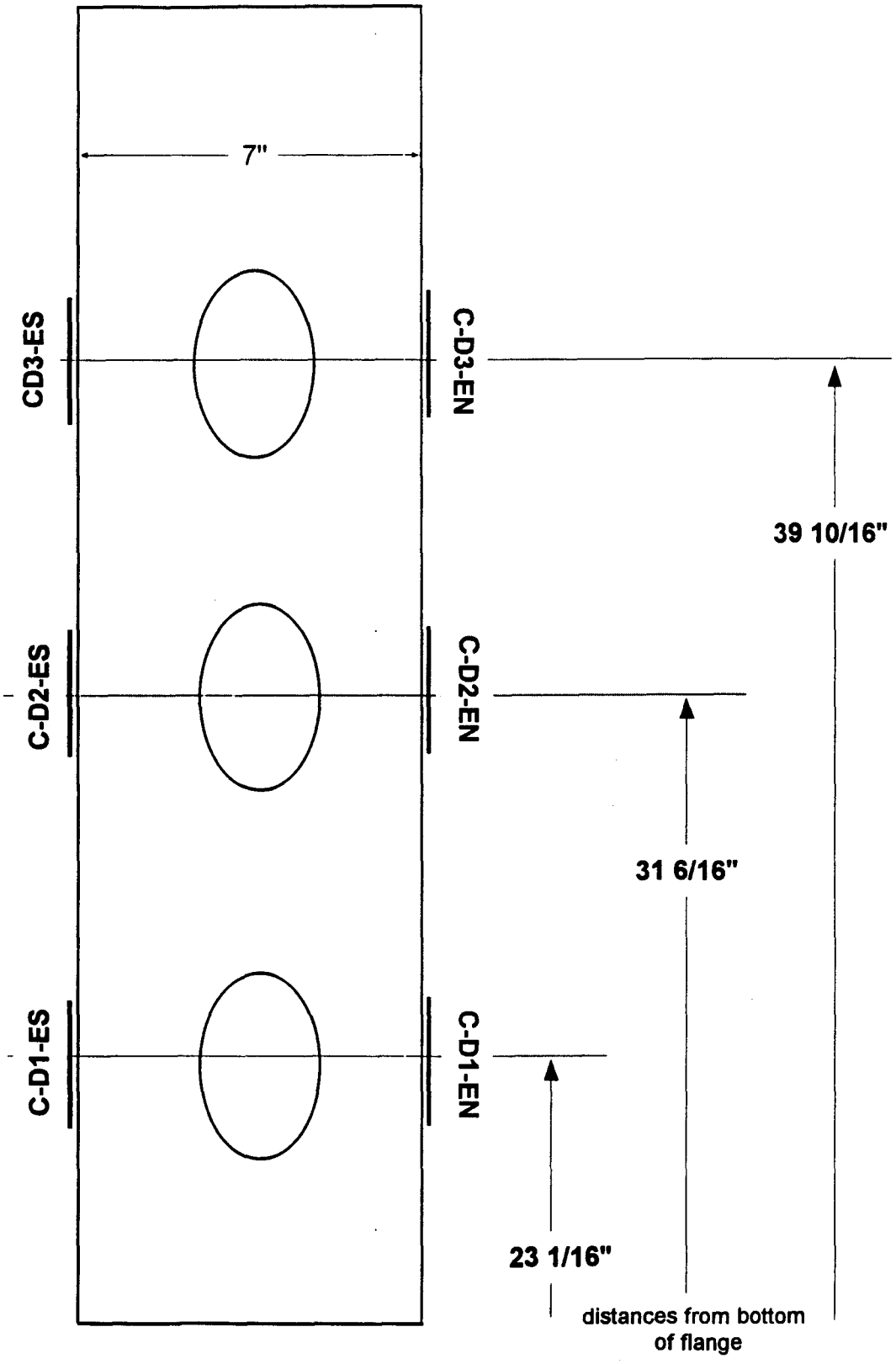

Figure 4.22 External Gages at Section C

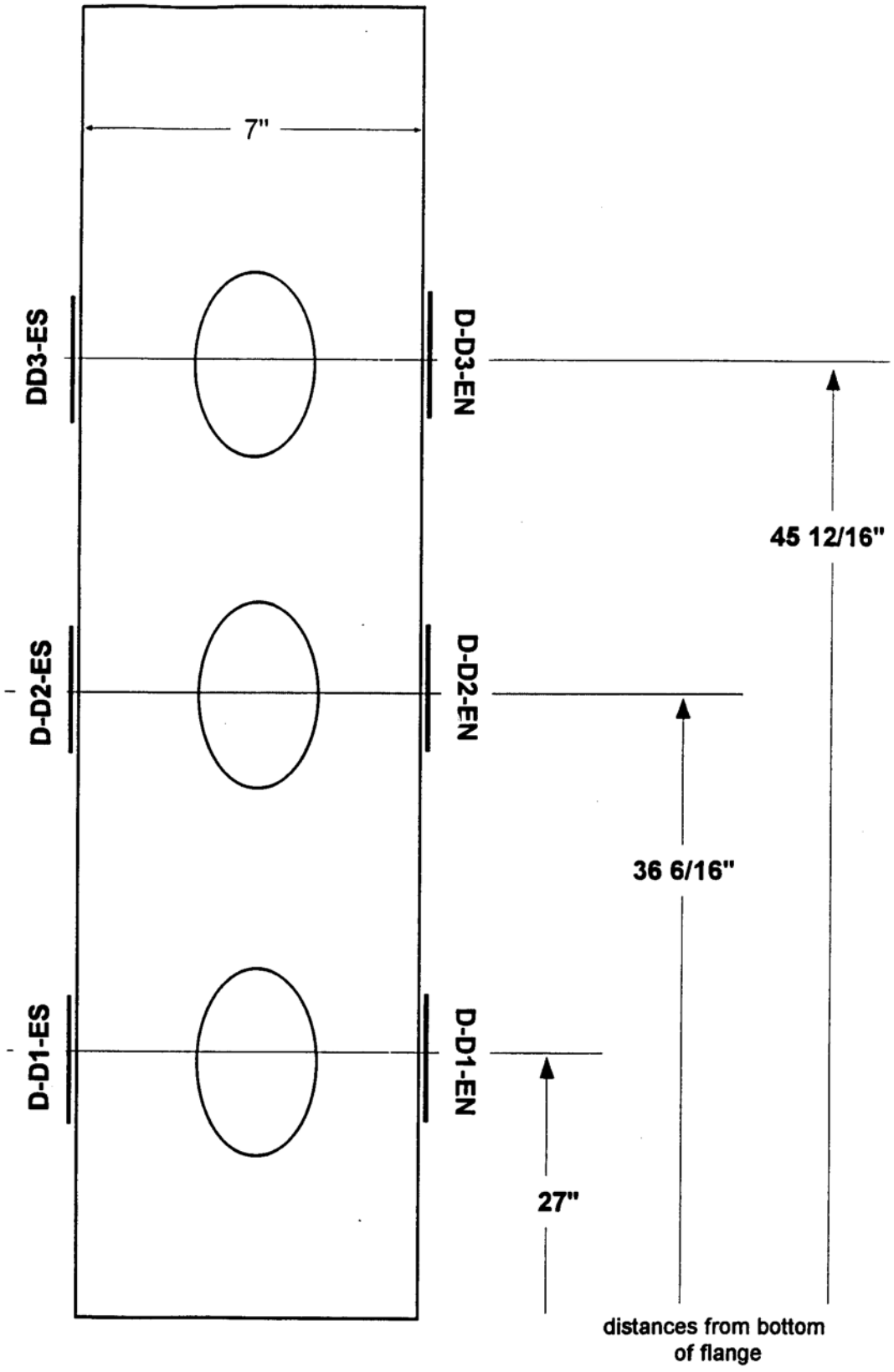

Figure 4.23 External Gages at Section D

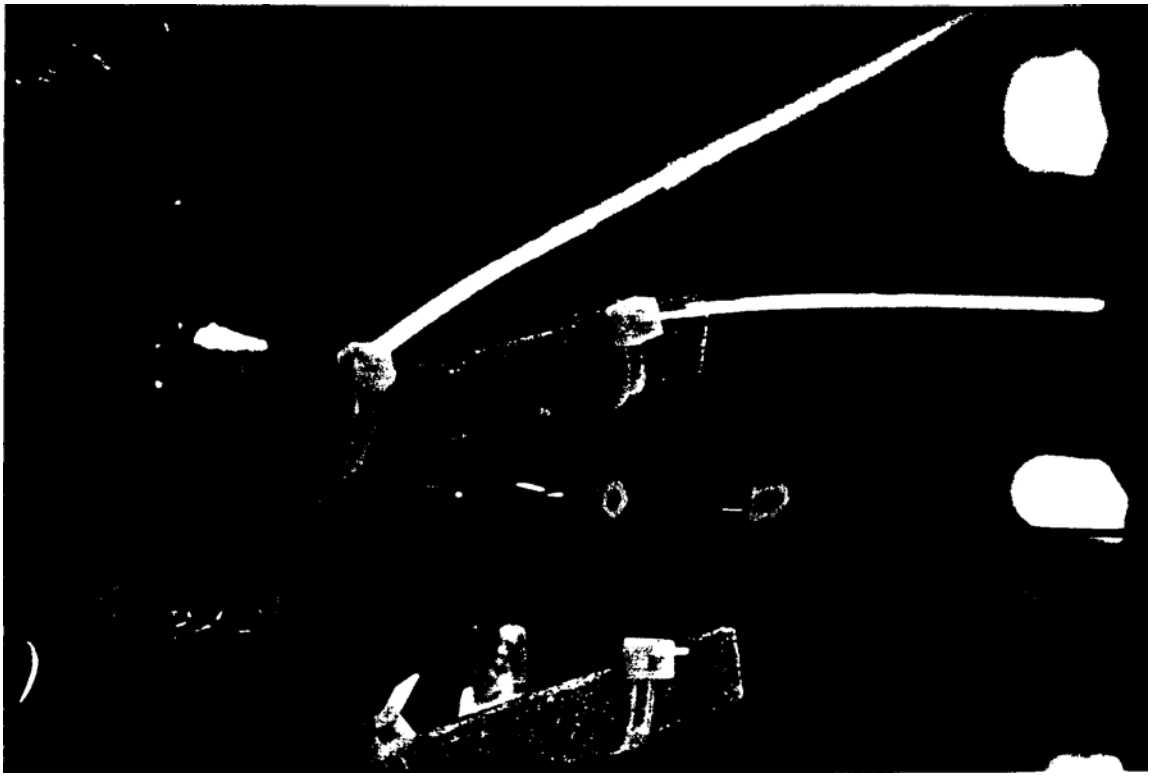

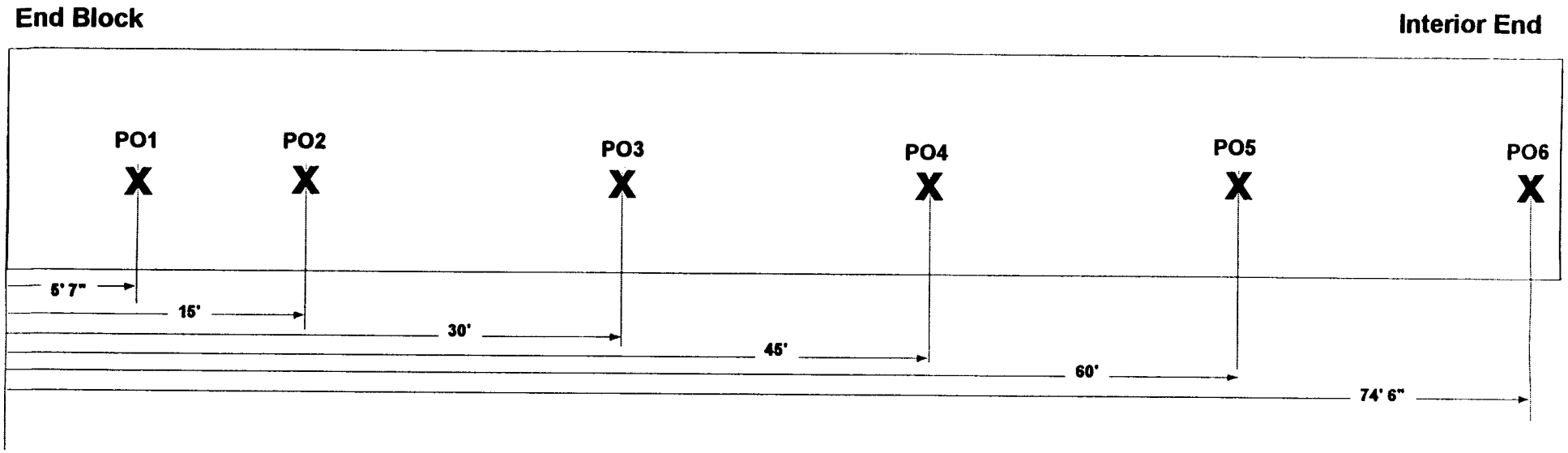

Figure 4.25 Location of Duct Strain Gages in Field Girder with Oval Ducts

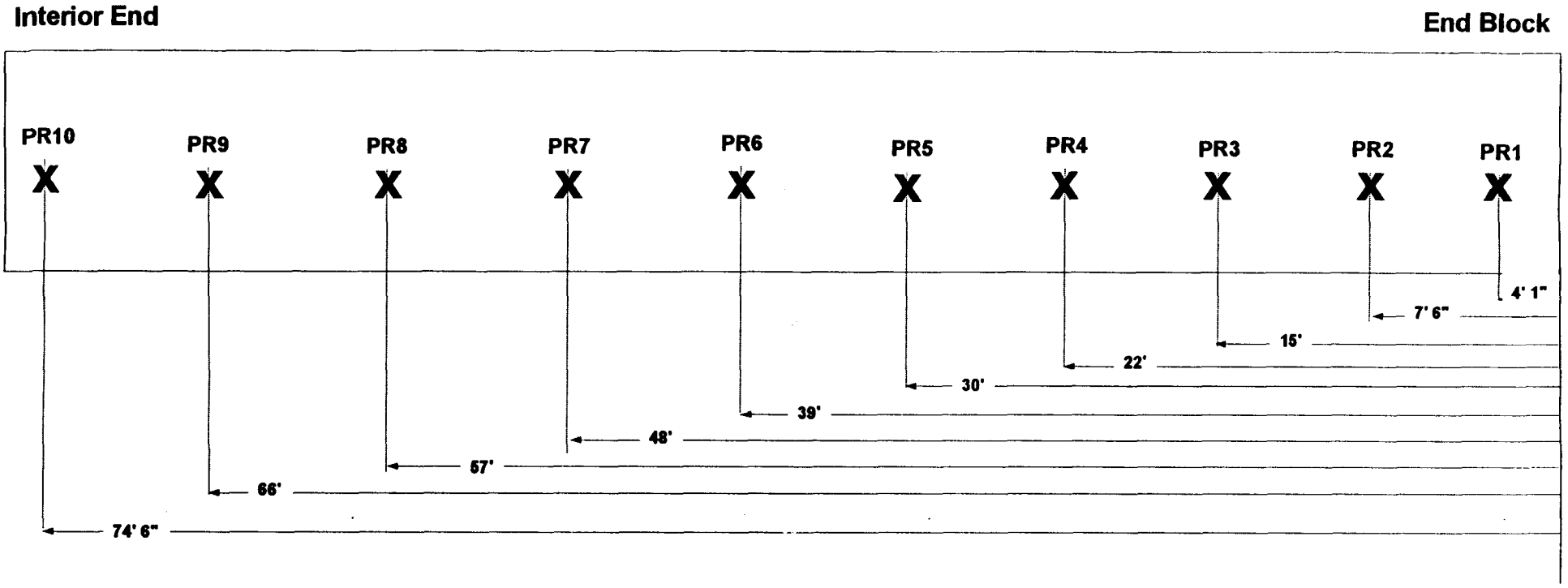

Figure 4.26 Location of Duct Strain Gages in Field Girder with Round Ducts

Figure 4.27 Protected Strain Gauge Applied to Round Steel Duct

Figure 4.28 Bundled Post-Tensioning Strands

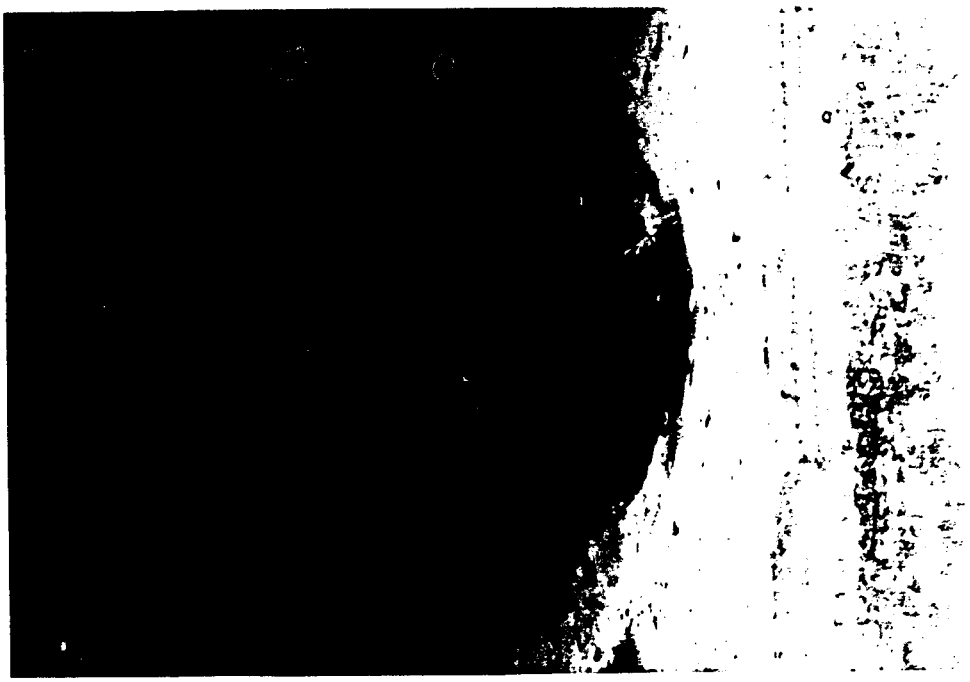

Figure 4.29 Bundled Post-Tensioning Strands Led into End Block

Figure 4.30 Strands in Duct 1 Secured (Prior to Post-Tensioning Strands in Duct 2)

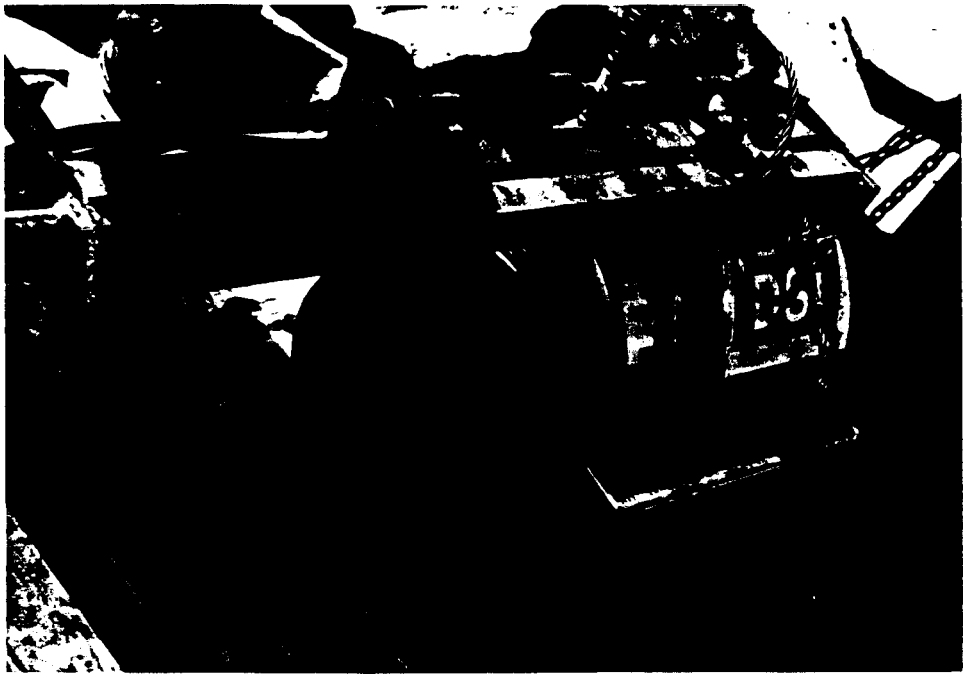

Figure 4.31 Post-Tensioning Jack Configured to Tension Nine

Chapter 5
Results

5.1 Results From Two Dimensional Finite Element Models

The stresses in the concrete girder from the pressure and wedging loads can be viewed in a number of different ways. In this section principal stresses will be used in each of the models for comparison. The stresses surrounding the ducts for a pressure of 100 psi is shown for the four types of ducts in Figures 5.1 to 5.4.

The results from all of the two dimensional models were reduced to tabular form for the purpose of comparison. The stress surrounding each duct at three different points will be used for comparison. At each duct, the stress on the web surface, the stress 1/2" directly above the duct in the center of the web and the stress 1" directly above the duct in the center of the web will be used for comparison. These locations are shown in Figure 5.5. Table 5.1 shows the results of the analysis using a linear concrete model and only pressure loading. Fable 5.2 shows the results using the same loading but with a nonlinear concrete model. The differences between the linear and nonlinear models is summarized in Table 5.3. It can be seen that the stress-strain model used for the concrete has little effect on the resulting stresses.

Table 5.4 shows the results using a linear concrete model with pressure and horizontal wedging forces. A non-linear model for this loading was not performed after reviewing the results from the previous non-linear models, where the use of a nonlinear concrete did not produce any significant changes.

An additional series of two-dimensional finite element were used to model the test girders. The supplier of the$_{m}$ oval duct increased the wall thickness of the duct while this project was being completed. As a result the test girders had a duct with a wall thickness slightly greater than the original two-dimensional models. The additional models were created using the actual duct thickness of the test girders. The results from these models were used to create a table that can be used to compare with the field test results. This table has the strains at the locations of the gauges in the test girders. These models were loaded with the same forces that were applied to the test girders. The

results are shown in Table 5.5. These results will be used with the three-dimensional finite element results and the field results to examine the web stresses in the Bulb-T.

5.2 Three Dimensional Finite Element Results

The three dimensional finite element model developed for the 72" Bulb-T was used to analyze stresses in the test girders. Four significant loading stages were analyzed using the three dimensional model. The first loading stage was completed after the strands in the lowest duct were posttensioned. The second loading stage was completed after the strands in the middle duct were posttensioned. The third loading stage was completed after a distributed load of 1,2001b/ft was applied to the top of the girder to compensate for the slab weight. The forth loading stage was completed after the strands in the third duct were post-tensioned.

The three-dimensional Bulb-T model shown in Figure 3.8 was analyzed using the four load cases discussed above. The results from the model can be used to examine the stresses in the critical sections. The three-dimensional models do not reflect horizontal wedging forces or grouting forces. Therefore, the results from two-dimensional models which do reflect these forces will be added to the three-dimensional results. The strain values were recorded at the locations of gauges in the test girders. The resulting strains are shown in Table 5.6. The three-dimensional strain results were added with the two-dimensional strain results which included the effects of strand wedging and grout pressure. These results are shown in Table 5.7.

5.2.1 Areas of Stress Concentration

The finite element models can be used to see if there are high stress concentrations near the transition zone in the Bulb-T girders. The cross sectional area of the Bulb-T girder changes considerably in the transition zone between the end block and interior sections of the girder. The end block section has over twice the area of the interior section. Thus the compressive stresses caused by prestressing will more than double after the transition zone. Essentially the web narrows and the flanges retain their sizes. So the compressive stresses will be redistributed through the transition zone.

A three dimensional finite element model was modified to determine if the redistribution of

compressive stresses causes a stress concentration in the web. The modified section had a large number of elements at the end of the transition zone. The spacing was reduced from two feet to four inches for a length of six feet. All forces in the z direction were removed, including self weight and applied loads. This was done so that the compressive stresses in the x direction were uniform throughout the depth of the girder. Thus the effects of stress redistribution through the transition zone will be isolated. Finally the compressive stress caused by prestressing was applied to the ends of the girder as a pressure acting evenly over the face of the girder. This was done to isolate the effects of the change in the girders shape in the transition zone.

Figure 5.6 shows the concrete stresses in the x direction for the model described above. The stresses in the end block are constant over the depth of the girder. Also the stresses away from the transition zone in the interior section are constant throughout the depth. However, through the transition zone and after the transition zone there is an uneven stress distribution. Figure 5.7 shows an enlarged view of the transition zone of Figure 5.6. There is a significant stress concentration at the end of the transition zone caused by the redistribution of the compressive stresses in the web. Figure 5.8 shows •.he same model with the vertical (y) direction stresses shown. Figure 5.9 shows a slice of the three dimensional model with the

5.3 Results From Full Scale Field Testing

The field testing of the test girders was performed during the week of September 19" to 23`d, 1994. The field testing was performed at the Hardaway facility in Tampa, Florida. Dr. Moussa Issa, FDOT Structures Research Center, and Mr. John Robertson, The Hardaway Company, and several research assistants from the FAMU/FSU College of Engineering assisted with the field testing. The post-tensioning equipment was supplied to the Hardaway Company from DSI International.

5.3.1 Observations During Girder Manufacture

The Hardaway Company has considerable experience in manufacturing Florida Bulb-T girders. The Hardaway manufactured the girders for the Edison Bridge and was manufacturing girders for the Merrill Barber Bridge at the time the test girders were manufactured and tested. Several observations regarding the construction techniques may lead to a better understanding of

problems with the cracking of the Bulb-T girders.

5.3.1.1 Collapse of Ducts

The Hardaway company did experience some problems with the collapsing of ducts during the manufacture of Florida Bulb-T girders for the Merrill Barber Bridge. Prior to girders being shipped from the Hardaway site, the Hardaway company checks to see that the ducts are not blocked. This test is performed by pulling a "rabbit" through each duct. The "rabbit" is slightly smaller than the duct and should be pulled through easily if there is no deformation of the ducts during the construction of the girders. Prior to shipment the Hardaway Company found that ducts on two of the girders had collapsed. The Hardaway Company hired a firm to inspect the interior of the duct using a remote video camera that is often used to inspect water and wastewater pipes. The video shows that the duct had completely collapsed. The two sides of the oval duct were nearly touching.

5.3.1.2 Construction Observations

Additional observations were made Owing the construction of the test girders. The profile of the post-tensioning ducts is designed as a parabolic shape. During the installation of the ducts the elevation, eccentricity, is measured at numerous stations along the length of the girder. The ducts arrive at the site in short lengths. These short segments are spliced together to make one duct of the required length. The oval duct is stiff in bending due to its relatively large depth of 5 inches. When the duct is placed in the girder two problems may result due to the stiffness of the duct. The duct is tied to two stirrups to secure it in place, sufficient force must be used to secure the duct so that it will not move during the placement of the concrete. In effect, the duct is compressed between the two stirrups. The spliced joints holding duct segments together are much less stiff than the duct segments. It was observed that when the spliced duct is secured in the girder there will be a significantly larger curvature immediately surrounding the spliced joint.

There was some difficulty feeding the strands through the post-tensioning ducts. The cross-sectional area of the round duct was 2.5 times larger than the area of the prestressing steel. The cross-sectional area of the oval duct was much larger than the area of the round duct. The difficulty in feeding the strands occurred when the strands reached the round duct. Eventually a fork lift was

used to pull the strands through the girder. While the ducts were being pulled through the duct nearly all of the strain gauges attached to the lowest duct failed.

5.3.2 Strand Elongation Results

The elongation of the post-tensioning strands was recorded during each stage of post-tensioning. The elongation results were compared with the estimated elongation results during post-tensioning. The estimated elongation was calculated using a coefficient of friction of 0.1. These results are shown in Table 5.8. The measured and predicted elongation results, along with the friction test results will be used to accurately determine the coefficient of friction, p.

5.3.3 Friction Test Results

To perform a friction test, a loadcell was used to measure the dead end force during the first stage of post-tensioning duct 1. During this stage the loadcell readings were significantly less than what was expected. However, the strand elongation was exactly as expected. Because of this apparent contradiction, it was decided to test the accuracy between the ioadcell and jack. The loadcell and post-tensioning jack were placed directly in line, with the jack bearing directly on the loadcell. Thus, the force indicated by the jack pressure gauge should be equal to the force measured by the loadcell. However, it was found that there was a significant error in the readings. Several data points were recorded so that a calibration could be performed. Because the estimated elongation was achieved using the jack pressure gauge, this gauge was used to measure post-tensioning forces for the remainder of the test. Table 5.9 shows the loadcell calibration data and the regression results used to calibrate the loadcell. Figures 5.10 and 5.11 show plots of the jack and loadcell readings before and after correction.

A friction analysis was then performed using the calibrated loadcell readings. The LRFD AASHTO Code specifies a wobble coefficient of 0.0002 and a coefficient of friction between 0.05 and 0.25 for galvanized rigid ducts. Five data points were recorded during the first stage of posttensioning duct 1. These data points are shown in Table 5.10. A coefficient of friction, p, of 0.1 was found to best fit the data

The elongation data can be used to further examine the friction in the ducts. For each data

point a coefficient of friction can be calculated so that the estimated elongation equals the actual measured elongation. These results are shown in Table 5.11. The average value for the coefficient of friction using the strand elongation data is 0.15. The major limitation in this analysis is the accuracy of the field elongation measurements. A change in the coefficient of friction of approximately 0.05 is required to change the estimated elongation 0.1 inch.

5.3.4 Deflection Results

Four deflection gauges were used to monitor the camber and deflection of the continuous girder during testing. The gauges were read after each stage of post-tensioning and loading. The three dimensional finite element model was used to estimate the expected camber and deflection at each of the loading stages. In addition the expected deflections were hand calculated using momentcurvature relationships. The restraint moments were calculated using the flexibility approach. Figures 5.12 to 5.13 show the expected and measured values for two of the loading

5.3.5 Strains Caused by Strand Wedging and Grouting

A computerized data acquisition system was used to record the strains of the internal and external gauges during the post-tensioning of the ducts. Because the test was conducted over a number of days, zero readings were taken immediately before each post-tensioning operation. The zero readings eliminated temperature effects and isolated the effects caused by each post-tensioning operation. The gauge readings were recorded several times during each post-tensioning operation. For example, as the strands were tensioned to 132 ksi (265 kips) at the oval end, data was recorded at jacking forces of 34 kips, 85 kips, 170 kips and 256 kips. Data was also recorded when the strands were tensioned to 189 ksi at the round end, and again when the final jacking force was applied at the oval end. Each of the readings for each gauge was plotted with the corresponding jacking force. A linear regression analysis was performed to determine the strain at the maximum jacking force. The use of linear regression reduces the dependance on a single reading and should give a better indication of the actual stresses in the girder. After all of the strands had been posttensioned and the slab dead load compensation had been applied, the ducts were ready to be grouted. The grouting process began at the top duct and preceded to the

and pumped at the oval end of the test girder. There was a pressure gauge located at the oval end and an additional pressure gauge located at the round end. The Hardaway personnel in charge of the post-tensioning and grouting operations had over 10 years of experience with post-tensioning segmental box girders and Florida Bulb-T girders. He had recently completed working on the construction and post-tensioning of the Edison Bridge. He performed the grouting as it is performed in the field.

The grout is initially pumped through the duct at a low pressure. The round end was left open until the grout flowing out of the round end was of the same consistency of the grout being pumped into the oval end. The round end was then sealed and the pressure gauge was attached. The grout pressure was then increased and the gauge readings were recorded using the data acquisition system. The grout pressure was not increased in a steady manner. Rather the pressure was increased in a step like fashion. In addition, it was difficult to maintain the pressure at a constant value. For these reasons the pressure at the round end never reached the pressure at the oval end. Several readings were taken as the pressure was increased from zero to the maximum value. During the grouting of the top duct the maximum pressure reached was 80 psi at the oval end. The maximum pressure reached during the grouting of the center duct was 90 psi. The maximum pressure reached during the grouting of the lowest duct was 40 psi and no useful data was recorded from this test. Similar to the wedging results, a regression analysis was performed on the data obtained from the grouting test.

The lowest duct was instrumented with strain gauges so that some information regarding the pressure gradient present during grouting could be obtained. However, as mentioned in section 4.3.1.2 the all of the strain gauges attached to the lowest duct failed during the feeding of the strands. Therefore, these gauges did not provide any information about the pressure gradient.

After the regression was completed for each of the gauges during each step of the posttensioning operation, a table was prepared showing the final results. Table 5.12 shows the final results for the field test.

Table 5.1 Principal Stresses Caused by Grout Pressure in Linear Concrete

	Location	Duct	Pressure (psi)			
			75	100	125	150
	Surface	1	160	214	268	322
		2	163	217	271	326
		3	164	219	274	329
Oval	1/2" above	1	106	141	176	213
Polyethylene		2	101	135	169	203
		3	127	169	211	254
	1" above	1	138	184	230	277
		2	123	164	205	247
		3	135	180	225	271
	Surface	1	111	148	185	222
		2	107	142	177	213
		3	110	147	184	220
Oval	1/2"above	1	98	130	162	195
Steel		2	99	132	165	197
		3	112	149	186	224
	1" above	1	57	76	95	114
		2	61	81	101	122
		3	67	89	111	134
	Surface	1	98	131	164	196
		2	102	136	170	204
		3	98	131	164	197
Round	1/2" above	1	55	73	91	110
Polyethylene		2	49	65	81	97
		3	56	74	92	111
	1" above	1	59	78	97	117
		2	66	88	110	133
		3	73	97	121	146
	Surface	1	15	20	25	30
		2	15	20	25	30
		3	15	20	25	31
Round	1/2" above	1	56	75	94	112
Steel		2	49	65	81	98
		3	53	70	87	105
	1" above	1	10	13	16	19
		2	9	12	15	17
		3	9	12	15	19

Table 5.2 Principal Stresses Caused by Grout Pressure in Non-Linear Concrete Models

Duct Type	Location	Duct	Pressure (psi)			
			75	100	125	150
Oval Polyethylene	Surface	1	160	214	267	321
		2	162	217	271	325
		3	166	222	277	332
	1/2" above	1	105	141	176	211
		2	101	135	169	203
		3	125	167	209	251
	1" above	1	137	183	229	275
		2	122	163	203	244
		3	135	181	226	271
Oval Steel	Surface	1	112	149	186	223
		2	106	141	176	211
		3	109	146	183	219
	1/2" above	1	98	130	162	195
		2	98	131	164	197
		3	111	148	185	223
	1" above	1	59	78	97	117
		2	63	84	105	125
		3	69	92	115	139
Round Polyethylene	Surface	1	97	129	162	194
		2	102	135	169	203
		3	98	130	162	195
	1/2" above	1	55	73	91	109
		2	48	64	80	96
		3	54	72	90	108
	1" above	1	59	79	98	118
		2	66	87	109	131
		3	71	95	119	142
Round Steel	Surface	1	15	20	25	30
		2	15	20	25	30
		3	15	20	25	30
	1/2" above	1	51	68	85	102
		2	44	58	73	87
		3	47	63	79	94
	1" above	1	10	13	16	20
		2	9	12	15	18
		3	9	13	16	20

Table 5.3 Differences Between Linear and Non-Linear Concrete Models (linear/non-linear)

Location	Duct	Oval Polyethylene	Oval Steel	Round Polyethylene	Round Steel
Surface	1	101%	100%	102%	96%
	2	101%	104%	100%	102%
	3	94%	97%	99%	100%
1/2" above	1	75%	92%	112%	115%
	2	85%	94%	110%	138%
	3	94%	98%	107%	257%
1" above	1	105%	108%	100%	105%
	2	104%	106%	101%	100%
	3	101%	101%	102%	96%

Table 5.4 Principal Stresses Caused by Grout Pressure and Strand Wedging

Duct Type	Location	Duct	Pressure (psi)			
			75	100	125	150
Oval Polyethylene	Surface	1	277	331	386	440
		2	237	292	348	403
		3	228	280	333	384
	1/2" above	1	292	326	361	395
		2	238	270	302	335
		3	238	279	320	361
	1" above	1	286	331	376	422
		2	220	260	301	341
		3	211	255	300	344
Oval Steel	Surface	1	192	228	264	300
		2	163	198	233	268
		3	157	195	233	271
	1/2" above	1	203	235	268	300
		2	182	215	248	281
		3	183	220	257	294
	1" above	1	107	126	145	164
		2	103	123	143	164
		3	103	125	148	170
Round Polyethylene	Surface	1	217	253	284	316
		2	183	219	250	284
		3	163	195	223	252
	1/2" above	1	191	208	227	245
		2	154	168	185	200
		3	141	157	176	195
	1" above	1	138	156	175	194
		2	146	158	189	211
		3	138	161	186	210
Round Steel	Surface	1	58	62	66	71
		2	50	55	60	66
		3	43	48	54	59
	1/2" above	1	74	89	104	119
		2	52	64	75	89
		3	56	71	86	101
	1" above	1	50	49	48	48
		2	39	38	37	37
		3	30	29	28	28

Table 5.5 Two-Dimensional Finite Element Analysis

	DOT-B	A-D1-H1	A-D1-H2	A-D1-H3	A-D2-H1	A-D2-H2	DOT-T	A-D1-VS	A-D2-VS	A-D1-ES	A-D1-EN	A-D2-ES	A-D2-EN	A-D3-ES	A-D3-EN
PT Stage 1	4	17	1	-2	0	0	0	-2	0	9	9	-1	-1	0	0
PT Stage 2	0	-1	-1	3	14	4	0	0	-2	0	0	7	7	-1	-1
PT Stage 3	0	0	0	0	-1	0	5	0	0	0	0	0	0	5	5
Grout Duct 2 (90 psi)	0	-3	0	33	31	5	0	1	3	-2	-2	35	35	-2	-2
Grout Duct 3 (80 psi)	0	0	0	0	-3	0	18	0	1	0	0	-2	-2	31	31
Sum	4	13	0	34	41	9	23	-1	2	7	7	39	39	33	33

	B-D1-H1	B-D1-H2	B-D1-H3	B-D2-H1	B-D2-H2	B-D1-VS	B-D2-VS	B-D1-ES	B-D1-EN	B-D2-ES	B-D2-EN	B-D3-ES	B-D3-EN
PT Stage 1	28	8	-3	-1	0	-4	0	9	9	-4	-4	0	0
PT Stage 2	-2	0	5	24	8	0	-3	-1	-1	13	13	-5	-5
PT Stage 3	0	0	0	-2	1	0	0	0	0	-1	-1	13	13
Grout Duct 2 (90 psi)	-2	1	30	27	3	0	13	-2	-2	35	35	-4	-4
Grout Duct 3 (80 psi)	0	0	0	-1	3	0	0	0	0	-2	-2	32	32
Sum	24	9	32	47	15	-4	10	6	6	41	41	36	36

	C-D1-H1	C-D1-H2	C-D1-H3	C-D2-H1	C-D2-H2	C-D1-VN	C-D2-VN	C-D1-ES	C-D1-EN	C-D2-ES	C-D2-EN	C-D3-ES	C-D3-EN
PT Stage 1	41	1	-3	-1	0	7	-1	26	26	-1	-1	0	0
PT Stage 2	-2	-2	20	32	-2	0	11	-1	-1	26	26	-1	-1
PT Stage 3	0	0	0	-2	-1	0	0	0	0	-1	-1	24	24
Grout Duct 2 (90 psi)	0	1	14	13	3	0	10	0	0	9	9	0	0
Grout Duct 3 (80 psi)	0	0	0	0	0	0	0	0	0	0	0	8	8
Sum	39	0	31	42	0	7	20	25	25	33	33	31	31

	D-D1-H1	D-D1-H2	D-D1-H3	D-D2-H1	D-D2-H2	D-D1-VS	D-D2-VS	D-D2-VN	D-D1-ES	D-D1-EN	D-D2-ES	D-D2-EN	D-D3-ES	D-D3-EN
PT Stage 1	19	-1	-1	0	0	5	0	0	16	16	0	0	0	0
PT Stage 2	0	-1	10	18	-1	0	5	5	-1	-1	13	13	0	0
PT Stage 3	0	0	0	0	-1	0	0	0	0	0	0	0	10	10
Grout Duct 2 (90 psi)	0	0	14	14	2	0	8	8	0	0	9	9	0	0
Grout Duct 3 (80 psi)	0	0	0	0	1	0	0	0	0	0	0	0	8	8
Sum	19	-2	23	32	1	5	13	13	15	15	22	22	18	18

Table 5.6 Three-Dimensional Finite Element Results at Gauge Locations

	DOT-B	A-D1-H1	A-D1-H2	A-D1-H3	A-D2-H1	A-D2-H2	DOT-T	A-D1-VS	A-D2-VS	A-D1-ES	A-D1-EN	A-D2-ES	A-D2-EN	A-D3-ES	A-D3-EN
PT Stage 1	-2	14	20	16	11	11	11	10	1	1	12	7	7	10	10
PT Stage 2	10	12	12	12	10	11	13	12	18	12	12	18	18	14	14
DL Compensation	0	0	0	0	0	0	2	0	0	0	0	0	0	2	2
PT Stage 3	10	10	11	12	13	13	13	12	12	10	10	12	12	12	12
Sum	18	36	43	40	34	35	38	34	31	22	34	37	37	37	37

	B-D1-H1	B-D1-H2	B-D1-H3	B-D2-H1	B-D2-H2	B-D1-VS	B-D2-VS	B-D1-ES	B-D1-EN	B-D2-ES	B-D2-EN	B-D3-ES	B-D3-EN
PT Stage 1	20	20	20	18	18	21	21	25	25	25	25	23	23
PT Stage 2	18	18	20	15	15	18	16	18	18	20	20	30	30
DL Compensation	-1	-1	-1	0	1	-4	-2	-4	-4	-2	-2	-1	-1
PT Stage 3	16	16	18	18	20	22	22	24	24	24	24	22	22
Sum	53	53	57	51	54	57	57	63	63	67	67	74	74

	C-D1-H1	C-D1-H2	C-D1-H3	C-D2-H1	C-D2-H2	C-D1-VN	C-D2-VN	C-D1-ES	C-D1-EN	C-D2-ES	C-D2-EN	C-D3-ES	C-D3-EN
PT Stage 1	25	21	19	20	17	21	21	25	25	25	25	23	23
PT Stage 2	19	19	21	17	15	16	16	18	18	19	19	28	28
DL Compensation	-1	-1	0	0	1	-4	-4	-4	-4	-4	-4	-1	-1
PT Stage 3	15	15	18	18	19	23	21	25	25	25	25	21	21
Sum	58	54	58	55	52	56	55	64	64	65	65	71	71

	D-D1-H1	D-D1-H2	D-D1-H3	D-D2-H1	D-D2-H2	D-D1-VS	D-D2-VS	D-D2-VN	D-D1-ES	D-D1-EN	D-D2-ES	D-D2-EN	D-D3-ES	D-D3-EN
PT Stage 1	18	23	16	13	13	12	6	6	13	13	6	6	12	12
PT Stage 2	13	13	13	11	11	13	18	18	17	17	21	21	18	18
DL Compensation	-1	0	0	0	1	-3	-1	-1	-3	-3	-1	-1	0	0
PT Stage 3	11	12	13	14	13	11	15	15	13	13	18	18	30	30
Sum	41	48	42	38	38	33	38	38	40	40	44	44	60	60

Table 5.7 Sum of Finite Element Results at Gauge Locations

	DOT-B	A-D1-H1	A-D1-H2	A-D1-H3	A-D2-H1	A-D2-H2	DOT-T	A-D1-VS	A-D2-VS	A-D1-ES	A-D1-EN	A-D2-ES	A-D2-EN	A-D3-ES	A-D3-EN
PT Stage 1	2	31	21	14	11	11	11	8	1	10	21	6	6	10	10
PT Stage 2	10	11	11	15	24	15	13	12	16	12	12	25	25	13	13
DL Compensation	0	0	0	0	0	0	2	0	0	0	0	0	0	2	2
PT Stage 3	10	10	11	12	12	13	18	12	12	10	10	12	12	17	17
Grout Duct 2 (90 psi)	0	-3	0	33	31	5	0	1	3	-2	-2	35	35	-2	-2
Grout Duct 3 (80 psi)	0	0	0	0	-3	0	18	0	1	0	0	-2	-2	31	31
Sum	22	49	43	74	75	44	61	33	33	29	41	76	76	70	70

	B-D1-H1	B-D1-H2	B-D1-H3	B-D2-H1	B-D2-H2	B-D1-VS	B-D2-VS	B-D1-ES	B-D1-EN	B-D2-ES	B-D2-EN	B-D3-ES	B-D3-EN
PT Stage 1	48	28	17	17	18	17	21	34	34	21	21	23	23
PT Stage 2	16	18	25	39	23	18	13	17	17	33	33	25	25
DL Compensation	-1	-1	-1	0	1	-4	-2	-4	-4	-2	-2	-1	-1
PT Stage 3	16	16	18	16	21	22	22	24	24	23	23	35	35
Grout Duct 2 (90 psi)	-2	1	30	27	3	0	13	-2	-2	35	35	-4	-4
Grout Duct 3 (80 psi)	0	0	0	-1	3	0	0	0	0	-2	-2	32	32
Sum	77	62	89	98	69	53	67	69	69	108	108	110	110

	C-D1-H1	C-D1-H2	C-D1-H3	C-D2-H1	C-D2-H2	C-D1-VN	C-D2-VN	C-D1-ES	C-D1-EN	C-D2-ES	C-D2-EN	C-D3-ES	C-D3-EN
PT Stage 1	66	22	16	19	17	28	20	51	51	24	24	23	23
PT Stage 2	17	17	41	49	13	16	27	17	17	45	45	27	27
DL Compensation	-1	-1	0	0	1	-4	-4	-4	-4	-4	-4	-1	-1
PT Stage 3	15	15	18	16	18	23	21	25	25	24	24	45	45
Grout Duct 2 (90 psi)	0	1	14	13	3	0	10	0	0	9	9	0	0
Grout Duct 3 (80 psi)	0	0	0	0	0	0	0	0	0	0	0	8	8
Sum	97	54	89	97	52	63	75	89	89	98	98	102	102

	D-D1-H1	D-D1-H2	D-D1-H3	D-D2-H1	D-D2-H2	D-D1-VS	D-D2-VS	D-D2-VN	D-D1-ES	D-D1-EN	D-D2-ES	D-D2-EN	D-D3-ES	D-D3-EN
PT Stage 1	37	22	15	13	13	17	6	6	29	29	6	6	12	12
PT Stage 2	13	12	23	29	10	13	23	23	16	16	34	34	18	18
DL Compensation	-1	0	0	0	1	-3	-1	-1	-3	-3	-1	-1	0	0
PT Stage 3	11	12	13	14	12	11	15	15	13	13	18	18	40	40
Grout Duct 2 (90 psi)	0	0	14	14	2	0	8	8	0	0	9	9	0	0
Grout Duct 3 (80 psi)	0	0	0	0	1	0	0	0	0	0	0	0	8	8
Sum	60	46	65	70	39	38	51	51	55	55	66	66	78	78

Duct	Operation	Predicted Elongation (in)	Measured Elongation (in)
Duct 1	Apply 132 ksi at Oval End	6.5	6.5
	Apply 189 ksi at Round End	2.8	2.5
	Apply 189 ksi at Oval End	0.96	1
Duct 2	Apply 132 ksi at Oval End	6	5.8
	Apply 189 ksi at Round End	2.6	2.5
	Apply 189 ksi at Oval End	0.83	1
Duct 3	Apply 132 ksi at Oval End	5.7	5.25
	Apply 189 ksi at Round End	2.5	2.375
	Apply 189 ksi at Oval End	0.7	0.625

Table 5.9 Loadcell Calibration Data

Jack (psi)	Jack (kip)	Loadcell (kip)	Error (jack-loadcell) (kip)
2,100	179.0	161.8	17.2
2,500	213.0	188.2	24.8
2,900	247.1	218.6	28.5
3,500	298.3	256.0	42.3
4,000	340.9	292.8	48.1
4,300	366.4	314.3	52.1

Regression Output:		
Constant		0.000
Std Err of Y Est		5.180
R Squared		0.995
No. of Observations		6.000
Degrees of Freedom		5.000
X Coefficient(s)	1.153	
Std Err of Coef.	0.009	

Corrected Loadcell = 1.153*Actual Loadcell

Table 5.10 Friction Losses in Duct 1

Jack Pressure (psi)	Jack Force (kips)	Dead End Force Corrected Loadcell (kips)	Dead End Force Predicted (kips)
400	34	14.3	22.1
1,000	85	51.0	55.3
2,000	170	111.5	110.6
2,500	213	140.6	138.3
3,000	256	166.1	166.0

Loadcell Correction Factor

Coefficient of friction = 0.1
Wobble Coefficient = 0.0002

Table 5.11 Measured Friction Coefficients from Strand Elongation

Duct	Operation	Predicted Elongation (in)	Measured Elongation (in)	Curvature Coefficient
Duct 1	Apply 132 ksi at Oval End	6.5	6.5	0.1
	Apply 189 ksi at Round End	2.8	2.5	0.2
	Apply 189 ksi at Oval End	0.96	1	0.08
Duct 2	Apply 132 ksi at Oval End	6	5.8	0.2
	Apply 189 ksi at Round End	2.6	2.5	0.15
	Apply 189 ksi at Oval End	0.83	1	0.05
Duct 3	Apply 132 ksi at Oval End	5.7	5.25	0.25
	Apply 189 ksi at Round End	2.5	2.375	0.16
	Apply 189 ksi at Oval End	0.7	0.625	0.17
			Average	0.15

Table 5.12 Field Test Results

	DOT-B	A-D1-H1	A-D1-H2	A-D1-H3	A-D2-H1	A-D2-H2	DOT-T	A-D1-VS	A-D2-VS	A-D1-ES	A-D1-EN	A-D2-ES	A-D2-EN	A-D3-ES	A-D3-EN
PT Stage 1	12	27	19	18	12	12	0	19	0	13	18	15	9	14	11
PT Stage 2	0	12	15	18	28	38	0	30	0	11	21	40	30	41	35
PT Stage 3	22	9	12	12	13	13	0	21	0	0	8	0	6	26	20
Grout Duct (90 psi)				15	1 s	2						22	13		
Grout Duct (80 psi)														25	9
Sum	34	48	46	63	69	65	0	70	0	24	47	77	58	106	75

	B-D1-H1	B-D1-H2	B-D1-H3	B-D2-H1	B-D2-H2	B-D1-VS	B-D2-VS	B-D1-ES	B-D1-EN	B-D2-ES	B-D2-EN	B-D3-ES	B-D3-EN
PT Stage 1	19	15	11	11	11	14	8	0	36	50	26	65	28
PT Stage 2	26	18	21	39	27	19	28	0	25	50	37	60	40
PT Stage 3	13	11	10	12	10	14	19	0	20	55	25	32	30
Grout Dud (90 psi)			9	16	3		7				11		
Grout Duct (80 psi)												15	9
Sum	58	44	51	78	51	47	62	0	81	155	99	172	107

	C-D1-H1	C-D1-H2	C-D1-H3	C-D2-H1	C-D2-H2	C-D1-VN	C-D2-VN	C-D1-ES	C-D1-EN	C-D2-ES	C-D2-EN	C-D3-ES	C-D3-EN
PT Stage 1	23	9	14	7	16	17	18	80	60	75	95	0	60
PT Stage 2	23	31	29	60	22	65	27	40	100	45	35	100	25
PT Stage 3	16	13	12	16	25	7	12	15	10	20	15	30	15
Grout Dud (90 psi)			s	6	2		6			8			
Grout Dud (80 psi)													6
Sum	62	53	63	89	65	89	63	135	170	148	145	130	106

	D-D1-H1	D-D1-H2	D-D1-H3	D-D2-H1	D-D2-H2	D-DINS	D-D2-VS	D-D2-VN	D-D1-ES	D-D1-EN	D-D2-ES	D-D2-EN	D-D3-ES	D-D3-EN
PT Stage 1	18	24	14	16	14	21	16	15	25	20	35	48	0	36
PT Stage 2	9	25	17	19	26	31	0	21	16	13	31	27	0	14
PT Stage 3	18	15	13	18	18	23	27	27	14	19	18	14	0	30
Grout Dud (90 psi)			7	4			6	8			5	5		
Grout Dud (80 psi)														5
Sum	45	64	51	57	58	75	49	71	55	52	89	94	0	85

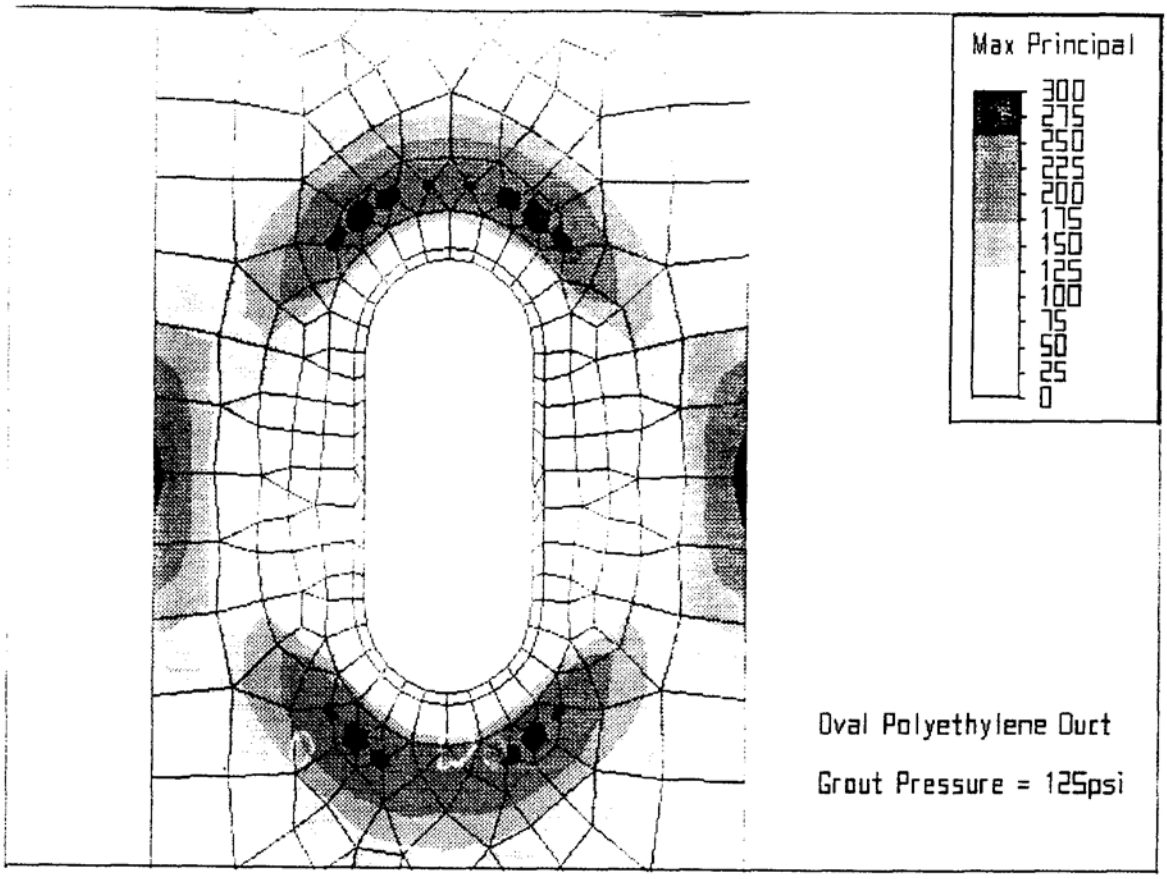

Figure 5.1 Principal Stresses in Oval Polyethylene Model Caused by Grout Pressure

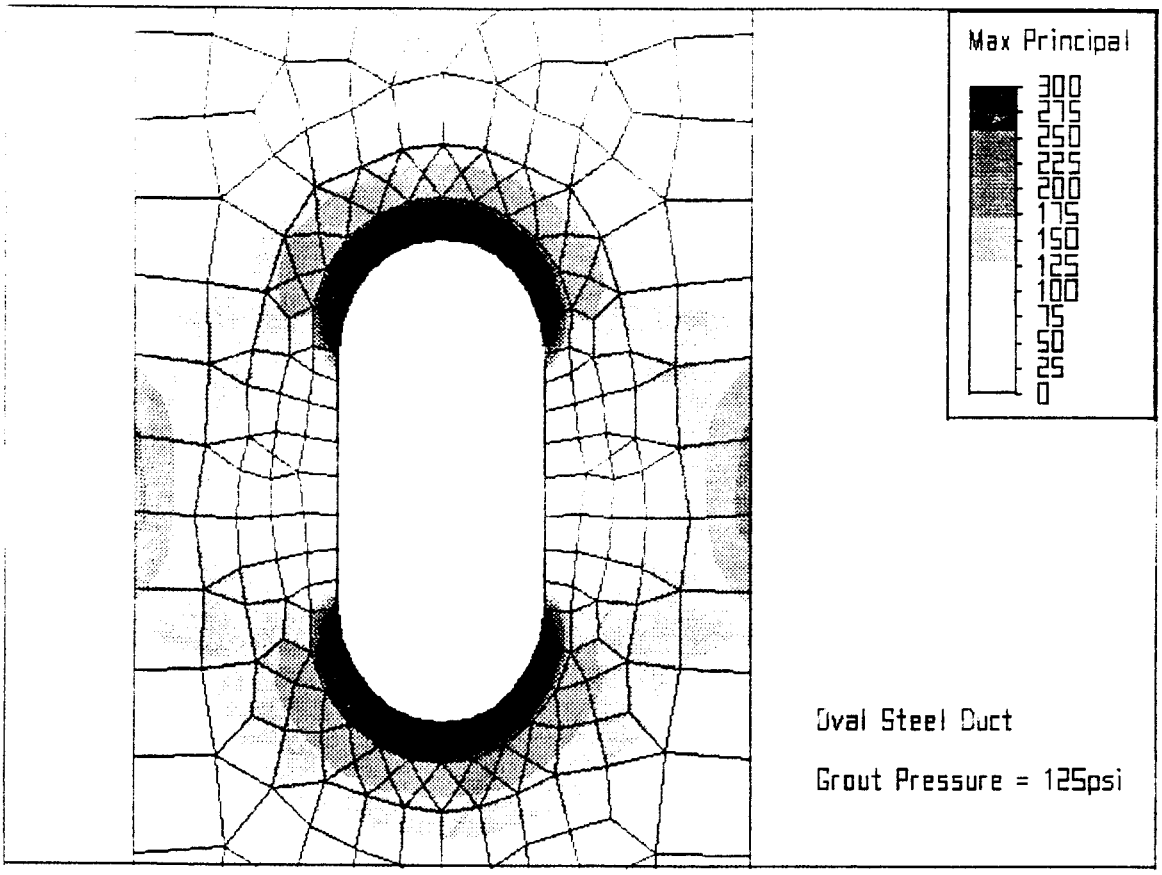

Figure 5.2 Principal Stresses in Oval Steel Model Caused by Grout Pressure

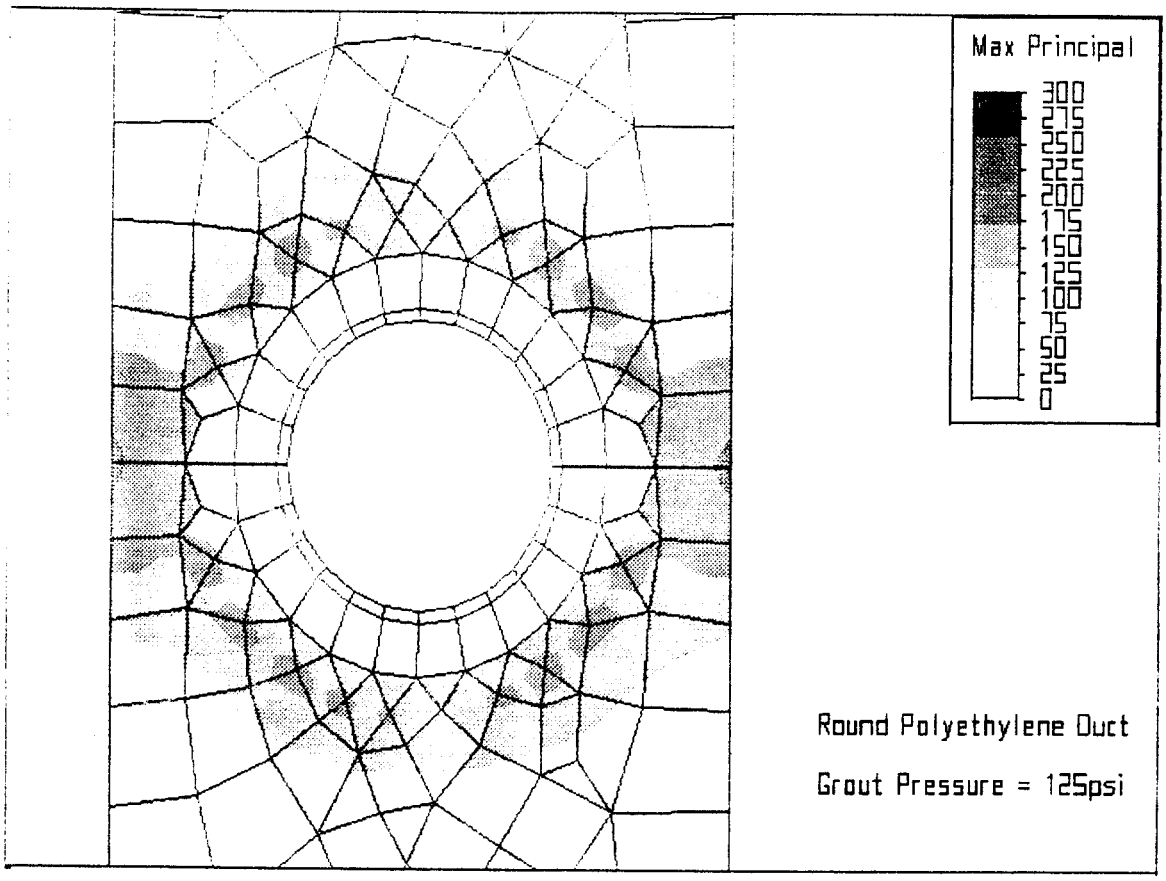

Figure 5.3 Principal Stresses in Round Polyethylene Model Caused by Grout Pressure

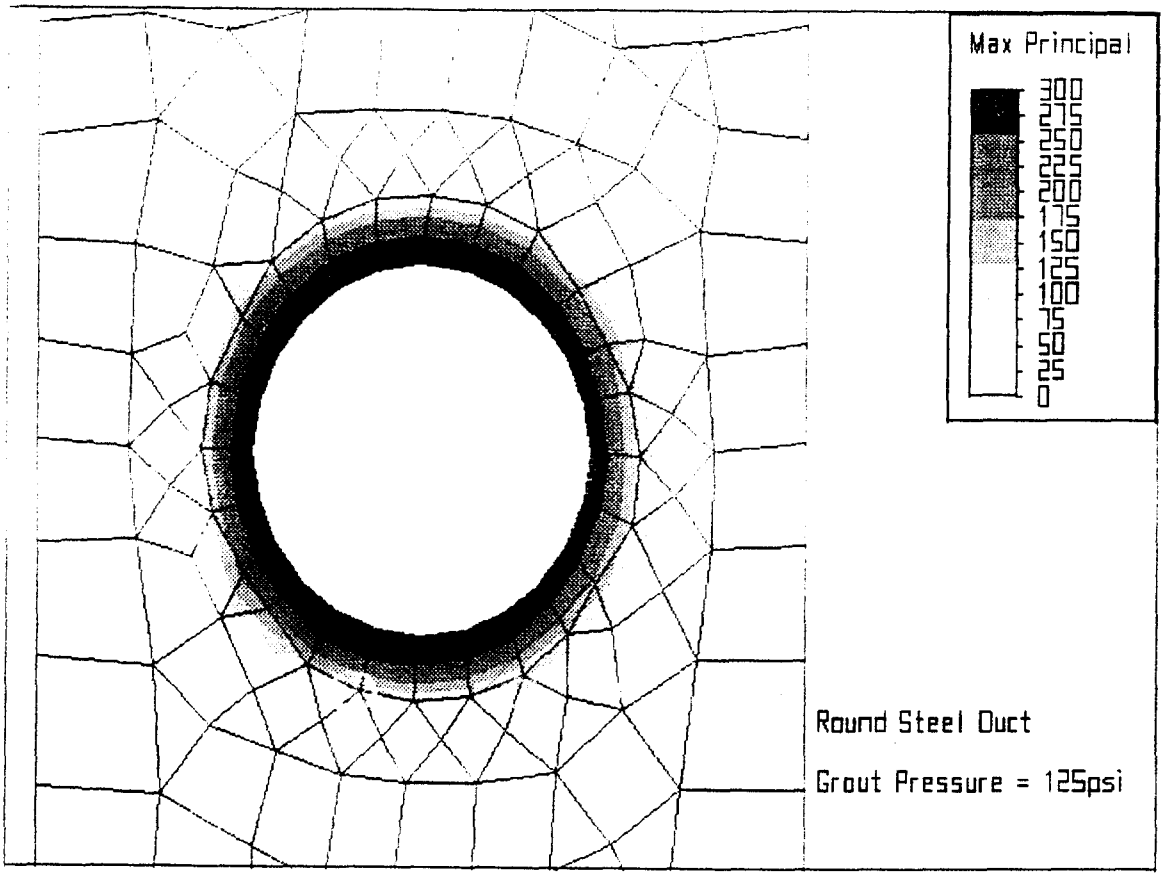

Figure 5.4 Principal Stresses in Round Steel Model Caused by Grout Pressure

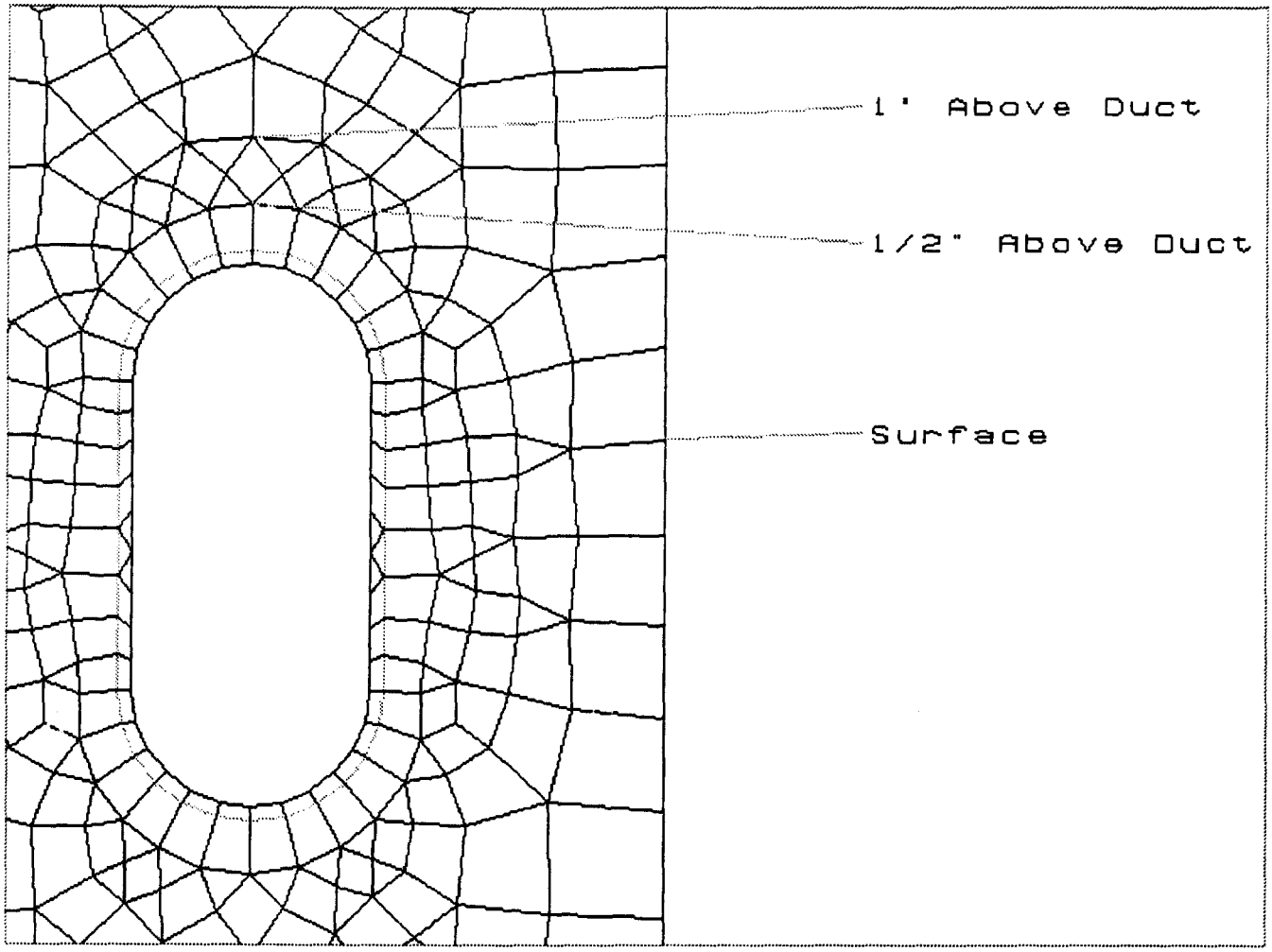

Figure 5.5 Locations of Stress Areas Used for Comparison

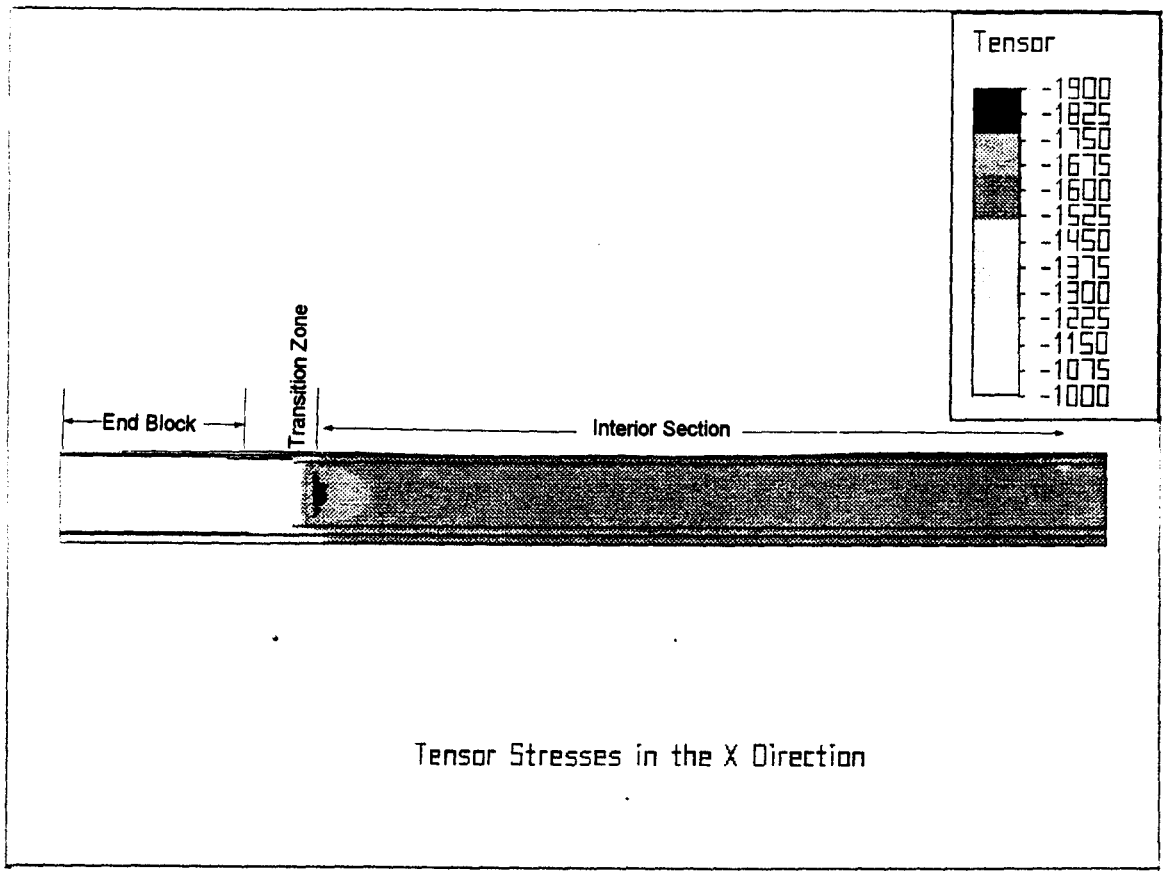

Figure 5.6 Stress Concentration at the End of the Transition Zone

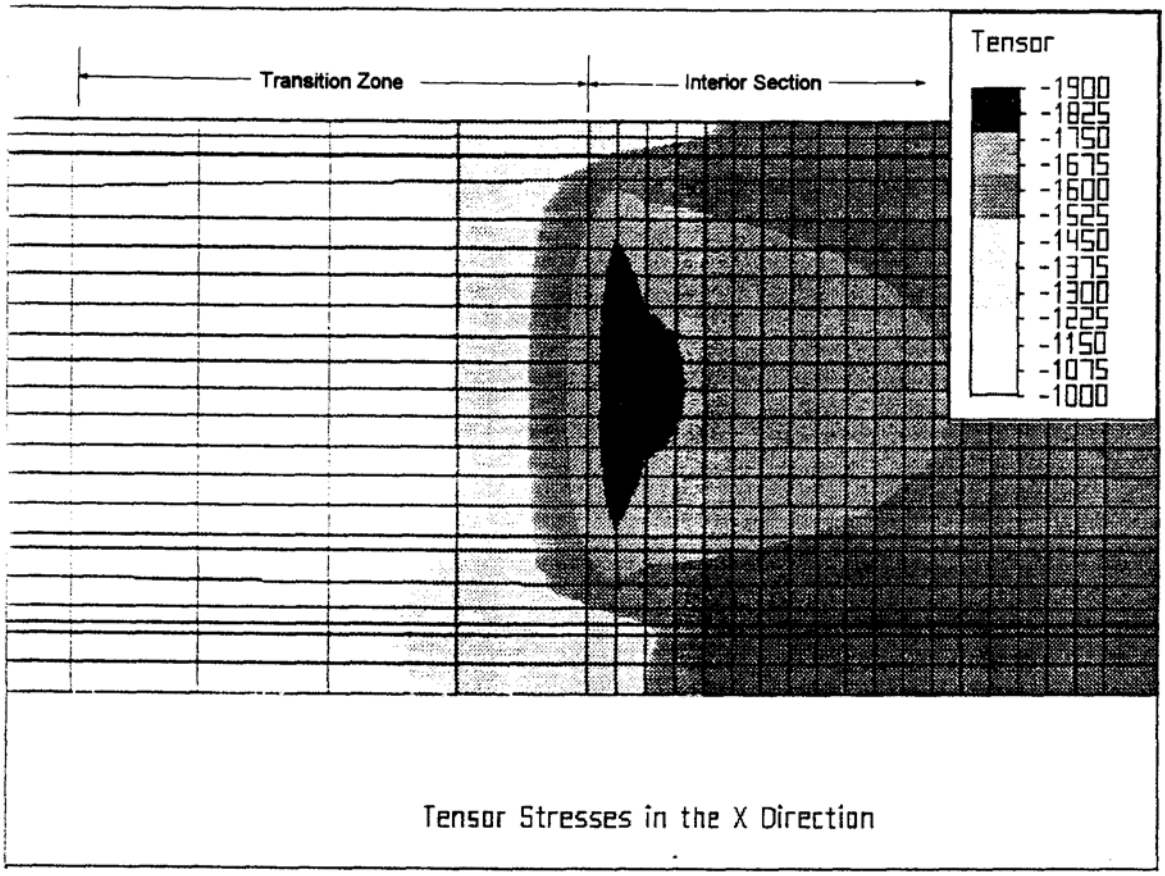

Figure 5.7 Enlarged View of Stress Concentration at the End of the Transition Zone

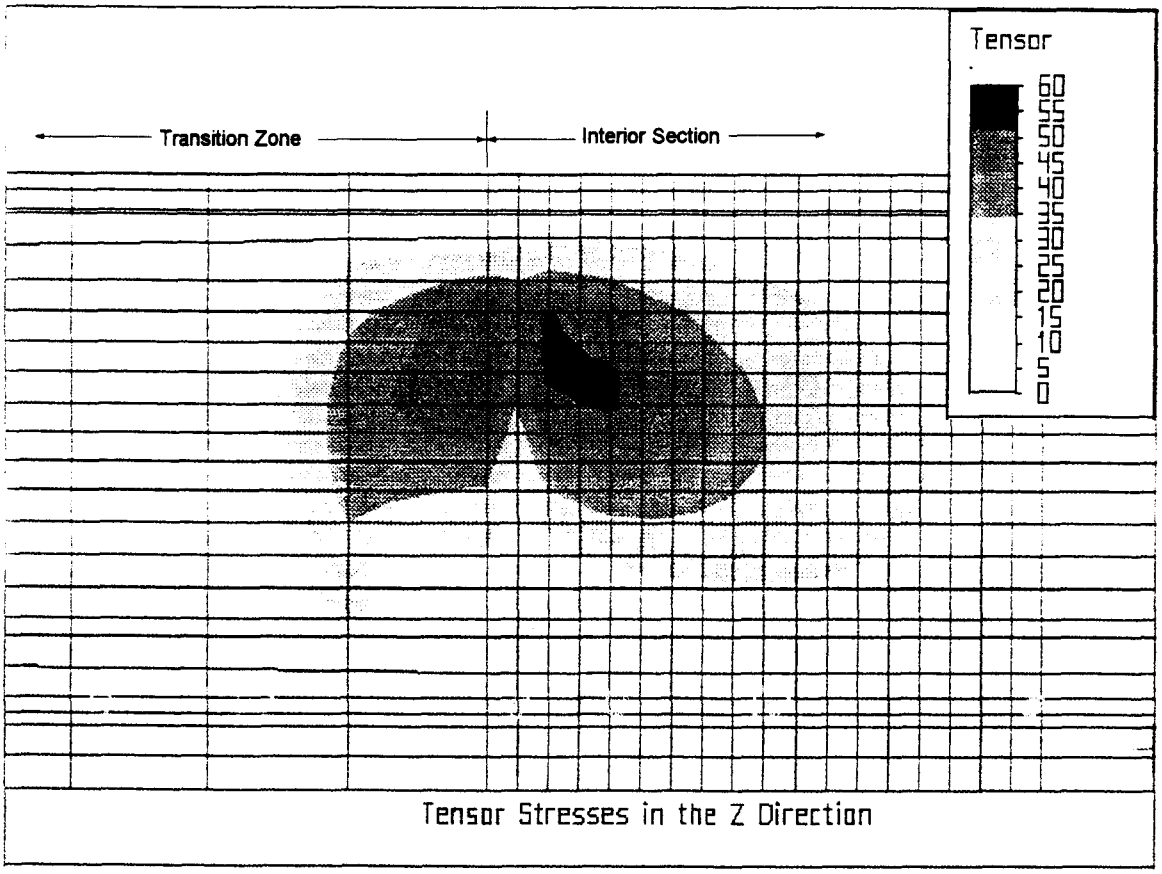

Figure 5.8 Vertical Component of Stress Concentration at the End of the Transition Zone

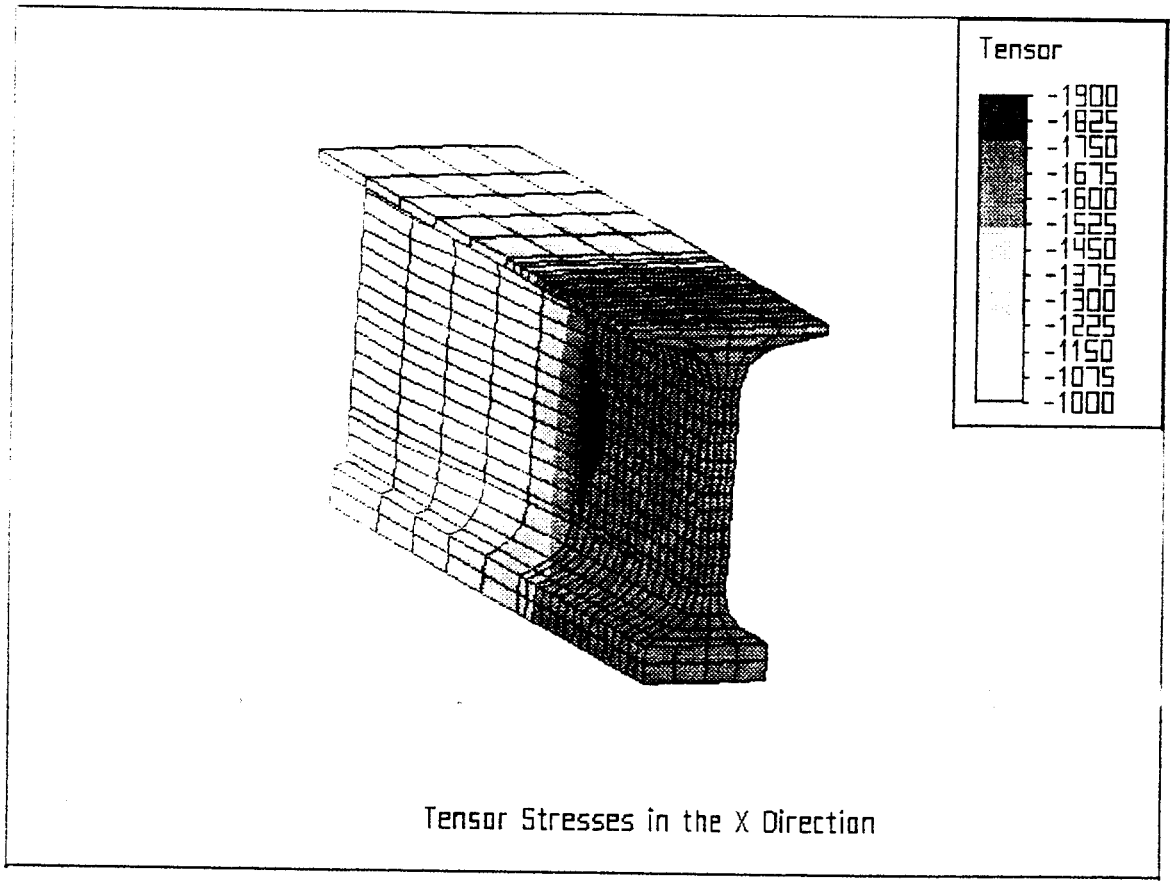

Figure 5.9 Three-Dimensional View of Stress Concentration at the End of the Transition Zone

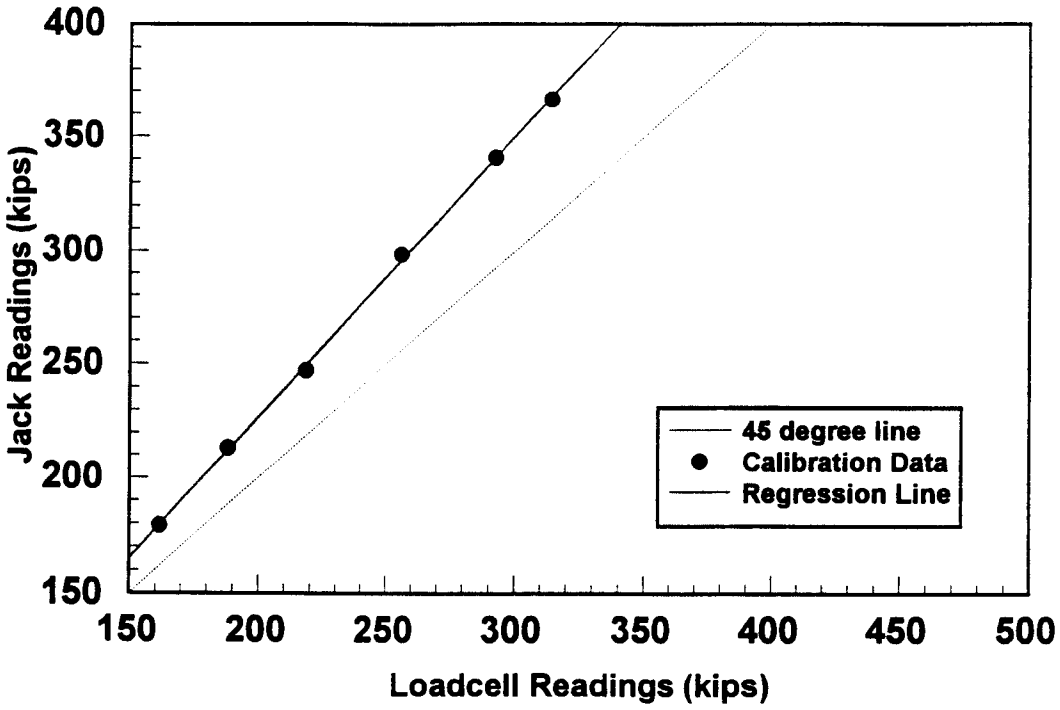

Figure 5.10 Error in Jack and Loadcell Readings

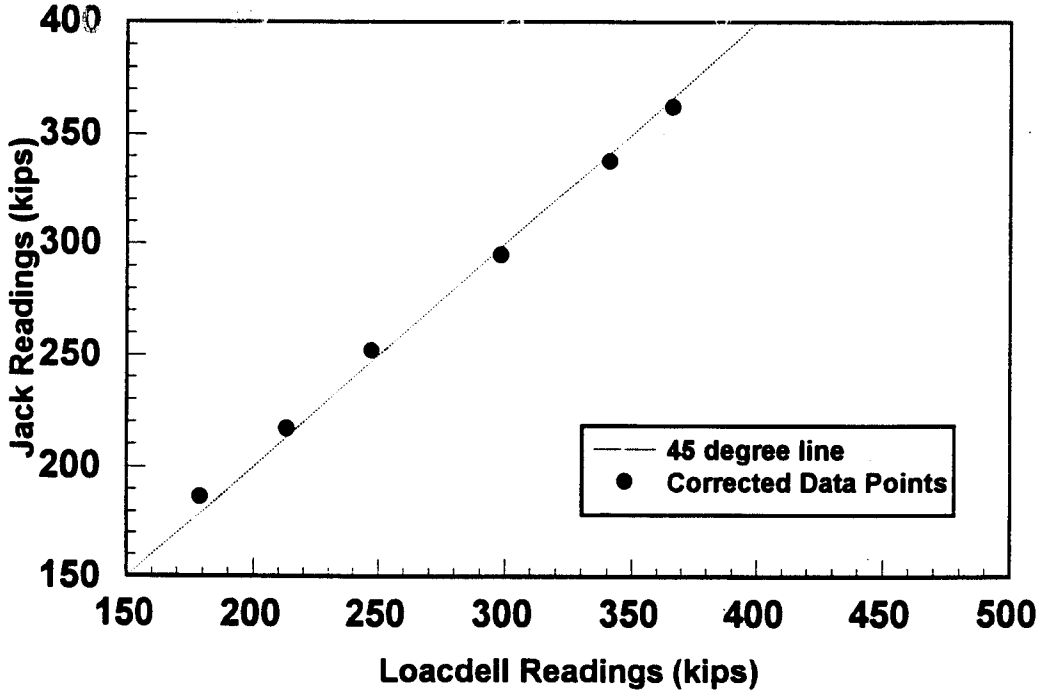

Figure 5.11 Jack and Loadcell Readings After Calibration

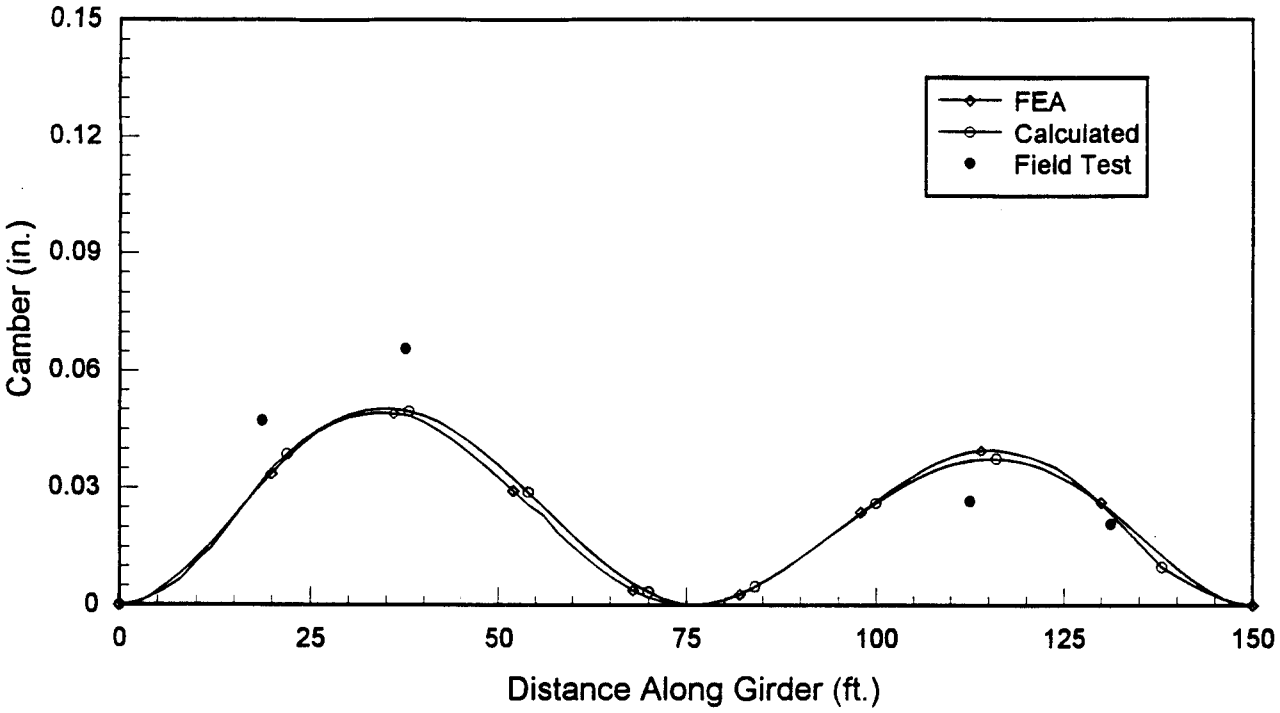

Figure 5.12 Camber After Stage 1 of Post Tensioning

(70 % of PT Force Applied at Live End)

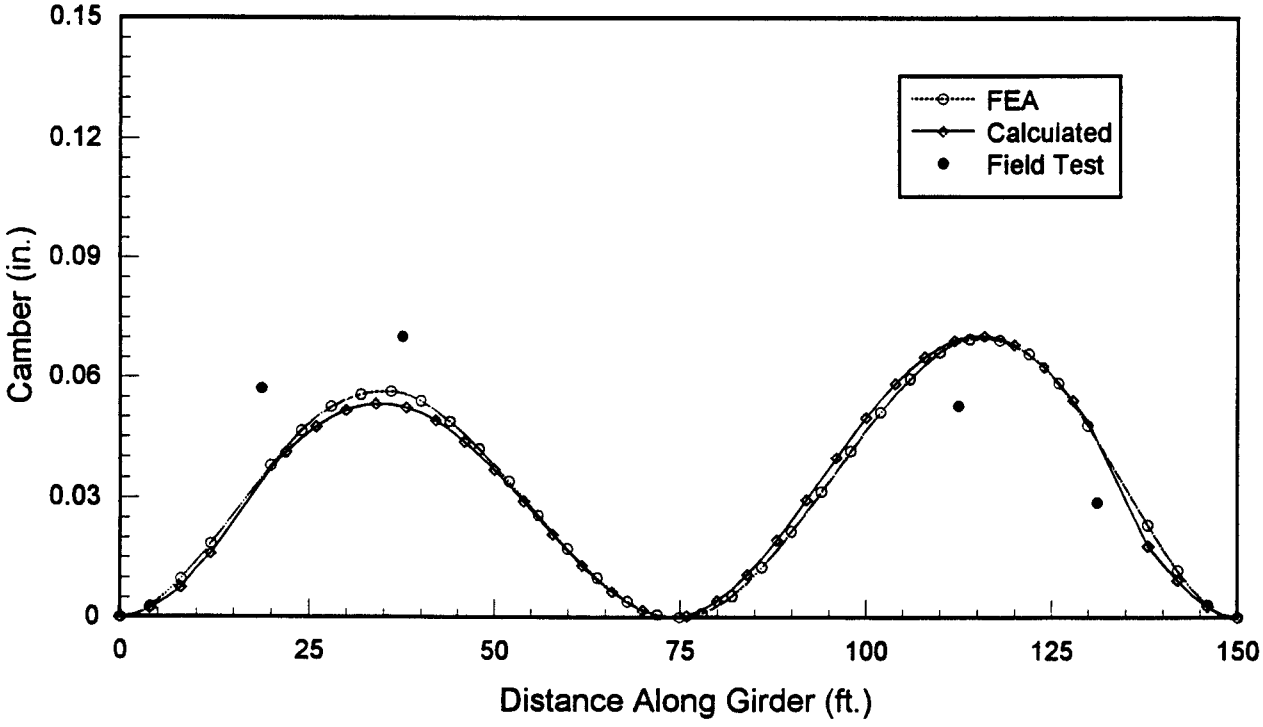

Figure 5.13 Camber After Stage 2 of Post Tensioning

(100% of PT Force Applied at Dead End)

Chapter 6 Discussion and Analysis

6.1 Finite Element Results

The two-dimensional models examined the effects of wedging and grout pressure for four different duct types. The three-dimensional models examined the other stresses in the Bulb-T which are independent of the duct type. The principal stress presented in Tables 5.1 through 5.4 can be used thoroughly examine stresses caused by pressure and wedging. The locations on the web surface, 1/2" above the center duct and 1" above the center duct will be used to compare the stresses between models with different ducts.

6.1.1 Principal Stresses vs Grout Pressure for a Given Duct Type

In this section the stresses caused by pressure and a constant wedging force will be examined. Figures 6.1 to 6.4 show plots of the stresses caused by varying grout pressure for the four different ducts being examined in this project. The results from the models using oval polyethylene duct, Figure 6.1, shows that the stress at the web surface are more critical than the stresses at the other locations.

Figure 6.2 shows the stresses in the model using the oval steel duct. This plot also shows that the stresses at the duct surface are most critical. However, the stresses 1/2" above the duct are nearly as large as the stresses on the web surface. The stresses 1" above the duct have the lowest magnitude.

Figure 6.3 shows the plot of the stresses for the round polyethylene duct. Again the stresses at the web surface are the most severe. The stresses 1" above the and 1/2" above the duct are approximately equal.

Figure 6.4 shows the plot of the principal stresses in the models with the round steel duct. In these models the stresses located 1/2" above the duct are greater than the stresses on the web surface.

6.1.2 Effects of Duct Type

Figures 6.5 to 6.7 show the principal stresses vs. grout pressure at the web surface, 1/2" above the duct and 1" above the duct respectively. In each of the Figures the models with the oval polyethylene duct have the highest stresses and the models with round steel ducts have the lowest stresses. On average, the stresses surrounding the models with oval polyethylene ducts were five times as large as the stresses surrounding the round steel ducts. It is apparent that both the duct shape and the duct material influence the stresses in the concrete surrounding the duct. The round shape appears more able to resist stresses than the oval shape. In addition, steel ducts are able to resist more stress than polyethylene ducts.

The primary reason models with oval ducts had higher stresses in the concrete than models with round ducts is that round shapes can develop high hoop stresses. Circular shapes under a pressure loading will deform equally in all directions due to the strain in the material, because the circular shape is the most efficient shape to resist internal pressure. On the other hand oval shapes will develop lower hoop stresses because of the inefficiency of the shape to resist internal pressures. The side.- of the duct will deform significantly at relatively low pressures.

Figure 6.8 shows a close view of the concrete between the duct and the web surface in an oval polyethylene model. The stresses shown in this Figure are vertical tensor stresses, stress in the Z direction. Figures 6.9 to 6.11 show this region of the concrete for each of the different types of ducts.The models with the round ducts show lower stresses than models with oval ducts. On average, the stresses surrounding the round ducts were 49% less than the stresses surrounding the models with oval ducts.

Figure 6.12 shows the tensor stresses in the Y direction for the oval polyethylene duct. Figures 6.13 to 6.15 show the same stresses for the other types of ducts. It can be seen that the models with steel ducts have lower stresses in the surrounding concrete than the models with polyethylene ducts. On average, the stresses surrounding the models with steel ducts were 50% less than the stresses surrounding the models with polyethylene ducts.

6.2 Field Test Results

6.2.1 Construction Techniques

Some of the construction techniques that were observed and discussed in section 5.3 may be contributing to the problems with the Florida Bulb-T during post-tensioning. The fact t at some of the ducts have completely collapsed during casting indicates that the ducts may not be strong enough to withstand the force exerted by the weight of the concrete during casting. The duct may have a tendency to collapse in areas where it has been tied to the reinforcing steel, and has a resulting inward force from the way it was tied. The oval shape is less efficient than a round shape in resisting external inward forces. It seems reasonable to assume that if the duct completely collapsed in some locations, then there may be numerous smaller deformations along the length of the duct. These smaller deformations may cause problems when the rabbit is pulled through the ducts. If the duct is slightly deformed then the rabbit may be able to be forced through the duct if the force allowed to pull the rabbit is not limited. If the rabbit is forced through the duct using excessive force, then very high point loads will result at the location of the inwardly deformed duct. These forces may damage the concrete surrounding the duct. It is quite possibly that the damage will not become apparent until additional forces are applied to the girder during post-tensioning and construction.

The curvature of the ducts near a splice may also cause problems during post-tensioning. The wedging forces calculated for the finite element model assumed a parabolic duct profile. While some deviation is expected in actual manufacturing conditions, large changes in curvature over a small distance may lead to significant wedging forces during post-tensioning. In a case where there is a large change in curvature the stresses that would normally be distributed over a large area will be isolated over a much smaller area.

6.3 Comparison Between Field Tests and Finite Element Results

The results from the two-dimensional finite element models, showing the effects of strand wedging and grouting, can be added to the results from the three-dimensional models, showing other out-of plane force effects, to get an estimate of the strains that are expected to be present in actual field girders. The finite element results correspond reasonably well with the field test results. Figures 6.16 to 6.23 show the finite element test results compared with the field test results for two gauges

from each of the instrumented sections A, B, C and D. It appears that there is a close correlation between the finite element results and the field test. These results indicate that full-scale Bulb-T girders can be successfully modeled using finite element analysis.

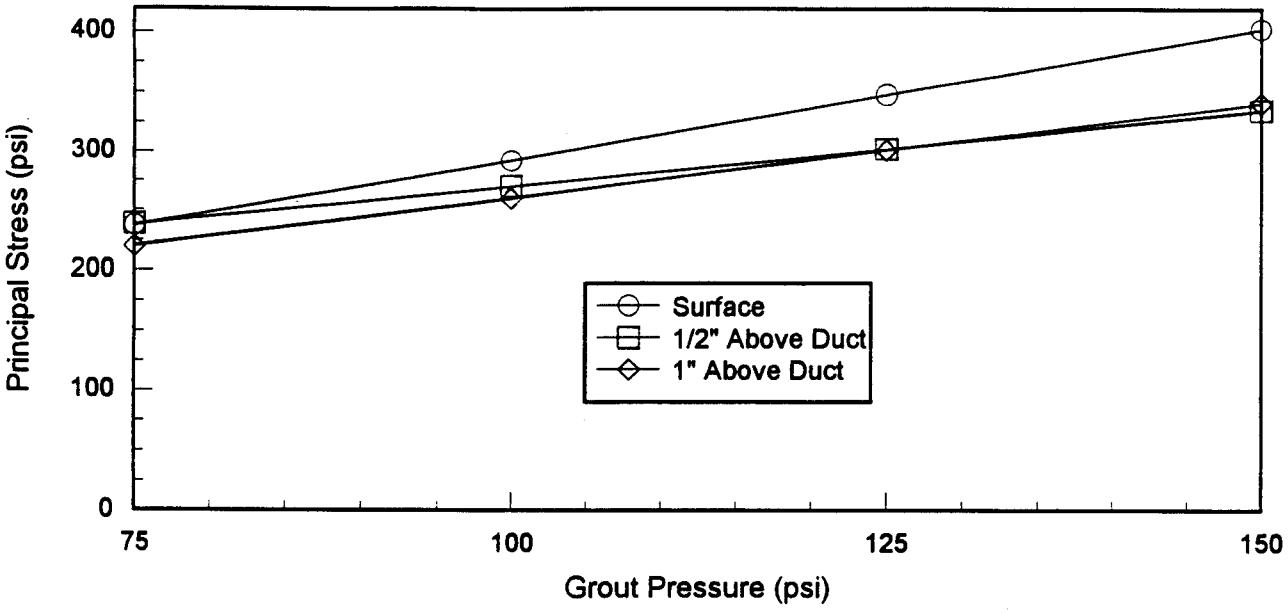

Figure 6.1 Principal Stress VS Grout Pressure In Oval Polyethylene Models

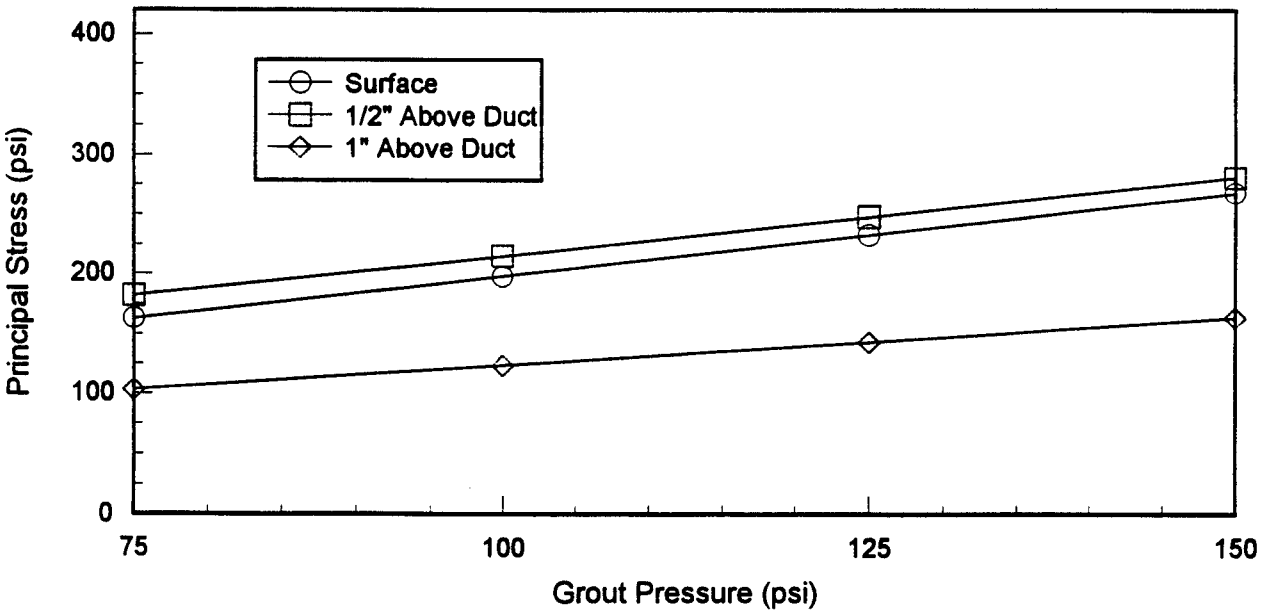

Figure 6.2 Principal Stress VS Grout Pressure In Oval Steel Models

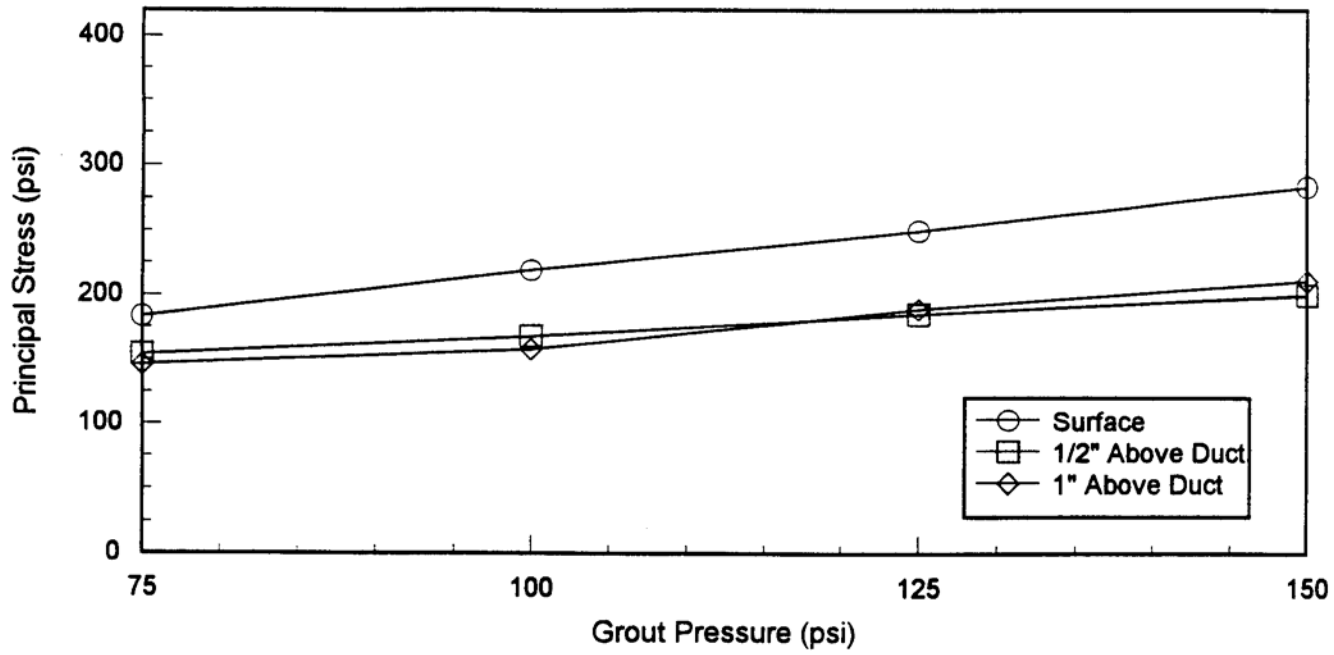

Figure 6.3 Principal Stress VS Grout Pressure In Round Polyethylene Models

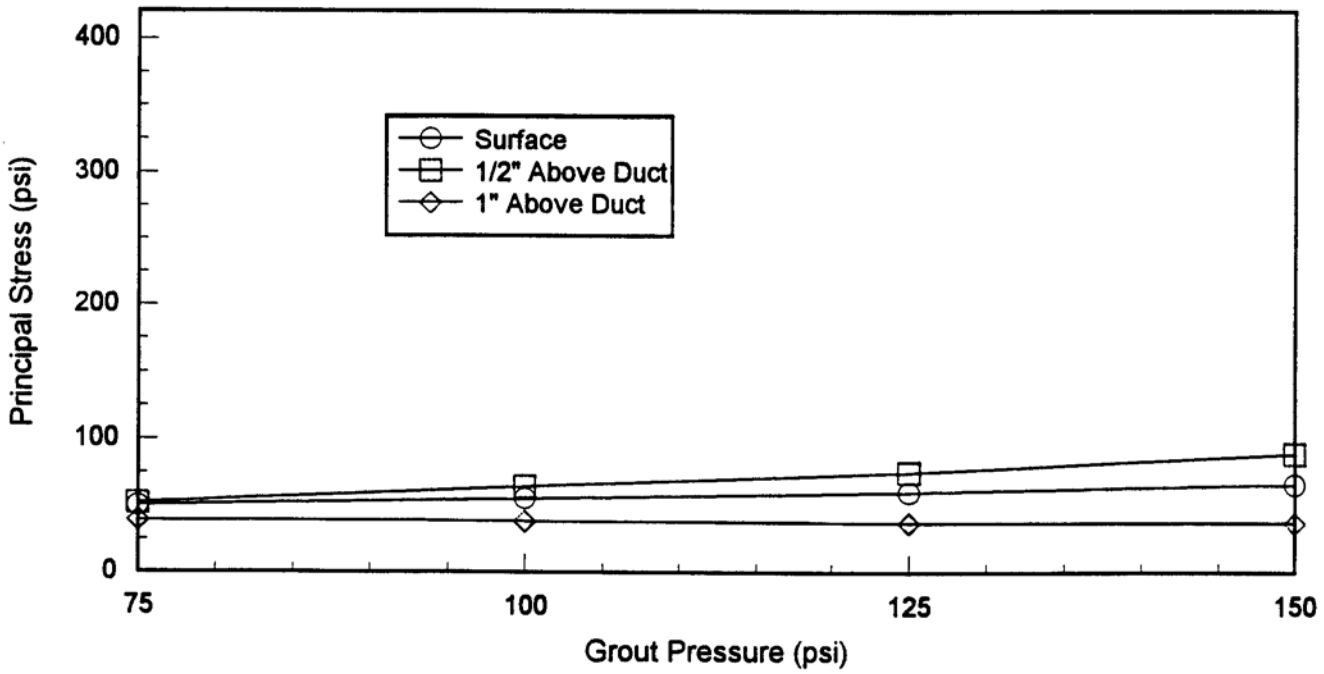

Figure 6.4 Principal Stress VS Grout Pressure In Round Steel Models

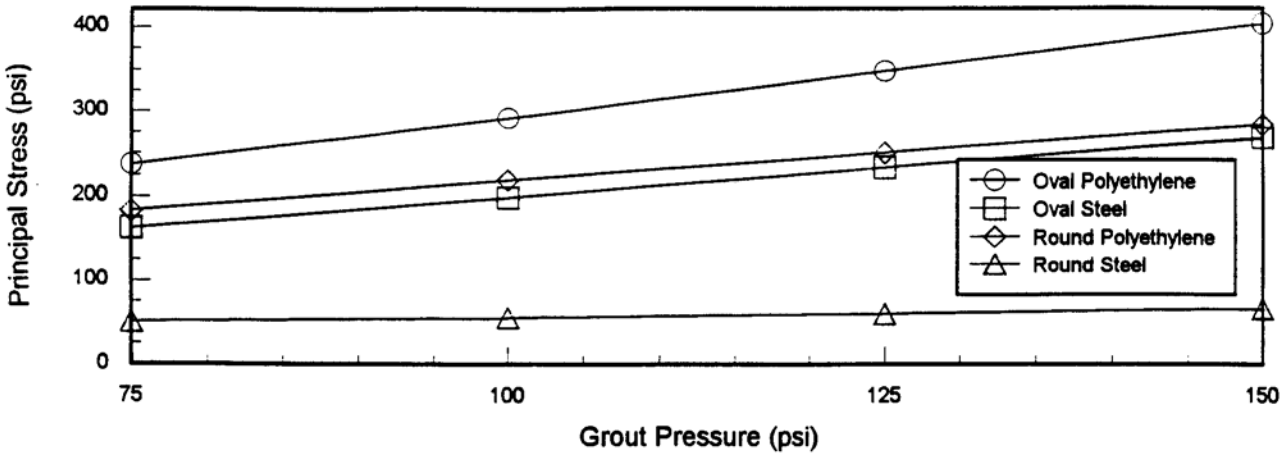

Figure 6.5 Principal Stress VS Grout Pressure at Web Surface

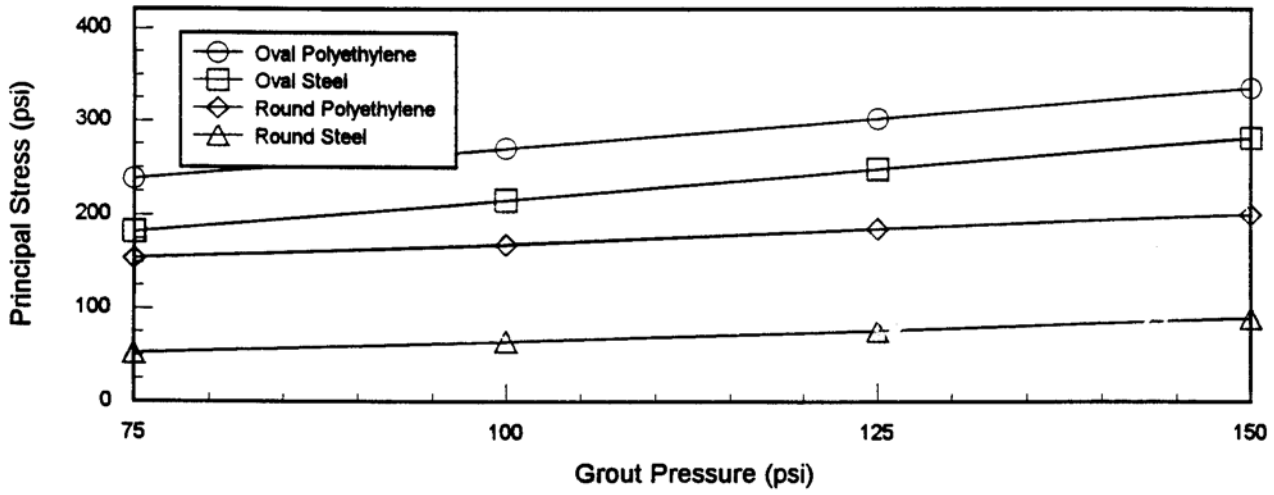

Figure 6.6 Principal Stress VS Grout Pressure 1/2" Above Duct

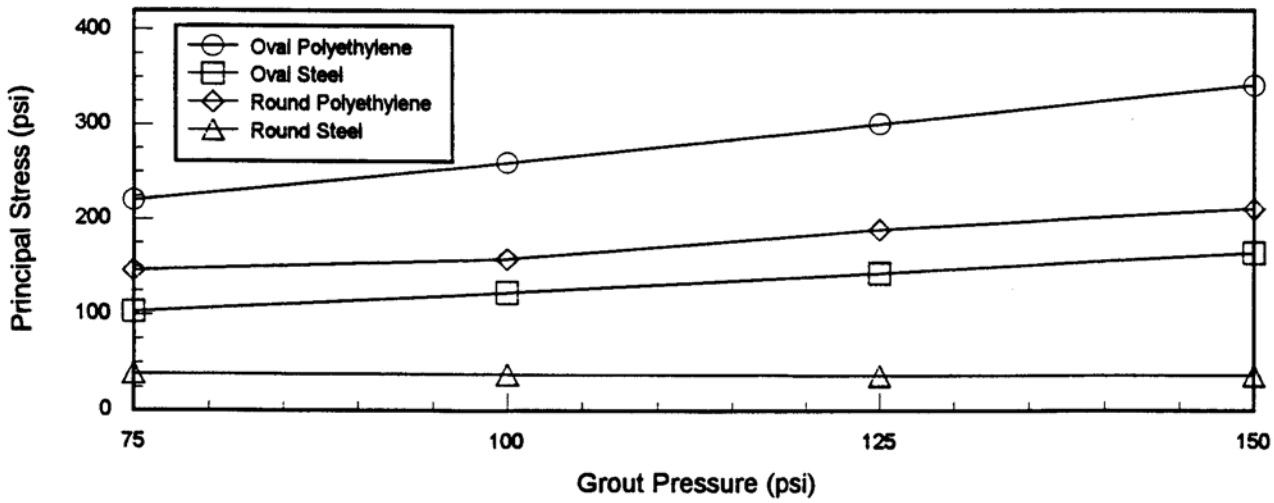

Figure 6.7 Principal Stress VS Grout Pressure 1" Above Duct

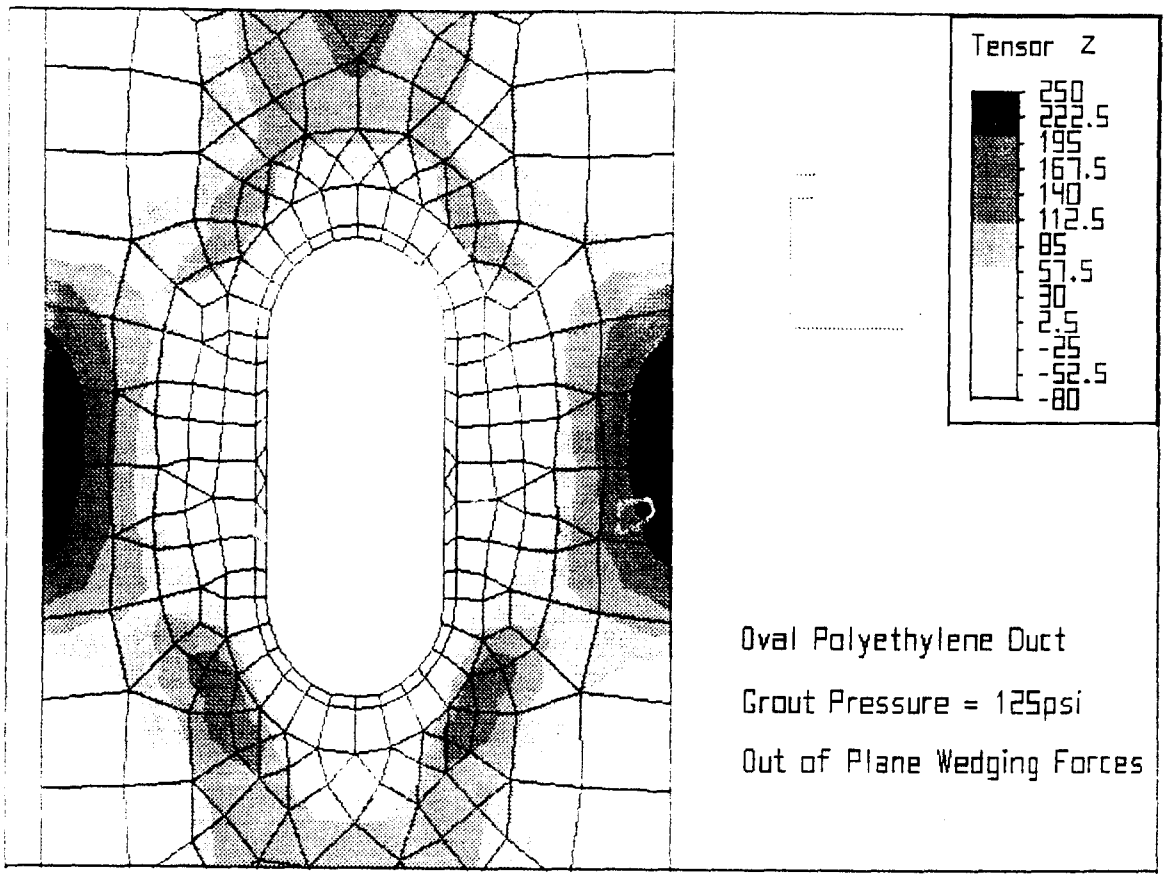

Figure 6.8 Tensor Z Stresses in Oval Polyethylene Model

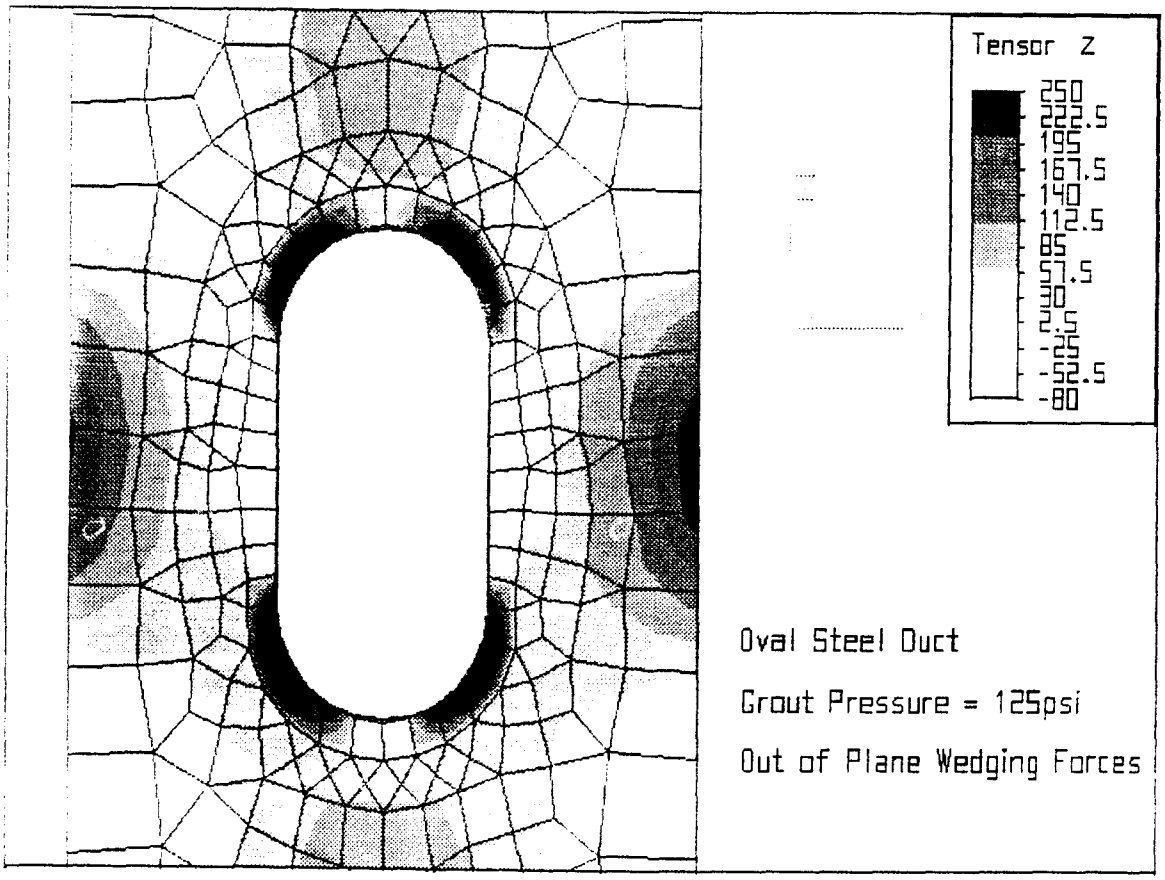

Figure 6.9 Tensor Z Stresses in Oval Steel Model

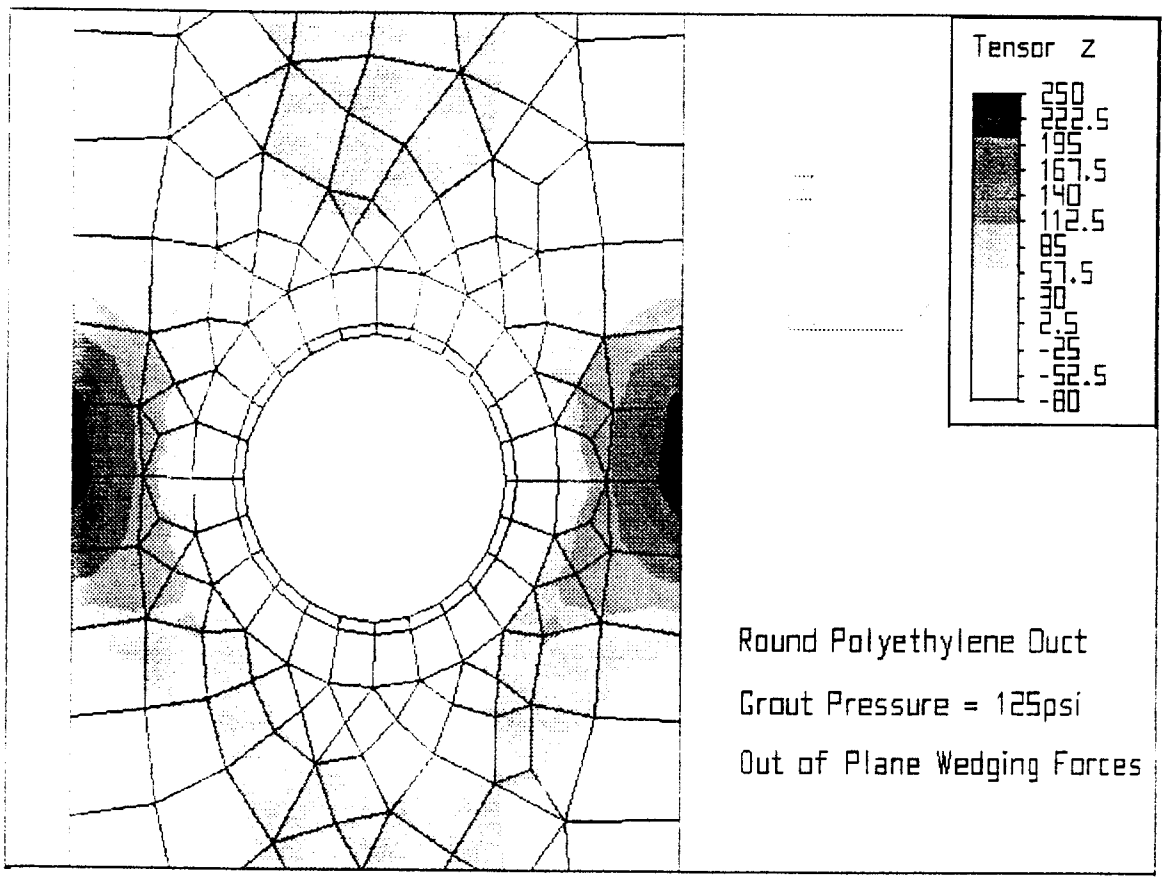

Figure 6.10 Tensor Z Stresses in Round Polyethylene Model

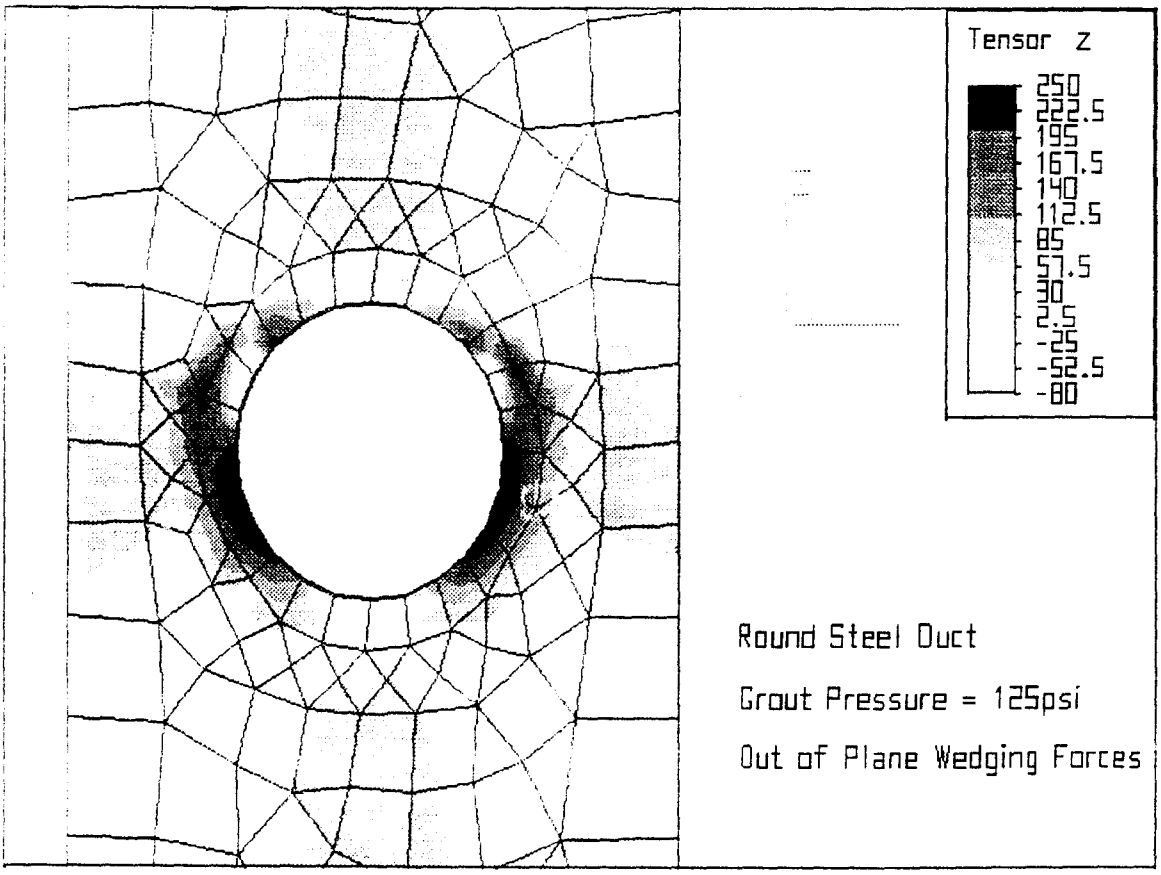

Figure 6.11 Tensor Z Stresses in Round Steel Model

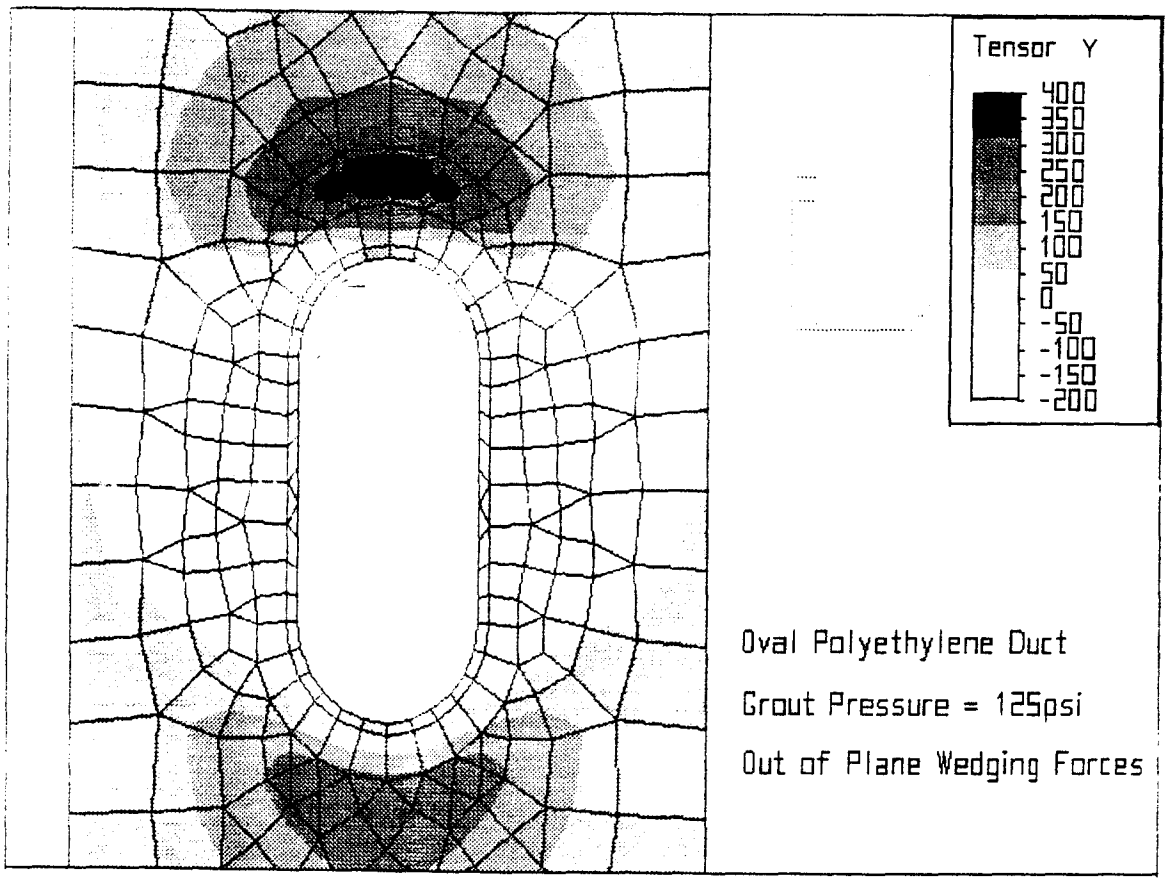

Figure 6.12 Tensor Y Stresses in Oval Polyethylene Model

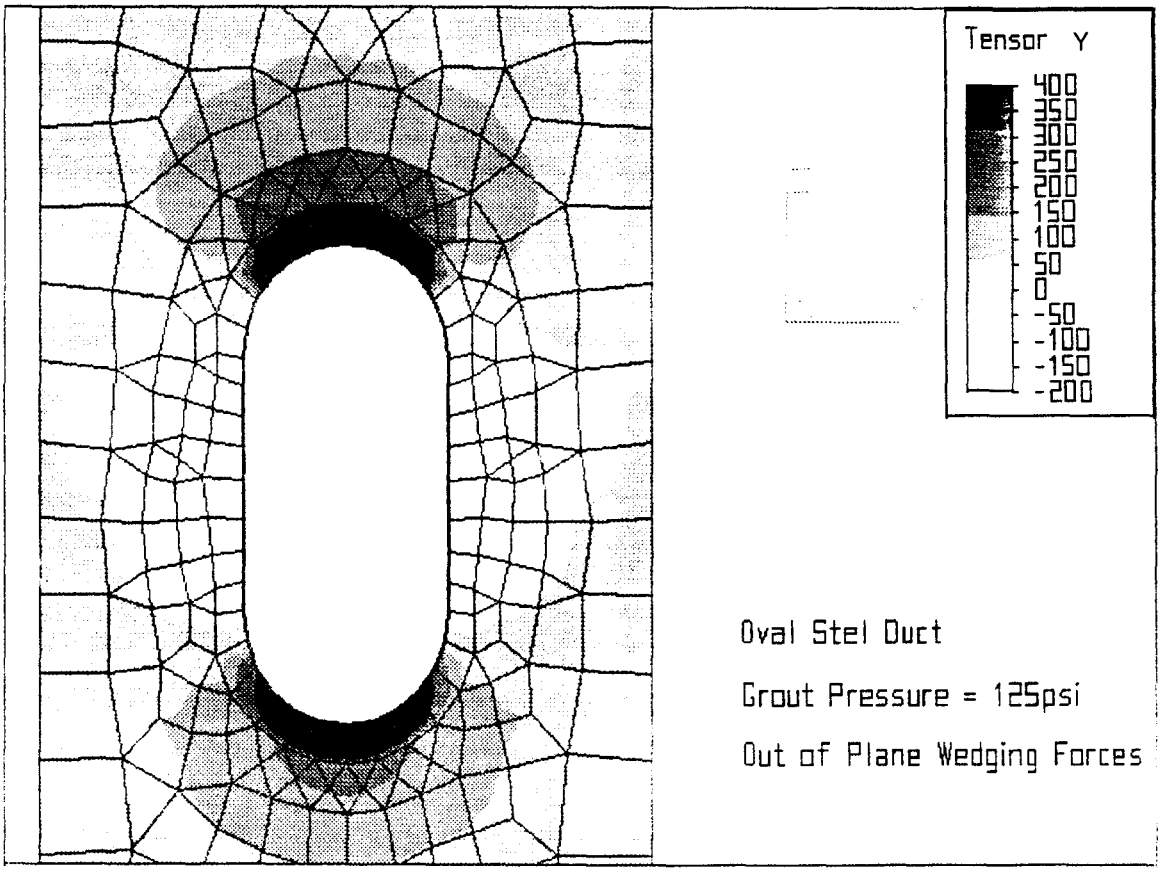

Figure 6.13 Tensor Y Stresses in Oval Steel Model

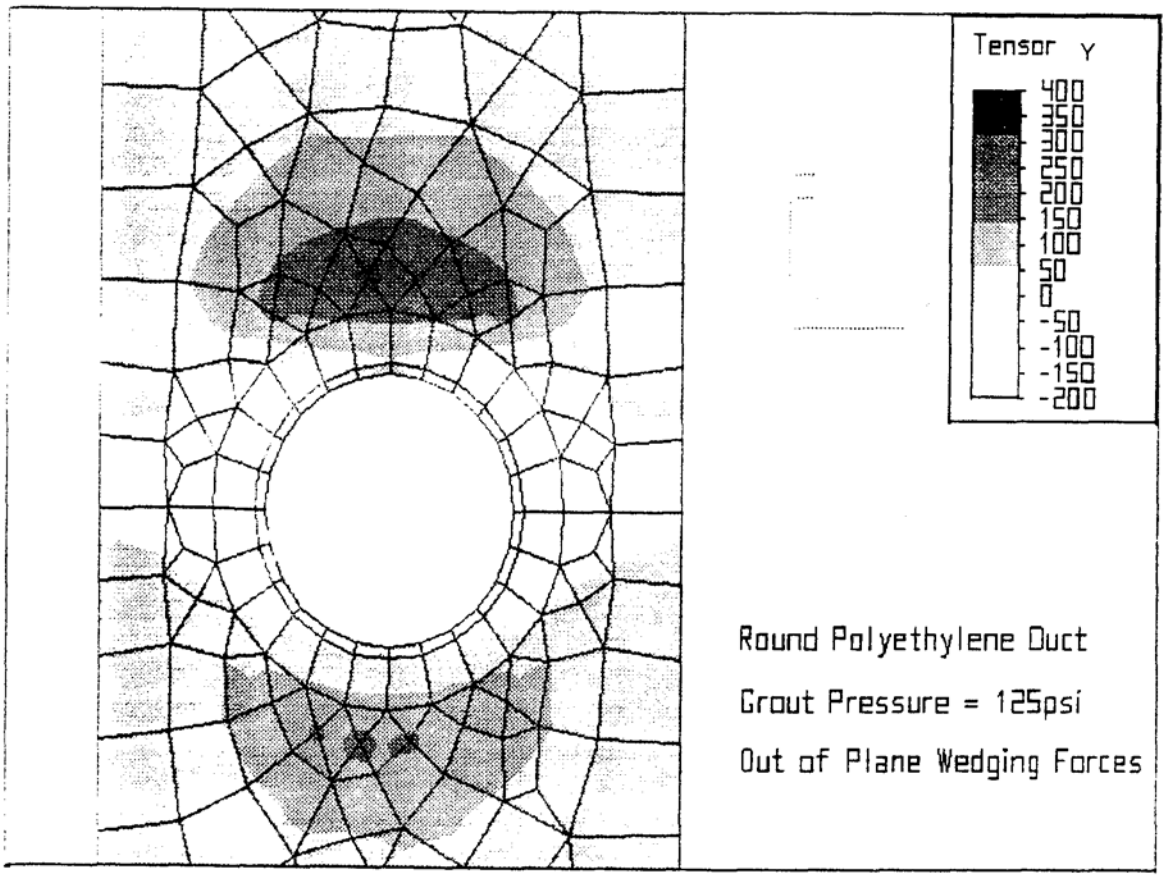

Figure 6.14 Tensor Y Stresses in Round Polyethylene Model

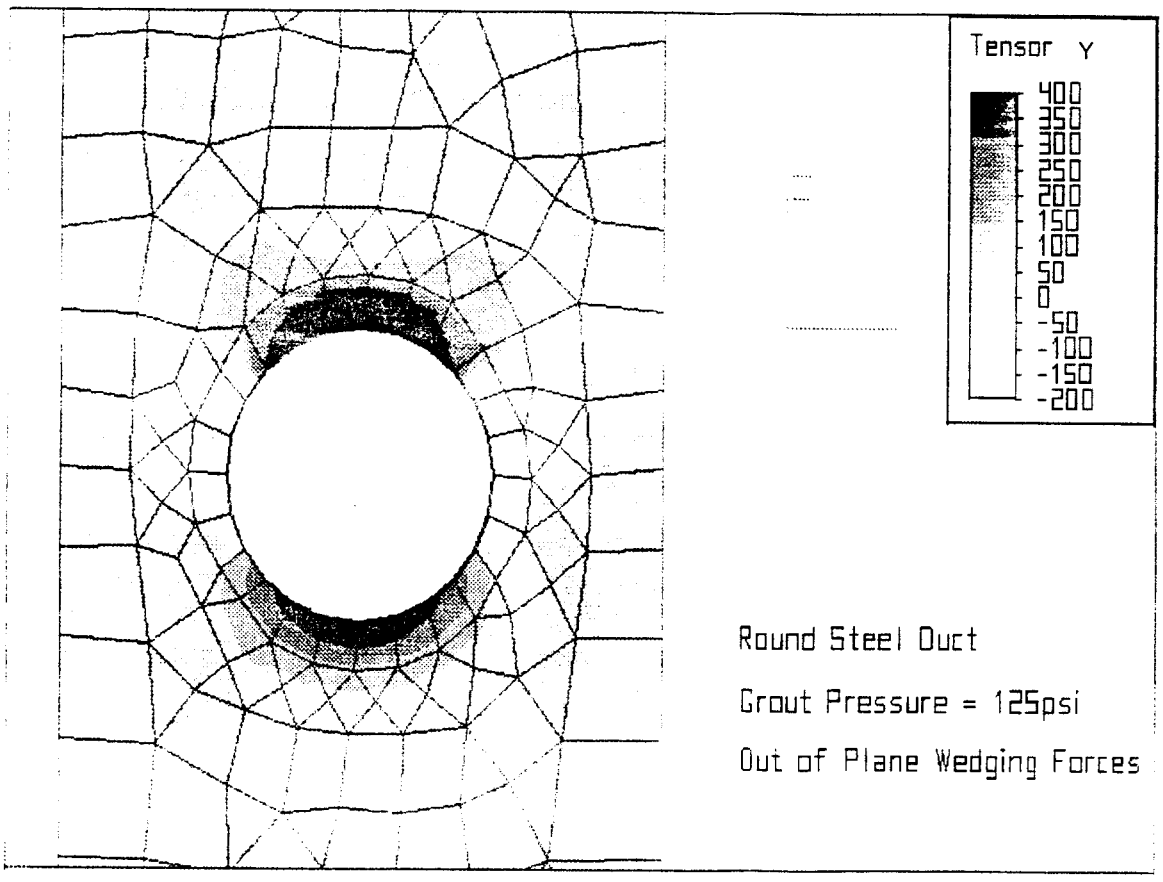

Figure 6.15 Tensor Y Stresses in Round Steel Model

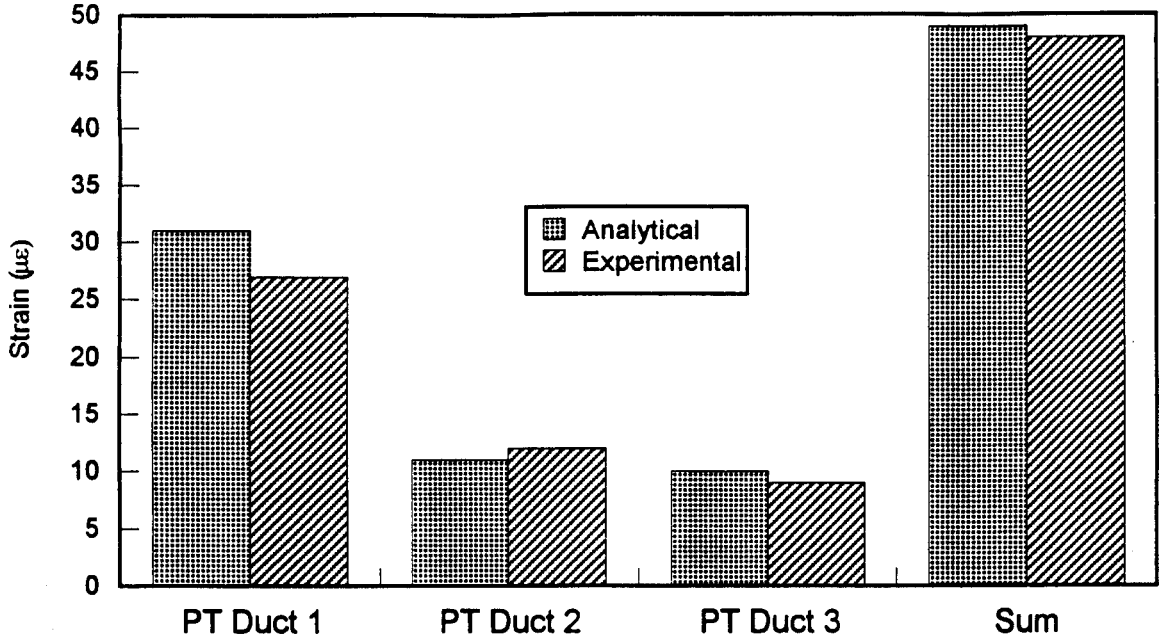

Figure 6.16 Predicted and Measured Strain for Gage A-D1-H1

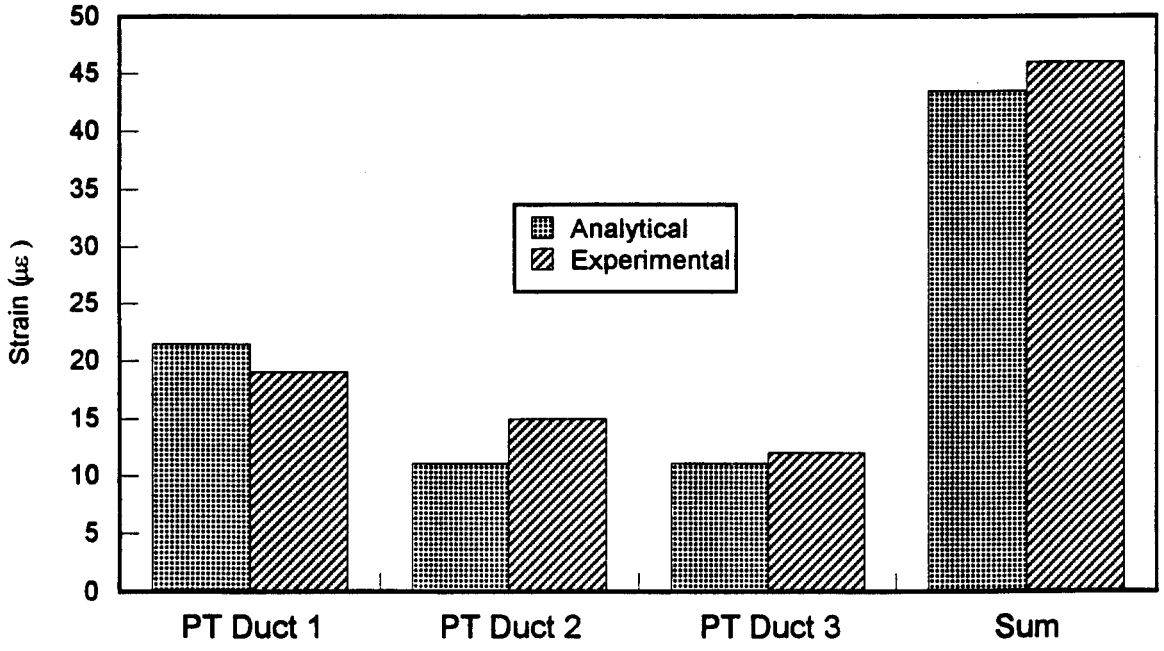

Figure 6.17 Predicted and Measured Strain for Gage A-D1-H2

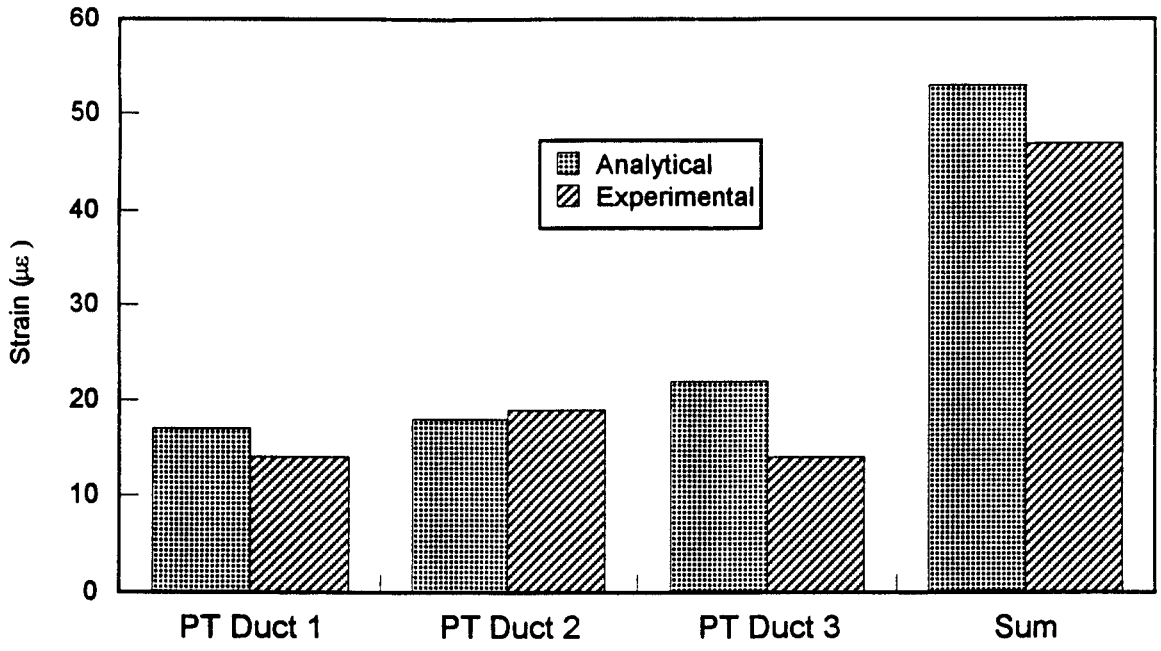

Figure 6.18 Predicted and Measured Strain for Gage B-D1-VS

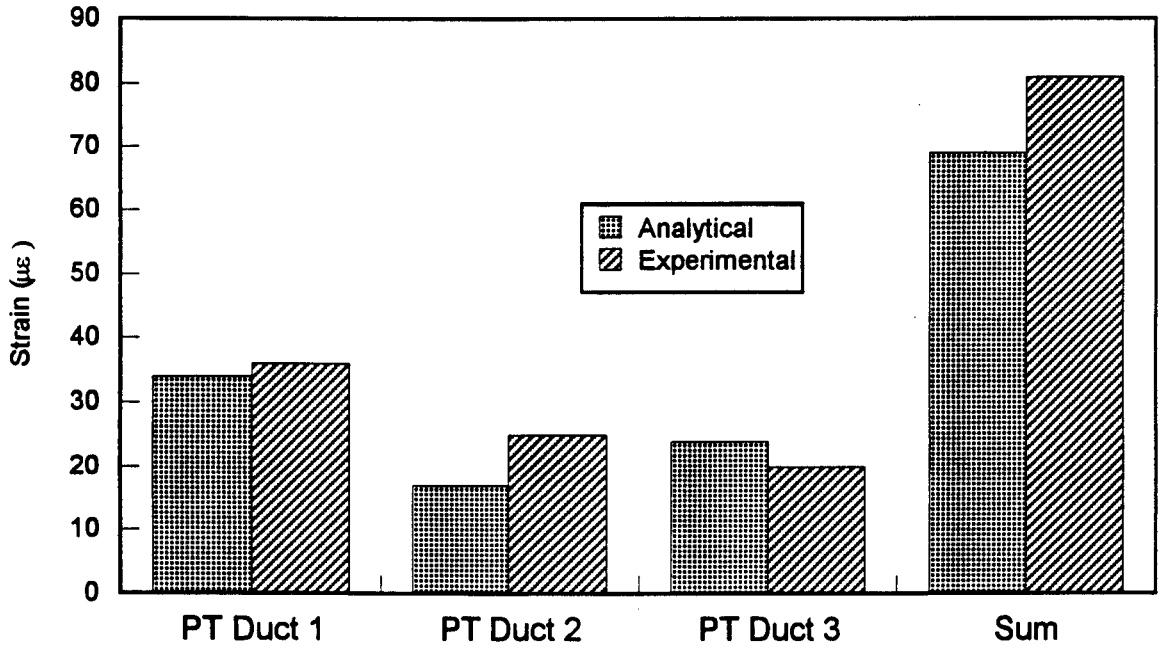

Figure 6.19 Predicted and Measured Strain for Gage B-D1-EN

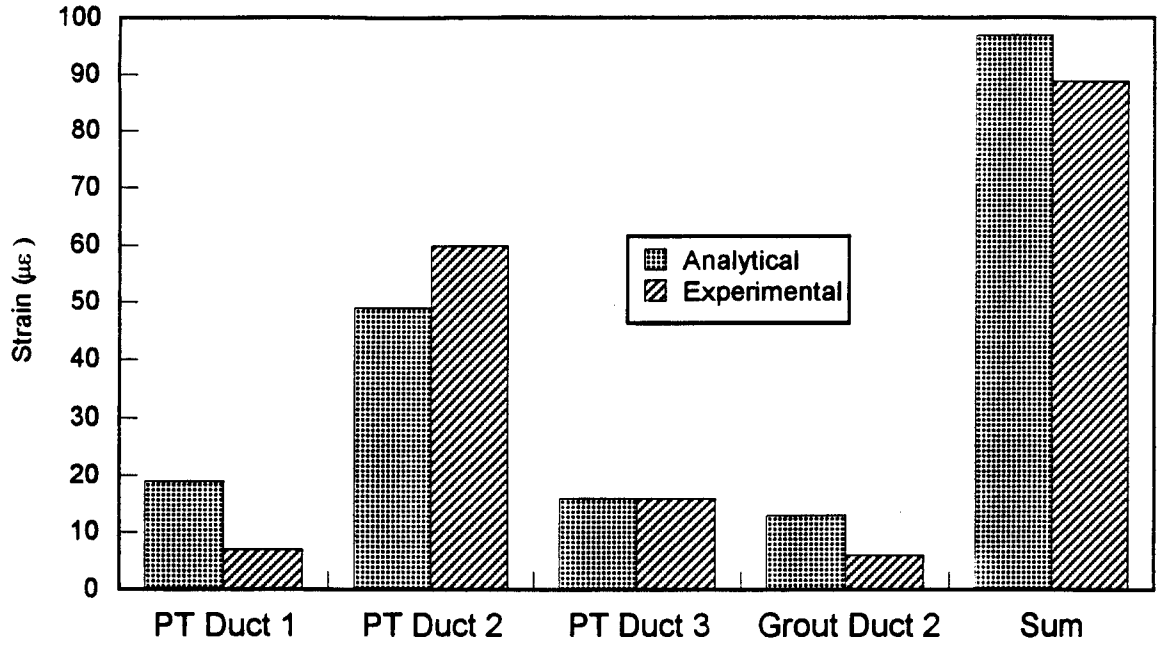

Figure 6.20 Predicted and Measured Strain for Gage C-D2-H1

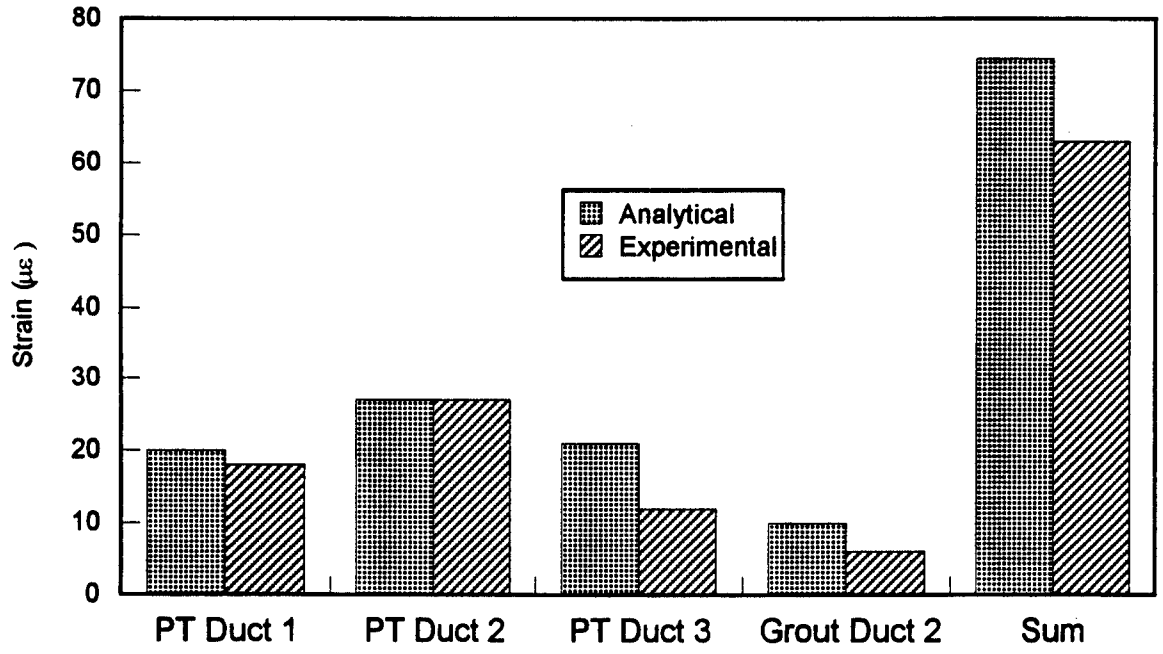

Figure 6.21 Predicted and Measured Strain for Gage C-D2-VN

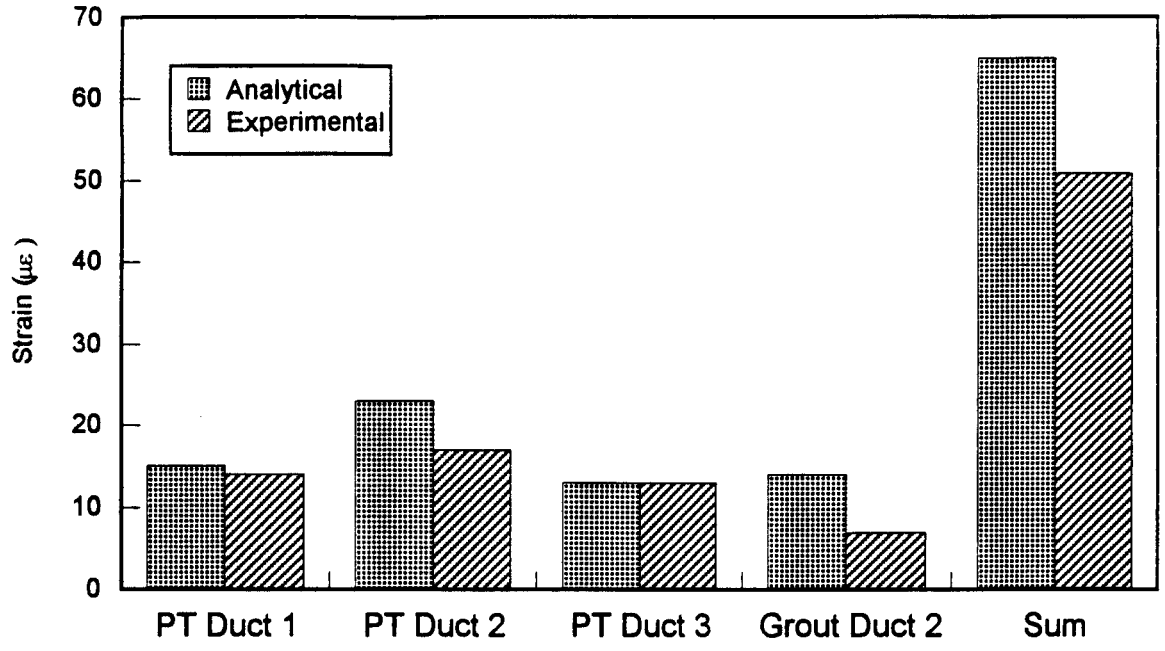

Figure 6.22 Predicted and Measured Strain for Gage D-D1-H3

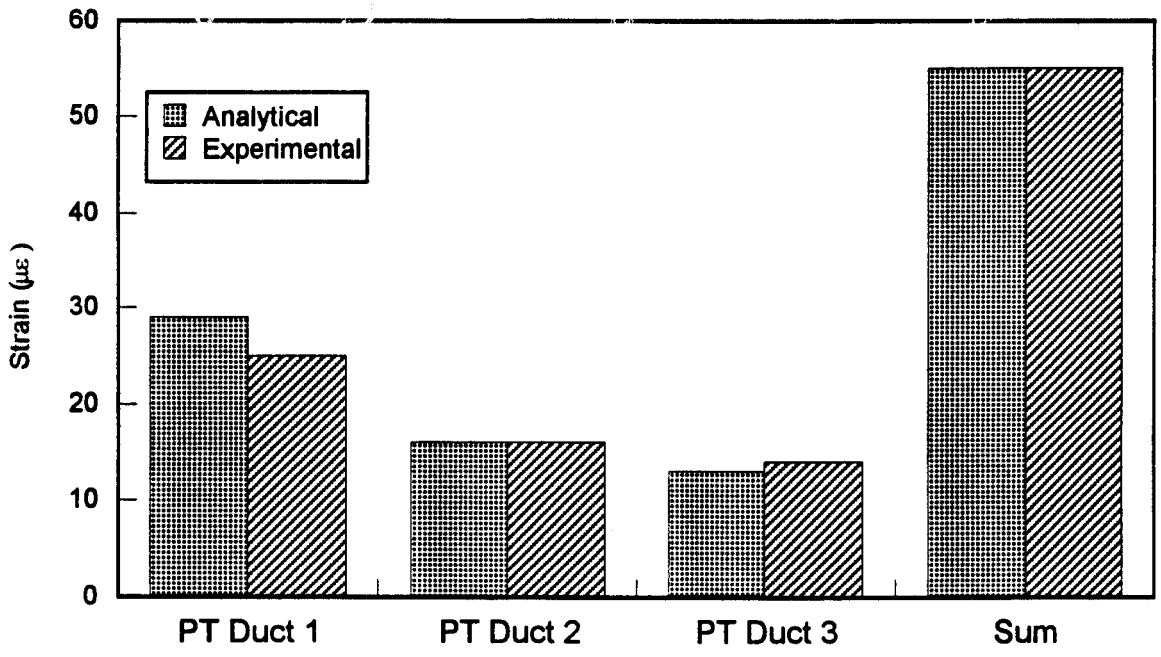

Figure 6.23 Predicted and Measured Strain for Gage D-D1-ES

Chapter 7
Conclusions and Recommendations

The following conclusions can be made from the results presented in this paper:

1. Strand wedging and grouting forces will cause significant stresses in the web of the Florida Bulb-T.
2. The use of round ducts will result in lower web stresses compared with oval ducts.
3. The use of steel ducts will result in lower web stresses compared with polyethylene ducts. 4. Locations of large curvature may occur where duct segments are spliced together during girder construction. There will be a significant concentration of wedging forces in these areas.
5. There is evidence that the oval ducts are closing inwards during the casting and curing of the concrete. If the "rabbit" is forced through a partially closed duct, high point loads will occur and cracks may form. These cracks may propagate during post-tensioning.
6. The measured friction coefficients fall within the range of recommended values in the LRFD AASHTO Code.

Based on the investigation the following recommendations are made:

1. Steel ducts should be used in the Florida Bulb-T. Polyethylene ducts should not be permitted in the Florida Bulb-T.
2. Whenever possible, round ducts should be used instead of oval ducts
3. The force required to pull the rabbit through the ducts should be monitored and limited.
4. Oval steel ducts with a wall thickness greater than 24 gage may be used successfully if the force used to pull the "rabbit" is limited.

References

1. "AASHTO LRFD Bridge Design Specifications," American Association of State Highway and Transportation Officials, 1994.

2. Bruce, R. N., Russell, H. G., Roller, J. J., and Martin, B. T., "Feasibility Evaluation of Utilizing High-Strength Concrete in Design and Construction of Highway Bridge Structures," Louisiana Transportation Research Center, January 1994.

3. Collins, Michael P. and Mitchell, Dennis, "Prestressed Concrete Structures," Prentice-Hall 1991.

4. Csagoly, Paul F. and Nickas, William N., "Florida Bulb-Tee and Double-Tee Beams," Concrete International, November, 1987 pp. 18-23.

5. Garcia, Antonio M., "Testing, Construction, and Aesthetics of Florida's Long Span Concrete Girders: Florida's Bulb-Tees," Florida Department of Transportation, October, 1992.

6. Issa, M., "Experimental Investigation of the Edison Bridge," Florida Department of Transportation, 1993.

7. Moreton, Alan, "Longitudinal Cracking of Webs and Spalls," Florida Department of Transportation, August, 1992.